THE UNIVERSITY OF CHICAGO

RECENT RESULTS IN DARK MATTER DIRECT DETECTION EXPERIMENTS

A DISSERTATION SUBMITTED TO
THE FACULTY OF THE DIVISION OF THE PHYSICAL SCIENCES
IN CANDIDACY FOR THE DEGREE OF
DOCTOR OF PHILOSOPHY

DEPARTMENT OF PHYSICS
BY
CHRISTOPHER MICHAEL KELSO
CHICAGO, ILLINOIS
AUGUST 2012

To Mindi.

It has been a long time coming, but I am finally finished.

TABLE OF CONTENTS

ABSTRACT

In this dissertation, we study the original excess of low energy events observed by the CoGeNT collaboration and the annual modulation reported by the DAMA/LIBRA collaboration, and discuss whether these signals could both be the result of the same elastically scattering dark matter particle. We find that, without channeling but when taking into account uncertainties in the relevant quenching factors, a dark matter candidate with a mass of approximately $\sim$7.0 GeV and a cross section with nucleons of $\sigma_{\rm DM-N} \sim 2 \times 10^{-40}\,{\rm cm}^2$ could account for both of these observations. We also compare the region of parameter space favored by DAMA/LIBRA and CoGeNT to the constraints from XENON 10, XENON 100, and CDMS (Si).

We proceed to make projections for the first full year of CoGeNT data, and for its planned upgrade. Not only will this body of data more accurately constrain the spectrum of nuclear recoil events, and corresponding dark matter parameter space, but will also make it possible to identify seasonal variations in the rate. In particular, if the CoGeNT excess is the product of dark matter, then one year of CoGeNT data will likely reveal an annual modulation with a significance of 2-3σ. The planned CoGeNT upgrade will not only detect such an annual modulation with high significance, but will be capable of measuring the energy spectrum of the modulation amplitude. These measurements will be essential to irrefutably confirming a dark matter origin of these events.

The CoGeNT collaboration then presented the results of their first 15 months of data, including the measurement of the spectrum of nuclear recoil candidate events, and the time variation of those events. These results appeared consistent with the signal anticipated from a relatively light dark matter particle scattering elastically with nuclei. We independently

analyze the data set collected by CoGeNT and explore the implications of these results for dark matter. We find that the observed spectrum and rate is consistent with originating from dark matter particles with a mass in the range of 4.5-12 GeV and an elastic scattering cross section with nucleons of approximately $\sim 10^{-40}$ cm^2. We confirm the conclusion of the CoGeNT collaboration that the data also includes a somewhat statistically significant (2.7σ) indication of annual modulation, with a phase, period, and amplitude consistent with that predicted for dark matter. CoGeNT's phase is also consistent with the annual modulation reported by the DAMA/LIBRA collaboration. We also discuss the null results reported by CDMS and XENON100, and comment on the prospects for other experiments to detect a dark matter particle with the properties implied by CoGeNT.

The first data release from the CRESST-II collaboration also reported signals which are not consistent with known backgrounds, but resemble that predicted for a dark matter particle with a mass of roughly $\sim$10 GeV and an elastic scattering cross section with nucleons of $\sim 10^{-41}$–10^{-40} cm^2. We compare the signals of all three experiments (DAMA/LIBRA, CoGeNT, and CRESST-II) and discuss whether they can be explained by a single species of dark matter particle, without conflicting with the constraints of other experiments. We find that the spectrum of events reported by CoGeNT and CRESST-II are consistent with each other and with the constraints from CDMS-II, although some tension with xenon-based experiments remains. Similarly, the modulation signals reported by DAMA/LIBRA and CoGeNT appear to be compatible, although the corresponding amplitude of the observed modulations are a factor of at least a few higher than would be naively expected, based on the event spectra reported by CoGeNT and CRESST-II. This apparent discrepancy could potentially be resolved if tidal streams or other non-Maxwellian structures are present in the local distribution of dark matter.

ACKNOWLEDGEMENTS

I owe many thanks to the following people:

My wife, Mindi, without whom I would have never finished (especially the references section)

My advisor Dan Hooper. It has been a great pleasure working with you and I especially want to thank you for helping me to find my love for physics again.

My committee: Juan Collar, Carlos Wagner, and Wendy Zhang for all their time and efforts.

Nobuko B. McNeil for all of her hard administrative work for me and all of the other physics students.

My collaborators, colleagues, and classmates at U of C and Fermilab.

Many of my professors and colleagues at CSM, especially Nathan Palmer, Bill Law, Tom Furtak, and Reuben Collins.

David Flammer for being a great friend for such a long time. We have been through so much together and I hope there is more to come.

Vince Kuo for being a great friend and helping me become a better teacher. I truely hope we will work together again as you are definitely one of my favorite people I have ever met.

All of my family and other friends for helping to make me the person I am as well as assisting and accompanying me along this journey.

Bob, for helping to keep me awake on those long physics nights.

LIST OF FIGURES

LIST OF TABLES

CHAPTER 1

INTRODUCTION

Although there exists an abundance of evidence that the vast majority of matter in our universe is non-baryonic and does not significantly emit, reflect, or absorb light, the nature of this dark matter remains unknown. Understanding the particle nature of dark matter is one of the most important outstanding problems in both cosmology and particle physics. We are currently experiencing what is arguably the most exciting time in the history of dark matter detection. The three main methods used to search for dark matter (direct detection, indirect detection, and colliders) have all reached a maturity level at which sensitivity is improving at a very rapid pace and is approaching theoretically relevant parameter space.

A wide variety of evidence supports dark matter's existence at many different distance scales. Zwicky's measurements of velocity dispersions in the Coma cluster led to the claim for the first time in 1933 that large quantities of non-luminous matter are required to be present to explain the motion of the galaxies in the cluster [1]. Additional observations on the scale of galactic clusters indicate the need for large amounts of dark matter [2]. In the bullet cluster, the locations of the baryonic matter (hot gas) and gravitational potential (as determined using X-ray observations and weak lensing), respectively are clearly spatially separated, giving very strong evidence for the presence of dark matter [3]. At galactic and sub-galactic scales, this evidence includes galactic rotation curves [4], and both weak [5] and strong [6] gravitational lensing. On cosmological scales, observations of the anisotropies in the cosmic microwave background by WMAP in conjunction with baryon acoustic oscillation data from the Sloan Digital Sky Survey have lead to a determination of the dark matter density of $\Omega_c h^2 = 0.1123 \pm 0.0035$ [7]. These same measurements, when combined with the

light chemical abundances predicted by big bang nucleosynthesis, find $\Omega_b h^2 = 0.02260 \pm 0.00053$ [8, 7]. The process of the formation of large scale structure is studied using N-body simulations of cold dark matter. These simulations produce filamentous structures that compare well with the observed structure in our universe seen in large scale surveys [9]. Hot dark matter, in contrast, underproduces the amount of large scale structure observed in our universe.

Although we have an overwhelming amount of evidence pointing towards gravitational interactions of dark matter, the particle nature of dark matter continues to be a mystery. Fig. 1.1 presents a schematic diagram of the different detection strategies that are currently being employed in the quest for dark matter discovery. Two legs of the diagram represent dark matter particles, while the other two legs represent some kind of Standard Model particles. The grey circle is some as yet to be determined interaction between the dark matter and the Standard Model particles. The three detection strategies differ in the red arrows that represent the flow of time. For indirect detection, we are searching for dark matter particles annihilating to produce Standard Model particles (time flows to the right). In colliders, standard model particles interact to produce dark matter particles (time flows to the left). Although the dark matter particles can not be measured by the detectors directly, their existence can be inferred by the subsequent Standard Model particles and missing momentum/energy coming from a collision. For direct detection, we are searching for an interaction of the dark matter particle with standard model particles directly, usually though a nuclear recoil caused by the scattering.

There are certainly many pros and cons to each of the three strategies. One universal theme is that understanding and eliminating backgrounds is where the vast majority of time and effort is spent. In many respects, the three strategies are complimentary. In fact, it is very likely that before the community accepts that particle dark matter has been discovered, at least two and probably all three of the strategies will have to be pointing to the same

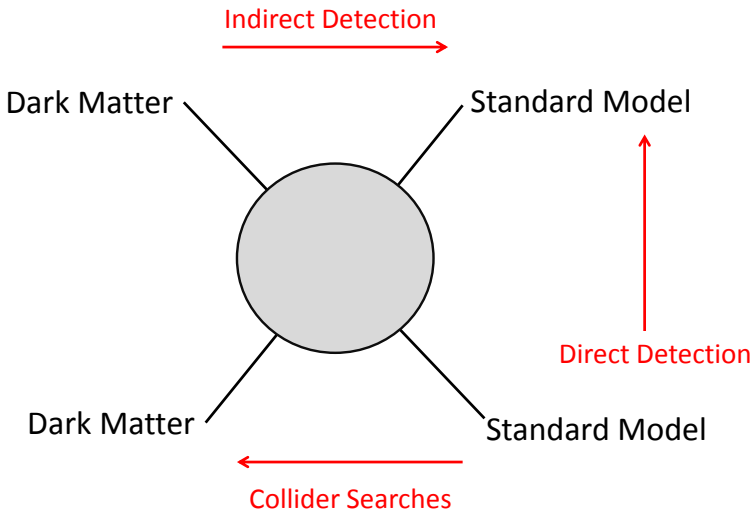

Figure 1.1: The three main detection strategies used to search for dark matter.

region of parameter space.

One of the most studied dark matter candidates are called Weakly Interacting Massive Particles (WIMPs). Many past, current, and planned experiments are searching for this particular type of dark matter. We will introduce some of the properties and motivatations for WIMPs in the next section.

1.1 Weakly Interacting Massive Particles (WIMPs)

Consider a stable particle, X, which interacts with Standard Model particles, Y, through some process $X\bar{X} \leftrightarrow Y\bar{Y}$. In the very early universe, when the temperature was much higher than m_X, the creation and annihilation processes of $X\bar{X}$ were equally efficient. This means X was present in large quantities with the other particles of the Standard Model in equilibrium with the photon thermal bath. As the temperature of the universe dropped below m_X, the process of $X\bar{X}$ creation became exponentially suppressed. The $X\bar{X}$ annihilations,

however, are not affected by the cooling of the thermal bath. If the particles remain in thermal equilibrium at temperatures $T \ll m_X$, then their number density is given by

$$n_{X,\,\mathrm{eq}} = g_X \left(\frac{m_X T}{2\pi}\right)^{3/2} e^{-m_X/T}, \tag{1.1}$$

where g_X is the number of internal degrees of freedom of X. If these particles were to remain in thermal equilibrium indefinitely, we see that their number density would quickly become increasingly suppressed as the universe cooled.

The exponential suppession of the number density of a particle species through self-annihilation can be interrupted by the competing effect of Hubble expansion. Once the universe expands to large enough size, the particles can not efficiently locate one another to annihilate. As the expansion and corresponding dilution of the particle increasingly dominates over the annihilation rate, the number density of X particles becomes sufficiently small that they cease to interact with each other, and thus survive to the present day. Quantitatively, the competing effects of expansion and annihilation are described by the Boltzmann equation:

$$\frac{dn_X}{dt} + 3Hn_X = - < \sigma_{X\bar{X}}|v| > (n_X^2 - n_{X,\,\mathrm{eq}}^2), \tag{1.2}$$

where n_X is the number density of WIMPs, $H \equiv \dot{a}/a = (8\pi^3\rho/3M_{\mathrm{Pl}})^{1/2}$ is the expansion rate of the universe, and $< \sigma_{X\bar{X}}|v| >$ is the thermally averaged $X\bar{X}$ annihilation cross section (multiplied by their relative velocity). The numerical solution for the Boltzmann equation is shown in Fig. 1.2.

As we see from Fig 1.2, the larger the thermally averaged annihilation cross section is, the longer the particle will track the equilibrium density, and the smaller its relic (final) comoving number density will be. The process of a particle species approaching a constant

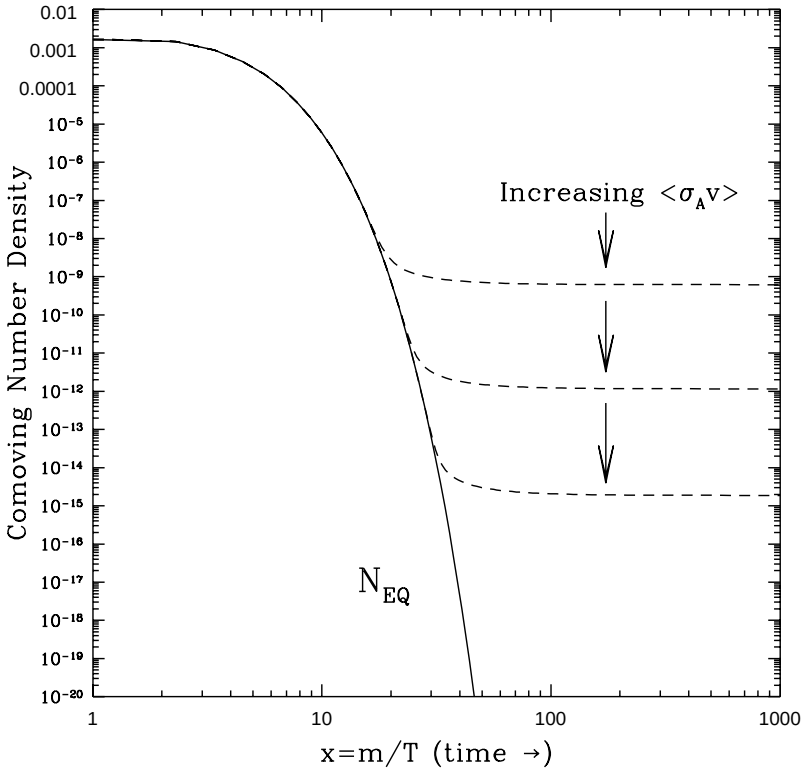

Figure 1.2: A schematic of the comoving number density of a stable species as it evolves through the process of thermal freeze-out [10].

comoving number density as the universe cools due to expansion is termed thermal freeze out.

Turning this argument around, a measurement of the relic (comoving) density of a particle species gives us insight into the annihilation cross section for that particle. If X has masses

in the GeV-TeV range, its relic abundance can be written as

$$\Omega_X h^2 \approx 0.1 \left(\frac{x_{\rm FO}}{20}\right)\left(\frac{g_\star}{80}\right)^{-1/2}\left(\frac{a+3b/x_{\rm FO}}{3\times 10^{-26}{\rm cm}^3/{\rm s}}\right)^{-1}, \tag{1.3}$$

where, $g_\star$ is the number of external degrees of freedom available (in the Standard Model, $g_\star \sim 120$ at $T \sim 1$ TeV and $g_\star \sim 65$ at $T \sim 1$ GeV), and a and b are terms in the non-relativistic expansion, $< \sigma_{X\bar{X}}|v| >= a + b < v^2 > +\mathcal{O}(v^4)$. We have also introduced the definition

$$x_{\rm FO} \equiv \frac{m_X}{T_{\rm FO}}\,, \tag{1.4}$$

with $T_{\rm FO}$ called the freeze-out temperature. This is the temperature when the annihilation rate is equal to the expansion rate, and the particle density starts to depart from its equilibrium value. In this mass range and for roughly weak-scale annihilation cross section, freeze-out occurs at $x_{\rm FO} \approx 20 - 30$.

Interestingly, the mass range and annihilation cross section necessary to produce the appropriate relic density for dark matter given by Eq. 1.3 is very similar to that for a generic weak-scale interaction. In particular, $\alpha^2/(100\,{\rm GeV})^2 \sim$ pb, which would give cross section (times c) $\sim 3 \times 10^{-26}$ cm^3/s. The similarly between this result and the value required to generate the observed quantity of dark matter is often referred to as the "WIMP miracle".

CHAPTER 2

THEORETICAL BACKGROUND

2.1 Introduction

The differential event rate (also referred to as energy spectrum) for the elastic scattering of dark matter with mass m_{DM} and a nucleus with mass m_N is given by

$$\frac{dR}{dE_r} = \frac{N_T\,\rho_{DM}}{m_{DM}} \int_{v_{min}} v f_E(\vec{v}) \frac{d\sigma}{dE_r}(v, E_r)\, d^3\vec{v}\,, \tag{2.1}$$

where N_T is the number of target nuclei per kilogram of the detector, ρ_{DM} is the local dark matter density, $\frac{d\sigma}{dE_r}(v, E_r)$ is the differential cross-section for the dark matter-nucleus elastic scattering , $\vec{v}$ is the velocity of the dark matter particle relative to the Earth, v_{min} is the minimum dark matter speed which can cause a recoil of energy E_R, and $f_E(\vec{v})$ is the the velocity distribution of the dark matter in the frame of the Earth (normalized to 1). We see that all dark matter particles with speeds above v_{min} will contribute to a signal at an energy E_r. This means that any strong features of the velocity distribution will be diluted to a certain degree by the integration, producing relatively smooth dark matter spectra.

In our galaxy, the dark matter-nucleon relative speed is of order 100 km/s, thus the elastic scattering occurs in the extreme non-relativistic limit and simple kinematics can be used to calculate the recoil energy of the nucleon in terms of the scattering angle (θ^*) in the center of mass frame:

$$E_r = \frac{\mu^2 v^2 (1 - \cos\theta^*)}{m_N}\,, \tag{2.2}$$

where we have introduced the dark matter-nucleus reduced mass,

$$\mu = \frac{m_{DM} m_N}{m_{DM} + m_N} \tag{2.3}$$

The lower limit of the integration over dark matter speeds in Eq. 2.1 is the minimum dark matter speed which can produce a recoil of energy E_r. This would correspond to the maximum momentum transfer to the nucleus, or $\theta^* = \pi$. Eq. 2.2 thus gives the minimum speed as

$$v_{min} = \sqrt{\frac{m_N E_r}{2\mu^2}}. \tag{2.4}$$

Within our galactic halo, the dark matter speeds are not expected to be arbitrarily large. The galactic escape velocity has recently been estimated to be 544 km/s[11]. When the Earth's motion is taken in to account, the minimum relative speed for a dark matter particle in our galaxy is thus likely to be $\sim$800 km/s. If a nuclear recoil of a given energy can be definitely identified as dark matter signal, then Eq. 2.4 with $v_{min}\sim$800 km/s provides a kinematic lower limit for the dark matter mass. Fig. 2.1 shows the minimum dark matter speed probed by some of the nuclear targets employed in current experiments near the current, low energy threshold of the detectors. We see that for low mass WIMPs ($\lesssim 10$ GeV), DAMA, CoGeNT and CRESST are all sensitive to similar velocity ranges. The current low energy threshold for the XENON100 collaboration, however, gives them no sensitivity to the low mass region. The collaboration has utilized statisitical techniques in their data analysis to try and extend their sensitivity to lower masses [12]. Uncertainties in their energy calibrations at lower energies, however, has led to debate about their conclusions in the low-mass region [13, 14].

Fig. 2.1 also shows that any potential signal coming from low-mass WIMPS in current detectors would be sourced exclusively by the high velocity tail of the dark matter dis-

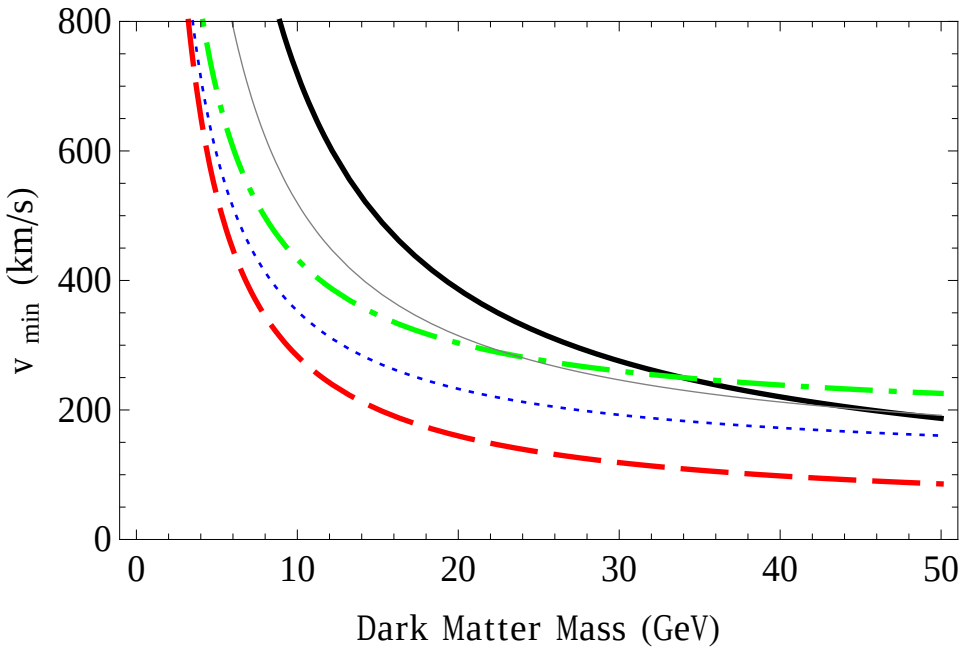

Figure 2.1: The minimum dark matter speed needed to produce a nuclear recoil (at the given threshold) for different dark matter masses. The thresholds for the different lines are as follows: sodium (blue,dotted) uses DAMA's 6 keV, the germanium (red,dashed) is 2 keV (CoGeNT and CDMS's low threshold analysis), xenon (black, thick) is 8 keV (XENON100), oxygen (green, dot-dashed) is 10 keV (CRESST II), and calcium (grey, thin) is also 10 keV (CRESST II).

tribution. This is the region of velocities where the dark matter distribution is the least well known. In particular, the departures from the standard assumptions about our halo (isotropic, Maxwell-Boltzman distribution) are expected to be greatest near the high veocity tail of the distribution (see, for example, Ref. [15] and references therein).

We see from Eq. 2.1, the expected signal at a direct detection experiment requires inputs from many different distance scales and areas of physics. The large distance scales of astrophysics play a role through ρ_{DM} and $f_E(\vec{v})$. We will find the intermediate distance scale of nuclear physics contributes through the form factors for the nuclear target. The fundamental particle physics is encoded in a dark matter-nucleus differential cross section. This cross section is calculated from an effective Lagrangian describing the interaction of

the particular dark matter candidate with quarks and gluons. Such a multi-scale problem leads to many potential areas where both experimental and theoretical uncertainties can be quite large or possibly even unknown. The following sections will describe the contribution of these inputs to the expected signal at a direct detection experiment.

2.2 Dark Matter Nucleus Scattering

The dark matter-nucleus cross section is typically separated into a spin-independent (scalar) and a spin-dependent contribution,

$$\frac{d\sigma}{dE_r} = \left(\frac{d\sigma}{dE_r}\right)_{SI} + \left(\frac{d\sigma}{dE_r}\right)_{SD} . \tag{2.5}$$

In general, the differential cross section is expressed as

$$\frac{d\sigma}{dE_r} = \frac{m_N}{2\mu^2 v^2}\left(\sigma_0^{SI} F^2(q) + \sigma_0^{SD} S(q)\right) , \tag{2.6}$$

where $\sigma_0^{SI,SD}$ are the spin-independent and spin-dependent cross sections at zero momentum transfer. The form factors, $F^2(q)$ and $S(q)$, describe the dependence on the momentum transfered to the nucleus, q. Dark matter-nucleus scatter occurs in the non-relativistic limit, so we can simpliy write $q = \sqrt{2m_N E_r}$. These functions account for the coherence loss as the momentum transfer is increased, which leads to a suppression in the event rate for higher recoil energies.

Additionally, one might consider non-trivial velocity or energy dependence for the scattering cross section coming from the dark matter sector. For example, the dark matter particle might have a "dark matter form factor," as commonly occurs in models of composite dark matter (see references 45-47 in [16]). A velocity dependence for the cross section might arise if the lowest order (isotropic, s-wave) scattering is suppressed. This work will not consider

these cases and will use the cross section as given by Eq. 2.6. The next two sections will provide a brief description of the particle and nuclear physics involved in determining the cross section. This will closely follow the discussion presented in [17].

2.2.1 Spin-independent contribution

Spin-independent contributions to the cross section may arise from scalar-scalar and vector-vector couplings in the Lagrangian:

$$\mathcal{L} \supset \alpha_q^S \bar{\chi}\chi\bar{q}q + \alpha_q^V \bar{\chi}\gamma_\mu\chi\bar{q}\gamma^\mu q\,. \tag{2.7}$$

The presence of these couplings depends on the particular particle physics model chosen for the dark matter candidate. In general one can write

$$\left(\frac{d\sigma}{dE_r}\right)_{SI} = \frac{m_N\sigma_0 F^2(E_r)}{2\mu^2 v^2}\,, \tag{2.8}$$

where the nuclear form factor, $F^2(E_r)$, is the Fourier transform of the nuclear charge density and has the effect of supressing the signal at large recoil energies (see Sec. 2.3).

The the scalar coupling leads to the following expression for the dark matter-nucleon cross section,

$$\sigma_0 = \frac{4\mu^2}{\pi}\left[Zf^p + (A-Z)f^n\right]^2\,, \tag{2.9}$$

with

$$\frac{f^p}{m_p} = \sum_{q=u,d,s}\frac{\alpha_q^S}{m_q}f_{Tq}^p + \frac{2}{27}f_{TG}^p\sum_{q=c,b,t}\frac{\alpha_q^S}{m_q}\,, \tag{2.10}$$

where the quantities f_{Tq}^p represent the contributions of the light quarks to the mass of the proton, and are defined as $m_p f_{Tq}^p \equiv \langle p|m_q\bar{q}q|p\rangle$. The second term is due to the interaction of dark matter and gluons through a colored loop diagram, with $f_{TG}^p = 1 - \sum_{q=u,d,s} f_{Tq}^p$. These

quantities are measured experimentally,

$$f_{Tu}^p = 0.020 \pm 0.004, \quad f_{Td}^p = 0.026 \pm 0.005, \quad f_{Ts}^p = 0.118 \pm 0.062, \tag{2.11}$$

with $f_{Tu}^n = f_{Td}^p$, $f_{Td}^n = f_{Tu}^p$, and $f_{Ts}^n = f_{Ts}^p$.

The vector coupling is only present in the case of a Dirac fermion but vanishes for Majorana particles. The sea quarks and gluons do not contribute to the vector current. This means that only valence quarks contribute, leading to the following expression

$$\sigma_0 = \frac{\mu^2 B_N^2}{64\pi}\,, \tag{2.12}$$

with

$$B_N \equiv \alpha_u^V (A + Z) + \alpha_d^V (2A - Z)\,. \tag{2.13}$$

For a general dark matter particle with both scalar and vector interactions, the spin-independent contribution to the scattering cross section can be written as

$$\left(\frac{d\sigma}{dE_r}\right)_{SI} = \frac{2\,m_N}{\pi v^2}\left[[Zf^p + (A-Z)f^n]^2 + \frac{B_N^2}{256}\right] F^2(E_r)\,. \tag{2.14}$$

Most direct detection experiments choose to parameterize the scalar part of the cross section instead in terms of a dark matter nucleon cross section (σ_n or σ_p)

$$\left(\frac{d\sigma}{dE_r}\right)_{SI} = \frac{m_N \sigma_i}{2v^2\mu_n^2}\,\frac{[Zf^p + (A-Z)f^n]^2}{f_i^2} F^2(E_r)\,, \tag{2.15}$$

where

$$\sigma_i = \frac{4\mu_i^2}{\pi} f_i^2\,, \tag{2.16}$$

with $(i = n)$ for the neutron, $(i = p)$ for the proton, and we have introduced the dark matter

nucleon reduced mass, μ_n. In most cases the dark matter coupling to neutrons and protons is assumed to be similar, $f^p \approx f^n$, and therefore the scalar contribution can be approximated by

$$\left(\frac{d\sigma}{dE_r}\right)_{SI} = \frac{m_N \sigma_i A^2}{2v^2 \mu_i^2} F^2(E_r). \tag{2.17}$$

The spin-independent contribution scales roughly as the square of the number of nucleons (A^2). This A^2 enhancement for spin-independent scattering has leFd many direct detection experiments to employ heavy targets (germanium, iodine, xenon, etc.) to try and boost a possible signal. Additionally, this A^2 dependence is a hallmark of SI dark matter scattering. A possible signal identified in two experiments with different target materials that displays the A^2 dependence would be strong evidence of spin-independent dark matter-nucleon scattering.

This work focuses primarily on spin-independent elastic scattering. However, for the sake of completeness, a brief discussion of spin-dependent scattering is included in the next section.

2.2.2 Spin-dependent contribution

The couplings of dark matter to the quark axial current, $\bar{q}\gamma_\mu\gamma_5 q$, produce the spin-dependent part of the dark matter-nucleus scattering cross section. For Fermionic dark matter, such as the lightest neutralino in supersymmetric models, the Lagrangian can contain the term

$$\mathcal{L} \supset \alpha_q^A (\bar{\chi}\gamma^\mu\gamma_5\chi)(\bar{q}\gamma_\mu\gamma_5 q)\,. \tag{2.18}$$

If the dark matter is a spin 1 field, as in the case of the lightest Kaluza-Klein particle, the interaction term takes the form,

$$\mathcal{L} \supset \alpha_q^A \epsilon^{\mu\nu\rho\sigma} (B_\rho \overset{\leftrightarrow}{\partial}_\mu B_\nu)(\bar{q}\gamma^\sigma\gamma_5 q)\,. \tag{2.19}$$

In both cases, the nucleus, N, matrix element can be written as

$$\langle N|\bar{q}\gamma_\mu\gamma_5 q|N\rangle = 2\lambda_q^N \langle N|J_N|N\rangle\,, \tag{2.20}$$

with λ_q^N relating the quark spin matrix elements to the angular momentum of the nucleons. These coefficients are often parametrized as

$$\lambda_q^N \simeq \frac{\Delta_q^{(p)}\langle S_p\rangle + \Delta_q^{(n)}\langle S_n\rangle}{J}\,, \tag{2.21}$$

where J is the total angular momentum of the nucleus, the quantities Δq^n are related to the matrix element of the axial-vector current in a nucleon, $\langle n|\bar{q}\gamma_\mu\gamma_5 q|n\rangle = 2s_\mu^{(n)}\Delta_q^{(n)}$, and $\langle S_{p,n}\rangle = \langle N|S_{p,n}|N\rangle$ is the expectation value of the spin content of the proton or neutron group in the nucleus . The total spin content in the proton and neutron groups is written as a sum over the quark contributions

$$a_p = \sum_{q=u,d,s} \frac{\alpha_q^A}{\sqrt{2}G_F}\Delta_q^p\,; \quad a_n = \sum_{q=u,d,s} \frac{\alpha_q^A}{\sqrt{2}G_F}\Delta_q^n\,. \tag{2.22}$$

Introducing the definition

$$\Lambda = \frac{1}{J}\left[a_p\langle S_p\rangle + a_n\langle S_n\rangle\right]\,, \tag{2.23}$$

Nucleus	Z	Odd Nuc.	J	$\langle S_p \rangle$	$\langle S_n \rangle$	$\frac{4\langle S_p \rangle^2 (J+1)}{3J}$	$\frac{4\langle S_n \rangle^2 (J+1)}{3J}$
^{19}F	9	p	1/2	0.477	-0.004	9.1×10^{-1}	6.4×10^{-5}
^{23}Na	11	p	3/2	0.248	0.020	1.3×10^{-1}	8.9×10^{-4}
^{27}Al	13	p	5/2	-0.343	0.030	2.2×10^{-1}	1.7×10^{-3}
^{29}Si	14	n	1/2	-0.002	0.130	1.6×10^{-5}	6.8×10^{-2}
^{35}Cl	17	p	3/2	-0.083	0.004	1.5×10^{-2}	3.6×10^{-5}
^{39}K	19	p	3/2	-0.180	0.050	7.2×10^{-2}	5.6×10^{-3}
^{73}Ge	32	n	9/2	0.030	0.378	1.5×10^{-3}	2.3×10^{-1}
^{93}Nb	41	p	9/2	0.460	0.080	3.4×10^{-1}	1.0×10^{-2}
^{125}Te	52	n	1/2	0.001	0.287	4.0×10^{-6}	3.3×10^{-1}
^{127}I	53	p	5/2	0.309	0.075	1.8×10^{-1}	1.0×10^{-2}
^{129}Xe	54	n	1/2	0.028	0.359	3.1×10^{-3}	5.2×10^{-1}
^{131}Xe	54	n	3/2	-0.009	-0.227	1.8×10^{-4}	1.2×10^{-1}

Table 2.1: Values of the atomic number Z, the total nuclear spin J, and the expectation values of the proton and neutron spins within the nucleus $\langle S_{p,n} \rangle$ for various nuclei with odd numbers of protons or neutrons, leading to the relative sensitivities to spin-dependent interactions shown, from Ref. [18].

the resulting differential cross section can then be expressed as

$$\left(\frac{d\sigma}{dE_r}\right)_{SD} = \frac{16 m_N}{\pi v^2} \Lambda^2 G_F^2 J(J+1) \frac{S(E_r)}{S(0)} \,. \tag{2.24}$$

Table 2.1 shows many of the nuclear properties relevant to spin-dependent direct detection experiments.

The form factor is typically decomposed into isoscalar, $a_0 = a_p + a_n$, and isovector, $a_1 = a_p - a_n$, couplings

$$S(q) = a_0^2 S_{00}(q) + a_0 a_1 S_{01}(q) + a_1^2 S_{11}(q) \,, \tag{2.25}$$

where the parameters S_{ij} are measured experimentally.

As we found in the previous section, the spin-independent contribution nuclear cross section scales roughly as the square of the number of nucleons (A^2). We have found in this

section, the spin-dependent cross section is instead proportional to a function of the nuclear angular momentum, $(J+1)/J$. Although in general both have to be taken into account, the scalar component dominates for heavy targets ($A > 20$). Nevertheless, dedicated experiments exist that are searching for spin-dependent dark matter coupling through the choice of targets with a large nuclear angular momentum, like flourine. Large volume detectors that contain large amounts of hydrogen (like Super Kamiokande and Ice Cube) can also search for spin-dependent dark matter interactions.

2.3 Form Factor

The form factor is typically a very important in nuclear scattering. When the momentum transfered to a nucleus during scattering is small, then the scattering is coherent, with each nucleon contributing. As the energy of the incoming particle is increased, however, the particle begins to resolve individual nucelons, and eventually the quark constituents. The form factor accounts for this loss of coherence and results in a supression of the scattering at higher energies.

The form factor is defined as the Fourier transform of the nuclear charge density

$$F(q) = \frac{1}{A(2\pi)^{3/2}} \int \rho(\vec{r}) e^{-i\vec{q}\cdot\vec{r}} d^3\vec{r}, \tag{2.26}$$

with $\rho(\vec{r})$ the charge density, A, the total charge of the nucleus, and $\vec{q}$ the momentum transfered during the scattering process. In direct detection experiments, the relative velocity between the dark matter and the nucleus are $\sim$100 km/s. In this extremely non-relativistic case, the magnitude of the transfered momentum can be be simply written as

$$q = \sqrt{2 m_N E_r} \tag{2.27}$$

with m_N the mass of the target nucleus.

Several different parameterizations of the form factor are commonly used. In this work we adopt the Helm form factor:

$$F(q) = \frac{3j_1(qR_1)}{qR_1}\ e^{-\frac{1}{2}q^2s^2}, \tag{2.28}$$

where j_1 is the second spherical bessel function and R_1 is given by

$$R_1 = \sqrt{c^2 + \frac{7\pi^2a^2}{3} - 5s^2}. \tag{2.29}$$

Here, $c \approx 1.23A^{1/3} - 0.60$ fm, $a \approx 0.523$ fm, and $s \approx 0.9$ fm having been determined by fits to nuclear physics data [19, 20, 21]. Fig. 2.2 plots the Helm form factor for three different target nuclei employed by current direct detection experiments. The plots show the form factor plays only a minor role for light nuclear targets. Many experiments, however, use heavy nuclei to take advantage of the anticipated A^2 enhancement for scalar, spin-independent dark matter-nuclear scattering. We see the loss of coherence at larger recoil energies encapsulated in the form factor will eventually overcome the A^2 enhancement. In fact, the form factor essentially sets an upper bound of $\sim$100 keV for xenon nuclear recoils.

2.4 The velocity integral

The majority of current direct detection experiments are seaching for elastic, spin-independent scattering between the dark matter particle and the target nucleus. In this case, Eqs. 2.1 and 2.15 can be used to write the spectrum of nuclear recoil events as

$$\frac{dR}{dE_r} = \frac{N_T\rho_{DM}m_N}{2m_{DM}\mu_n^2}\,\frac{\left[f_pZ + f_n(A-Z)\right]^2}{f_i^2}\sigma_i\,F^2(q)g(v_{min})\,, \tag{2.30}$$

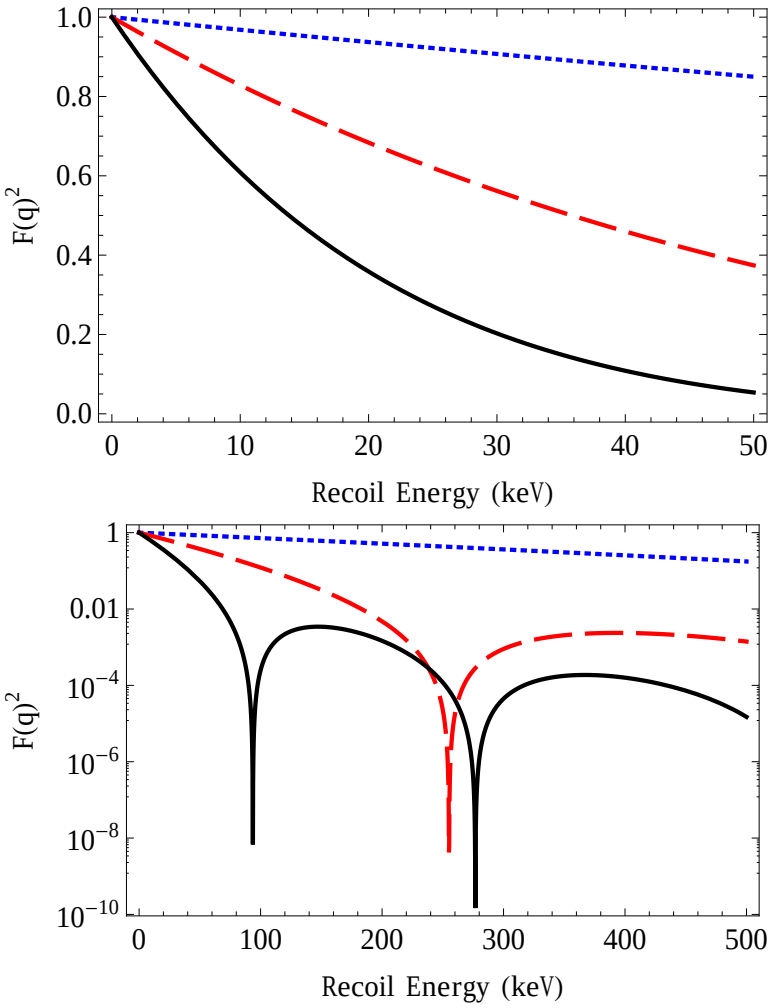

Figure 2.2: The Helm form factor adopted in these calculations for three nuclear targets in current direct detection experiments: blue (dotted) is sodium, red (dashed) is germanium, and black (solid) is xenon. The upper frame shows the form factor over a nuclear recoil range relevant for direct detection experiments, while the lower frame provides a wider energy range for comparison.

where N_T is the number of target nuclei per kilogram of the detector, m_N is the mass of the target nucleus, ρ_{DM} is the local dark matter density, m_{DM} is the dark matter mass, μ_n is the reduced mass of the dark matter particle and nucleon (proton or neutron), Z and A are the atomic and mass numbers of the nucleus, $F(q)$ is the nuclear form factor (see Sec. 2.3), and $f_{n,p}$ are the coupling strengths of the dark matter particle to neutrons and protons,

respectively. The signal can be written in terms of the dark matter scattering cross section with either the neutron ($i = n$) or proton ($i = p$). All of the dependence on the velocity distribution of the dark matter is collected in the phase-space integral

$$g(v_{min}) = \int_{v>v_{min}} \frac{1}{v} f_e(\vec{v}, t) d^3\vec{v} = \int_{v>v_{min}} \frac{1}{v} f(\vec{v} + \vec{v}_e(t)) d^3\vec{v}. \tag{2.31}$$

In the above expression, f_e represents the velocity distribution of the dark matter in the frame of the Earth, f is the velocity distribution in the galactic halo's rest frame, $\vec{v}$ is the velocity of the dark matter particle relative to the Earth, and $\vec{v}_E(t)$ is the velocity of the Earth in the halo's rest frame. We also recall $v_{min} \sim \sqrt{E_r}$, as given in Eq. 2.4.

The motion of the Earth through the halo will result in a direct detection experiment experiencing a time-dependent "wimp wind" striking the detector. The time scale for the orbital motion of the Earth is many orders of magnitude below the time scale for changes in the galactic dark matter distribution. This means that f can be considered to be time independent over the lifetime of any dark matter direct detection experiment. The second integral expression above highlights this fact with the only time dependence coming from $\vec{v}_e(t)$.

Additionally, the length scale for the earth's orbital motion is also expected to be many orders of magnitude below the length scale for spatial variations of the distribution of dark matter. For this reason, the velocity distribution is expected to be spatially uniform on the scale of the solar system. In the following sections we will introduce velocity distributions that are commonly utilized in dark matter literature and discuss the annual modulation induced by the orbital motion of the earth.

2.4.1 The Orbital Motion of the Earth

The net motion of the Earth through the galaxy should induce an annual modulation of a dark matter signal in a direct detection experiment. This section presents the relevant velocities needed to predict the effects of the orbital motion of the Earth on a dark matter signal following a discussion similar to that presented in Ref. [22]. Throughout this section, when explicit vectors are given, they use a coordinate system with the first unit vector towards the Galactic Center, the second unit vector in the direction of disk rotation, and the third unit vector towards the North Galactic Pole.

In the galactic halo's rest frame, the net motion of the earth can be written as

$$\vec{v}_e(t) = \vec{v}_\odot + v_\oplus \left[\hat{\boldsymbol{\varepsilon}}_1 \cos\{\omega(t-t_1)\} + \hat{\boldsymbol{\varepsilon}}_2 \sin\{\omega(t-t_1)\}\right] \tag{2.32}$$

In this expression, $\vec{v}_\odot$ is the motion of the sun, $v_\oplus = 29.8\,\mathrm{km/s}$ is the orbital speed of the Earth, $\hat{\boldsymbol{\varepsilon}}_1$ and $\hat{\boldsymbol{\varepsilon}}_2$ are the direction of the Earth's orbital motion around the sun at the Spring equinox ($t_1 = 80$, March 21) and Summer solstice, respectively. The sun's motion around the galaxy is typically further broken down into the motion of the local standard of rest and it's peculiar velocity

$$\vec{v}_\odot = \vec{v}_{LSR} + \vec{v}_{pec}, \tag{2.33}$$

with $\vec{v}_{LSR} = (0, v_0, 0)$ and $\vec{v}_{pec} = (10, 13, 7)\,\mathrm{km/s}$. The unit vectors defining the orbital motion of the earth are given by

$$\hat{\boldsymbol{\varepsilon}}_1 = (0.9931, 0.1170, -0.01032)\,, \tag{2.34}$$

$$\hat{\boldsymbol{\varepsilon}}_2 = (-0.0670, 0.4927, -0.8676)\,. \tag{2.35}$$

The time dependence of the speed of the earth can be written in terms of a single cosine

function

$$v_e(t) = \sqrt{v_\odot^2 + v_\oplus^2 + 2\,b\,v_\odot v_\oplus \cos\{\omega(t - t_m)\}} \tag{2.36}$$

with t_m the time when the Earth's speed is maximized. The time is found using

$$\cos\{\omega(t_m - t_1)\} = \frac{b_1}{b}\,, \quad \sin\{\omega(t_m - t_1)\} = \frac{b_2}{b}\,. \tag{2.37}$$

where $b_i \equiv \hat{\boldsymbol{\varepsilon}}_i \cdot \hat{v}_\odot$ and $b = \sqrt{b_1^2 + b_2^2}$. Using the typical value of $v_0 = 220\,\mathrm{km/s}$, we find that $b = 0.49$ and the time when the Earth's speed is maximized is $t_c = 152\,\mathrm{days}$ (June 1). As we will see in the next section, this is also the time that the dark matter signal from a Maxwellian halo is expected to be maximized.

2.4.2 Standard Halo Model (SHM)

This is the velocity distribution that is most commonly employed when analyzing direct detection data. Dark matter is assumed to be uniformly distributed throughout an isothermal sphere. The velocity distribution for this Standard Halo Model (SHM) is

$$f_{SHM}(\vec{u}) = \begin{cases} \frac{1}{N v_0^3 \pi^{3/2}} e^{-u^2/v_0^2}, & \text{if } u < v_{esc} \\ 0, & \text{otherwise.} \end{cases} \tag{2.38}$$

with $\vec{u}$ the velocity of the dark matter particles (in the halo rest frame), v_{esc} the escape velocity of the galaxy, and N the normalization constant given by

$$N = \mathrm{erf}\left(\frac{v_{esc}}{v_0}\right) - \frac{2 v_{esc}}{v_0\sqrt{\pi}} e^{-v_{esc}^2/v_0^2}, \tag{2.39}$$

which ensures that $\int f(\vec{u}) d^3\vec{u} = 1$. The velocity dispersion (v_0) is the most likely speed for a dark matter particle with this velocity distribution.

Substituting this distribution into Eq. 2.31 gives

$$g_{SHM}(v_{min}, v_e) = \begin{cases} g_l(v_{min}, v_e), & \text{if } v_{min} < v_{esc} - v_e, \\ g_h(v_{min}, v_e), & \text{if } v_{esc} - v_e < v_{min} < v_{esc} + v_e, \\ 0 & \text{if } v_{min} > v_{esc} + v_e, \end{cases} \tag{2.40}$$

with

$$g_l(v_{min}, v_e) = \frac{\text{erf}\left(\frac{v_e + v_{min}}{v_0}\right) + \text{erf}\left(\frac{v_e - v_{min}}{v_0}\right)}{2Nv_e} - \frac{2}{Nv_0\sqrt{\pi}} e^{-\frac{v_{esc}^2}{v_0^2}} \tag{2.41}$$

$$g_h(v_{min}, v_e) = \frac{\text{erf}\left(\frac{v_{esc}}{v_0}\right) + \text{erf}\left(\frac{v_e - v_{min}}{v_0}\right)}{2Nv_e} - \frac{(v_{esc} + v_e - v_{min})}{Nv_e v_0\sqrt{\pi}} e^{\frac{-v_{esc}^2}{v_0^2}}. \tag{2.42}$$

The expression for g in Eq. 2.40 is used in Eq. 2.30 to calculate the signal expected in a germanium detector and is shown as the solid line in Fig. 2.3. When giving scientific talks, many dark matter direct detection collaborators often state that they are searching for a "featureless exponential" signal. As is evident by the best fit exponential also plotted in Fig. 2.3, an exponential does indeed provide a good description of the expected signal. This work, however, uses the expressions in Eq. 2.40 rather than an exponential. As we will see below, these analytic expressions are especially useful when trying to calculate the expected modulation signals due to the orbital motion of the Earth.

The orbital motion of the Earth is a relatively small perturbation of its overall galactic motion $\mathcal{O}(v_\oplus/v_\odot)$. The expression for the Earth's speed given in Eq. 2.32 can be used to expand Eqs. 2.41 and 2.42 with respect to the small parameter $\varepsilon \equiv v_\oplus/v_\odot = 0.13$, for $v_0 = 220\,\text{km/s}$. We find

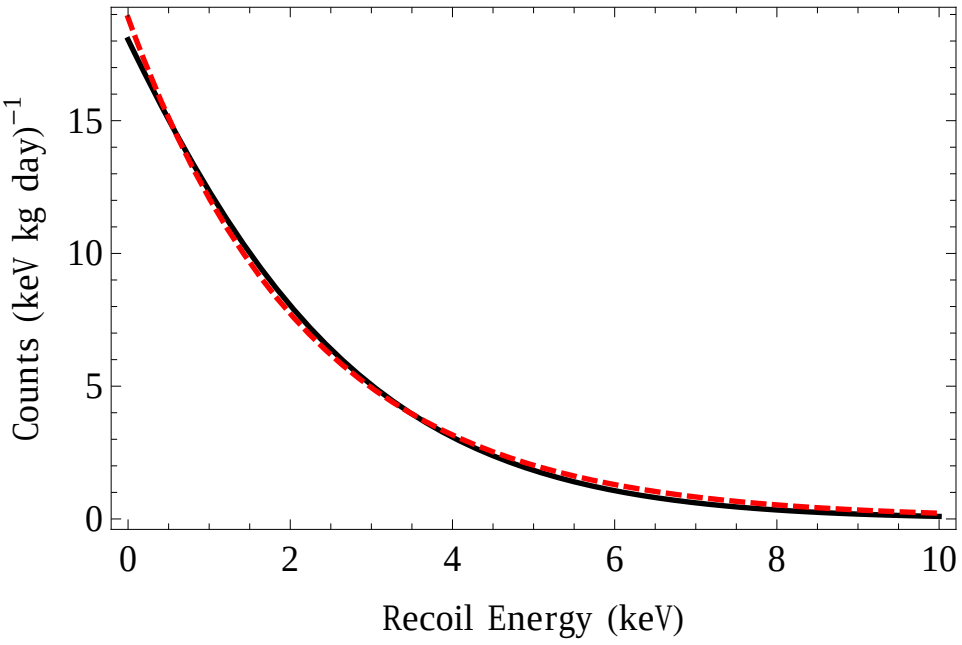

Figure 2.3: The solid line shows the spectrum in a germanium detector for a dark matter particle with a mass of 10 GeV and spin-independent, elastic scattering cross section with nucleons of $10^{-40}\,\mathrm{cm}^2$ from the SHM with $v_0 = 220\,\mathrm{km/s}$ and $v_{\mathrm{esc}} = 544\,\mathrm{km/s}$. The dashed line is the best fit exponential for this spectrum.

$$\widetilde{g}_l(v_{min}, t) = A_0(v_{min}) + A_1(v_{min}) \cos\left[\omega\,(t - t_m)\right] \tag{2.43}$$

$$\widetilde{g}_h(v_{min}, t) = B_0(v_{min}) + B_1(v_{min}) \cos\left[\omega\,(t - t_m)\right]. \tag{2.44}$$

The above approximations introduce the following definitions

$$A_0(v_{min}) = g_l(v_{min}, v_\odot) + \frac{\varepsilon^2}{2}\left[h(v_{min} - v_\odot, v_{min} + v_\odot) - g_l(v_{min}, v_\odot)\right] + \mathcal{O}(\varepsilon^4) \tag{2.45}$$

$$A_1(v_{min}) = \varepsilon\, b\, \left[h(v_{min} - v_\odot, v_{min} + v_\odot) - g_l(v_{min}, v_\odot)\right] + \mathcal{O}(\varepsilon^3) \tag{2.46}$$

$$B_0(v_{min}) = g_h(v_{min}, v_\odot) + \frac{\varepsilon^2}{2}\left[h(v_{min} - v_\odot, v_{esc}) - g_h(v_{min}, v_\odot)\right] + \mathcal{O}(\varepsilon^4) \tag{2.47}$$

$$B_1(v_{min}) = \varepsilon\, b\, \left[h(v_{min} - v_\odot, v_{esc}) - g_h(v_{min}, v_\odot)\right] + \mathcal{O}(\varepsilon^3) \tag{2.48}$$

$$h(v_1, v_2) = \frac{e^{-v_1^2/v_0^2} + e^{-v_2^2/v_0^2} - 2e^{-v_{esc}^2/v_0^2}}{N\sqrt{\pi}v_0} \tag{2.49}$$

We can see from the expansions for g_{SHM} in Eqs. 2.43 and 2.44, the velocity integral for a Maxwellian halo will typically have a sinusoidal annual modulation. The velocity integral modulation amplitude for the Maxwellian halo is plotted in Fig. 2.4. The actual signal measured in a direct detection experiment is proportional to this function times the form factor, as given by Eq. 2.30. The form factor is time independent and thus will not introduce additional time variation. The form factor leads to supression of the event rate for large recoil energies. For light targets such as sodium, this supression is quite small. For larger targets, the effects of the form factor will also be relatively small if the dark matter is light. In the case of large dark matter masses, however, the effect can be more significant. For example, in the limit of large dark matter mass, a xenon target will have any modulation above $\sim$200 km/s effectively cut off by the form factor supression. When viewing any figure plotting the the velocity integral (or its modulation), one must keep in mind the additional form factor supression that may be present in the actual signal expected at a direct detection experiment.

From the inset, we see that the fractional modulation increases to 100% as v_{min} increases. This fact is due to the presence of the galactic escape velocity, which sets a maximum speed for the dark matter particles. In the summer (at t_m), the Earth has its largest speed relative

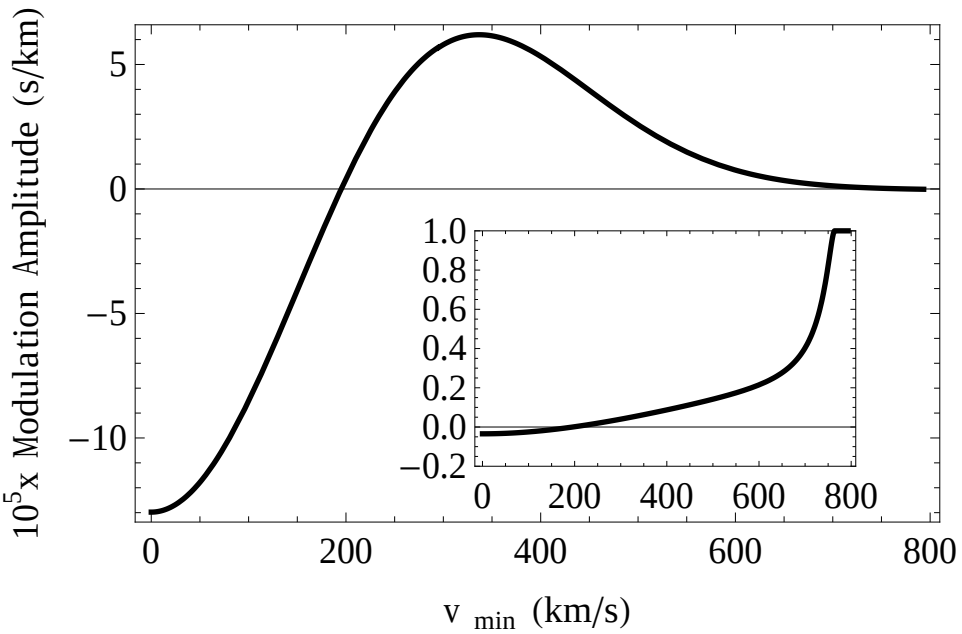

Figure 2.4: The modulation amplitude for g_{SHM} as given by A_1 and B_1 in Eqs. 2.46 and 2.48 for $v_0 = 220\,\mathrm{km/s}$ and $v_{esc} = 544\,\mathrm{km/s}$. The actual modulation measured in a direct detection experiment is proportional to this function times the form factor. A large dark matter mass and large nuclear target mass would lead to a supression of the signal at high speeds from the form factor. The inset shows the fractional modulation for this situation.

to the WIMP wind. This occurs when the component of the earth's orbital motion along the direction of the sun's galactic motion is maximized. Alternatively, in the winter, this component is minimized, producing a lower effective escape velocity. This means that there is a region in v_{min} space that is populated by dark matter in the summer and completely depopulated of dark matter in the winter, resulting in the 100% modulation. Although the fractional modulation is very large in this case, the signal itself is becoming vanishingly small because there are not very many particles in the high velocity tail of a Maxwellian halo.

As mentioned in the previous section, we find that a dark matter signal will be maximimized or minimized at t_m depending on the sign of A_1 or B_1. Another interesting feature of Fig. 2.4 to note is the modulation vanishes for a particular value of v_{min}. Above this value of v_{min} a dark matter signal would have a maxima at t_m (see Eq. 2.37), whereas the signal

is minimized at t_m for v_{min} below this critical value.

The value of v_{min} where the phase flip occurs will be the solution of $A_1 = 0$ if $v_{min} < v_{esc} - v_e$ or the solution of $B_1 = 0$, otherwise. The equations must be solved numerically and will depend on the value of v_0. Interestingly, A_1 has no v_{esc} dependence, while there is a slight v_{esc} dependence for the B_1 solutions. Fig. 2.5 plots the solutions as a function of v_0 for three different values for v_{esc}.

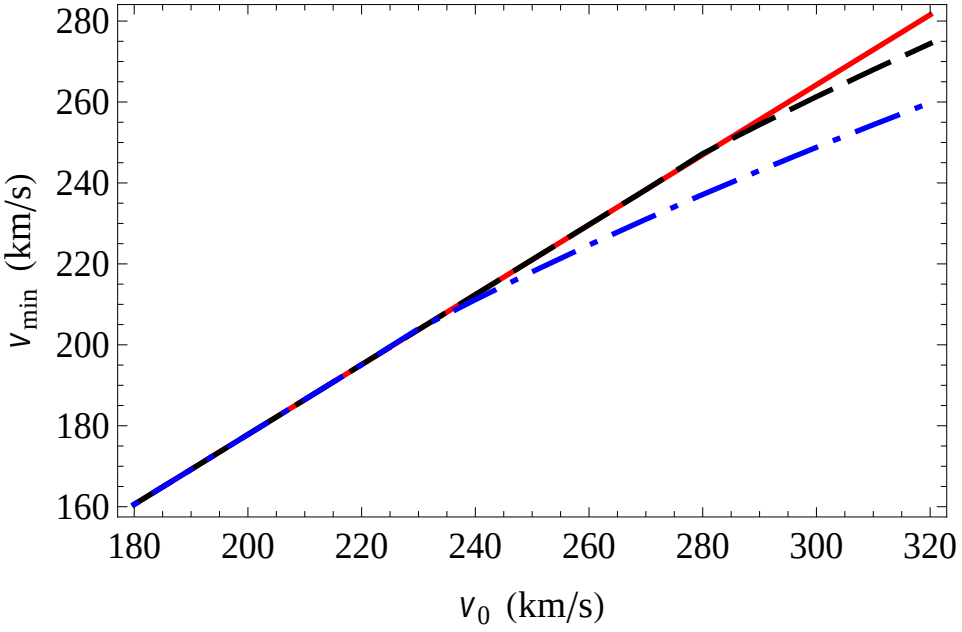

Figure 2.5: The value of v_{min} where the modulation of a dark matter signal should vanish and the phase flip occurs. Above this value the modulation's maximum phase occurs at t_m (June 1), whereas below this value the modulation will have its minimum phase at t_m. The three lines show the slight v_{esc} dependence with the red (solid) line $v_{esc} = 650\,\mathrm{km/s}$, the black (dashed) line $v_{esc} = 544\,\mathrm{km/s}$, and the blue (dot-dashed) line $v_{esc} = 450\,\mathrm{km/s}$.

Measuring the recoil energy where this phase flip occurs gives a direct measure of the dark matter mass through $v_{min} = \sqrt{\frac{E_r m_N}{2\mu^2}}$. Fig. 2.6 shows the recoil energy where this phase change would occur for various target nuclei that are employed by current direct detection experiments using the current best measurements of $v_0 = 220\,\mathrm{km/s}$ and $v_{esc} = 544\,\mathrm{km/s}$. Unfortunately, we see that to measure this phase change for low mass WIMPs requires

detector thresholds well below 5 keV independent of target nucleus. On the other hand, for dark matter of masses larger than 50 GeV, current detector thresholds are sufficient to measure the phase flip.

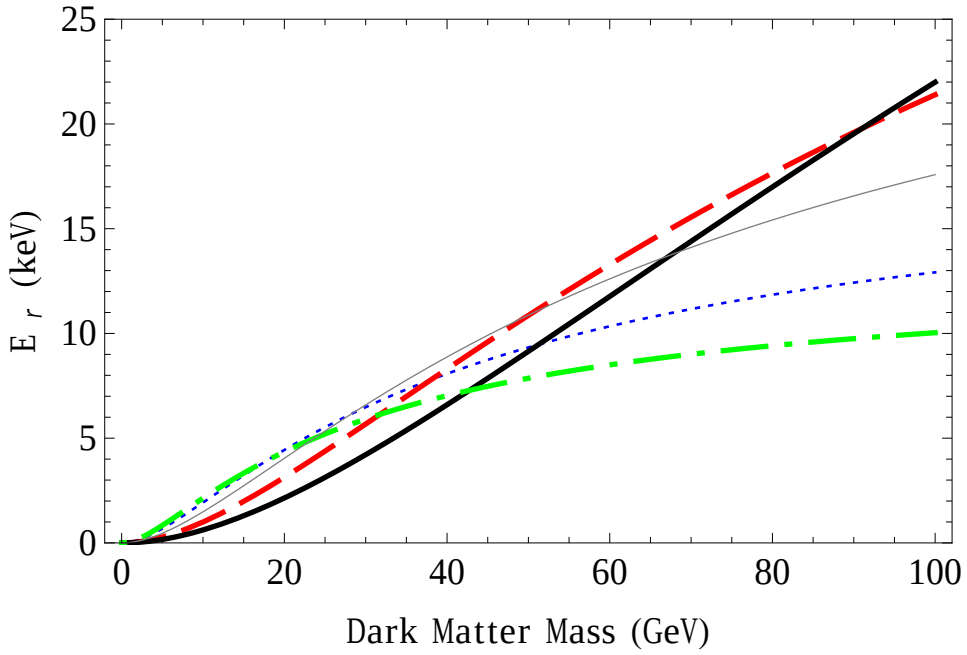

Figure 2.6: The recoil energy where the annual modulation phase change would occur for various target nuclei for $v_0 = 220\,\mathrm{km/s}$ and $v_{esc} = 544\,\mathrm{km/s}$. The target materials shown are: sodium (blue,dotted), germanium (red,dashed), xenon (black, thick), oxygen (green, dot-dashed) and calcium (grey, thin).

2.4.3 Velocity Streams

Numerical simulations of the formation and evolution of Milky Way-like dark matter halos have become increasingly sophisticated in recent years. These simulations find that although simple halo models with Maxwellian distributed velocities are likely to represent a reasonable zeroth order description of the distribution of dark matter in our galaxy, significant departures from such models are expected [23, 24, 25, 26].

When considering relatively light dark matter particles, as we are in this paper, the

behavior of the velocity distribution near the escape velocity of the galaxy is of particular importance. In order to produce a measurable nuclear recoil, a low-mass dark matter particles requires greater speeds than would be necessary for a heavier particle. As a result, a detector may only be sensitive to the high velocity tails of the dark matter distribution, where departures from Maxwellian behavior are expected to be most significant [15].

Small-scale structure of the Milky Way's halo can also play an important role in interpreting signals from direct detection experiments. The dark matter halo of our galaxy formed through a sequence of mergers of many smaller halos; a process known as hierarchial structure formation. High resolution simulations have found that many smaller halos survive this process and remain intact today, residing as substructures within larger halos [27, 23, 28, 29, 30]. Furthermore, many of these subhalos have a great deal of their outer mass stripped, resulting in the formation of cold tidal streams. These streams have a localized dark matter distribution with a collective flow in the direction of motion of the subhalo.

The presence of such streams in or around the Solar System would introduce departures from the Maxwellian velocity distribution. While such streams could potentially effect the spectrum of dark matter-induced events that are observed in direct detection experiments [31, 32], these effects are often far more pronounced in the modulation signals of such experiments [33]. The presence of such streams can significantly enhance a modulation signal, as well as shift the phase of the modulation relative to that predicted in more simple halo models [34, 22, 33, 35].

A stream with a non-zero velocity dispersion will have a velocity distribution very similar to a Maxwellian halo. The velocity dispersion for streams found in N-body simulations are typically fairly small, $v_{0s} \sim 20\,\mathrm{km/s}$ [33]. The dark matter particles in streams are not necessarily bound to the galaxy and thus are also not a priori required to have speeds below the galactic escape velocity. For this reason, and for the ease of calculation, the upper limit

for dark matter speeds in a stream can be effectively taken to be infinite. The only additional change is the Gaussian is now centered around $\vec{v}_{str}$ rather than zero:

$$f_{str}(\vec{u}) = \frac{1}{v_0^3 \pi^{3/2}} e^{-|\vec{u}-\vec{v}_{str}|^2/v_{0s}^2}. \tag{2.50}$$

The velocity integral can then be easily computed using Eq. 2.40 in the limit $v_{esc} \to \infty$ and with the replacement $v_e \to |\vec{v}_e - \vec{v}_{str}| \equiv v_{e,str}$. The resulting expression is

$$g_{stream}(v_{min}) = \frac{1}{2v_{e,str}} \left[\text{erf}\left(\frac{v_{e,str} + v_{min}}{v_{0s}} \right) + \text{erf}\left(\frac{v_{e,str} - v_{min}}{v_{0s}} \right) \right], \tag{2.51}$$

with $v_{e,str}$ the speed of the earth relative to the stream. This speed is related to the stream speed in the halo's rest frame (v_{str}) by

$$v_{e,str}^2 = v_e^2 + v_{str}^2 - 2\vec{v}_e \cdot \vec{v}_{str} \tag{2.52}$$

One additional case to consider is a stream with essentially no dispersion. This corresponds to the case of $v_{0s} \to 0$, and the velocity distribution in the halo rest frame is $\propto \delta^3(\vec{v} - \vec{v}_{str})$. The velocity integral can again be easily calculated using Eq. 2.51 in the limit $v_{0s} \to 0$. In this limit, we find

$$g_\delta(v_{min}) = \frac{1}{v_{e,str}} \theta(v_{e,str} - v_{min}). \tag{2.53}$$

Fig. 2.7 plots the velocity integral for several different stream configurations. We see the presence of a non-zero dispersion acts to soften the hard cut-off of a dispersionless stream. The plot also shows the time dependence of the cut-off coming from the time dependence of v_e in Eq. 2.52.

The time dependence of the signal can be found using similar logic as when finding the time dependence of the Earth's motion in the halo rest frame (see Sec. 2.4.1). The process

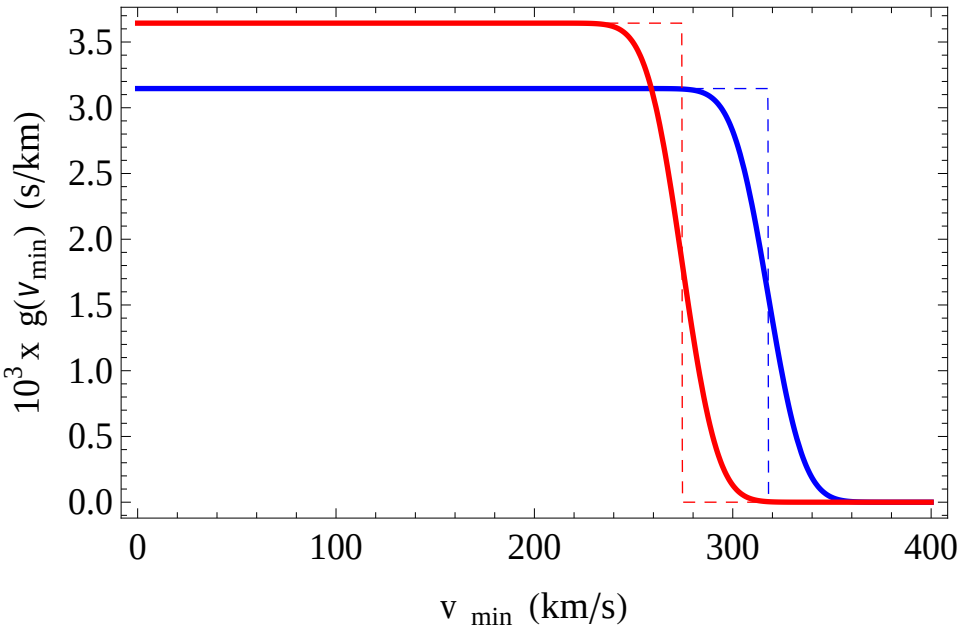

Figure 2.7: The velocity integral for a stream with the maximum speed relative to the earth (at $t_{m,str}$) are shown in blue. The red lines show the velocity integral when the speed is minimized (at $t_{m,str} + 365/2$). The dashed (solid) lines correspond to a dispersion of $0\,(20)$ km/s.

will be exactly the same with only the replacement $\vec{v}_\odot \to \vec{v}_\odot - \vec{v}_{str} \equiv \vec{v}_{\odot,str}$ with $\vec{v}_{\odot,str}$ being the velocity of the sun relative to the stream. We thus find

$$v_{e,str}(t) = \sqrt{v_{\odot,str}^2 + v_\oplus^2 + 2\,b_{str}\,v_{\odot,str} v_\oplus \cos\{\omega(t - t_{m,str})\}} \tag{2.54}$$

with $t_{m,str}$ the time when the Earth's speed relative to the stream is maximized. This time is found using

$$\cos\{\omega(t_{m,str} - t_1)\} = \frac{b_{1,str}}{b_{str}}\,, \quad \sin\{\omega(t_{m,str} - t_1)\} = \frac{b_{2,str}}{b_{str}}\,. \tag{2.55}$$

where $b_{i,str} \equiv \hat{\boldsymbol{\varepsilon}}_i \cdot \hat{v}_{\odot,str}$ and $b_{str} = \sqrt{b_{1,str}^2 + b_{2,str}^2}$. As there is no a priori reason why the stream should point in any particular direction, the time when the Earth's speed is maximized relative to the stream can happen at any time during the year.

The annual modulation behavior for a stream can be understood using Fig. 2.7. At low values of v_{min}, the modulation will be negative and relatively small $\mathcal{O}(\frac{v_\oplus}{v_{\odot,str}^2})$. This is of similar magnitude to the modulation of the Maxwellian halo. For values of v_{min} above the low velocity cut-off at $v_{e,str}(t_{m,str} + 365/2)$, there will be part of the year when there are no dark matter particles with enough energy to create detectable nuclear recoils. For these values of v_{min}, the modulation is now $\mathcal{O}(\frac{1}{v_{\odot,str}})$. In this region of v_{min} space, a signal is not scaled down by the additional factor $\mathcal{O}(\frac{v_\oplus}{v_{\odot,str}})$. The annual modulation signal for a stream will thus have a large peak in the range $v_{e,str}(t_{m,str})$ to $v_{e,str}(t_{m,str} + 365/2)$.

The modulation signal as described above is shown in Fig. 2.8 as the blue, dashed line. This stream has only 5% of the dark matter density compared to the Maxwellian halo shown as the red, solid line. We see that even though the stream has much lower density than the halo, it can still have a profound effect on the annual modulation signal.

In Fig. 2.9 the same scenario is plotted showing the non-modulating part of the signal. In this plot we see the stream creates only a very small perturbation above the signal from the Maxwellian halo at low values of v_{min}. This is in stark contrast to the drastic effect the signal has on the modulating part of the signal shown in Fig. 2.8. A strong effect on the annual modulation signal with relatively little effect on the non-modulating part of the signal is one of the most important features of a stream.

The cut-off in v_{min} space for a stream will translate into a cut-off in the recoil energy for an experiment at $E_{cut} = \frac{2\mu^2 v_{cut}^2}{m_N}$. This is a purely kinematical cut-off, and will thus occur independent of the nature of the scattering, as long as it is elastic. The true cut-off occurs in v_{min} space, which leads to the interesting effect that the energy cut-off will occur at different energies in different detectors. The relationship between the energy cut-off in the two experiments will be

$$E_{co,2} = \frac{\mu_2^2 m_{N_1}}{\mu_1^2 m_{N_2}} E_{co,1} \tag{2.56}$$

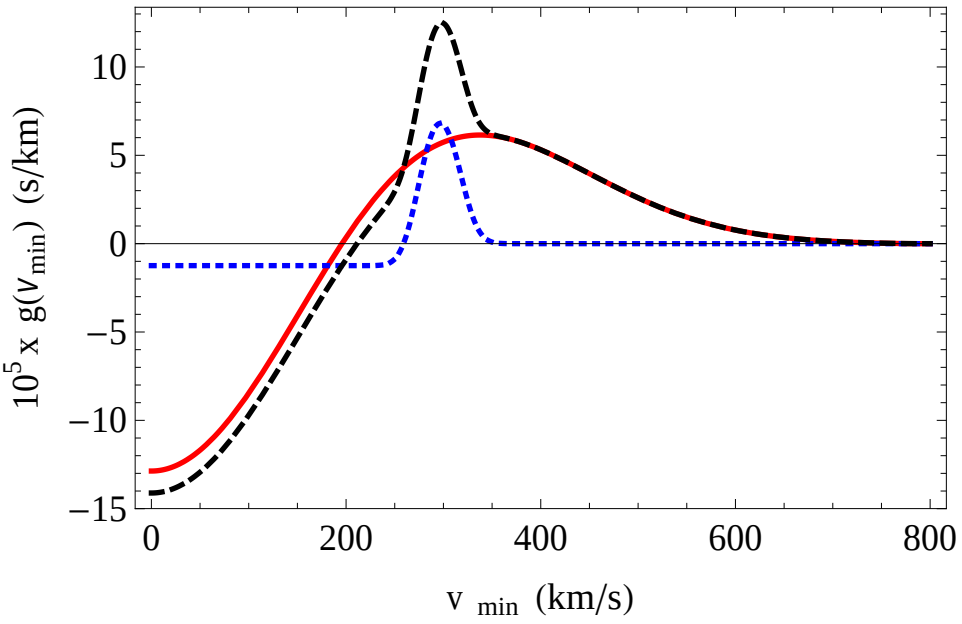

Figure 2.8: The effect of a stream with 5% of the density of dark matter in the Maxwellian halo on the modulation amplitude of the velocity integral. The stream was deliberately chosen to enhance the Maxwellian halo's modulation by making the stream's velocity point opposite to that of the Earth's orbital velocity at t_m. The stream speed is 100 km/s in the halo's rest frame and has a dispersion of 20 km/s. The solid red line shows the modulation for the Maxwellian halo, the dotted blue line the stream, and the black dashed line the halo + stream.

The idea that the same features in v_{min} space will occur at different energies in different experiments will be extended in Sec. 2.4.5 to develop a technique to make comparisons between two experiments independent of the dark matter's velocity distribution.

As we saw above, the presence of a stream is much easier to detect by searching for a peak in the annual modulation signal. If a stream is able to be detected by two experiments using different targets masses, then the relationship in Eq. 2.56 can given an independent measure of the mass of the dark matter particle. As difficult as these direct detection experiments are to execute, the more independent checks that we have, the better.

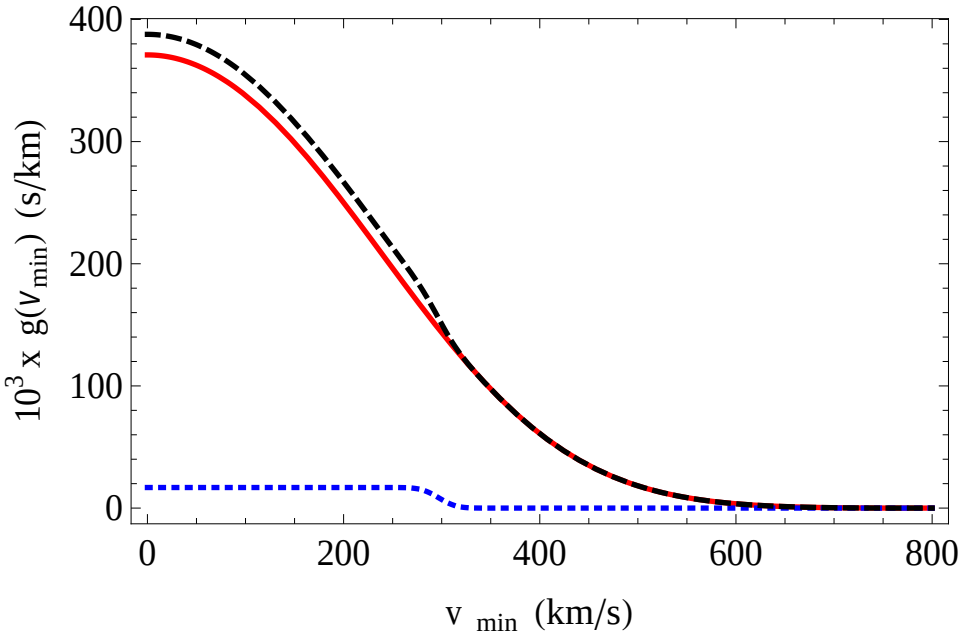

Figure 2.9: The same situation as in Fig. 2.8 but now plotting the average signal (nonmodulating part).

2.4.4 Debris Flow

Another type of substructure expected to be present in the galactic halo that has generated recent interest is termed debris flow [36]. Unlike a stream that is spatially localized, debris flow is relatively spatially homogeneous, but still retains velocity substructure distinct from the host halo. While the dark matter in streams is typically quite cold (small velocity dispersion), dark matter in debris flow can retain a much larger dispersion until it is thermally mixed with the surrounding halo. The debris flow is created by tidal stripping of subhalos as they make multiple orbits around the galactic center. This process is especially strong during the gravitational shock that occurs for a pericenter passage. Eventually, debris flow that is relatively old will become thermalized with the host halo, and no longer be identifiable as velocity substructure.

In Ref. [36], the authors examined the Via Lactea simulation of the formation of a Milky Way-type galactic halo and found that debris flow can compose a large fraction of the dark

matter particles, especially at larger speeds. Fig. 2.10 shows the fraction of dark matter particles with speeds above v_{min} that can be identified as debris flow found in Ref. [36]. At the higher speeds that are often most relevant to low-mass WIMPs, we see that over 80% of the the dark matter particles exist as debris flow. This type of velocity substructure could thus have a profound effect on the expected signal in a direct detection experiment.

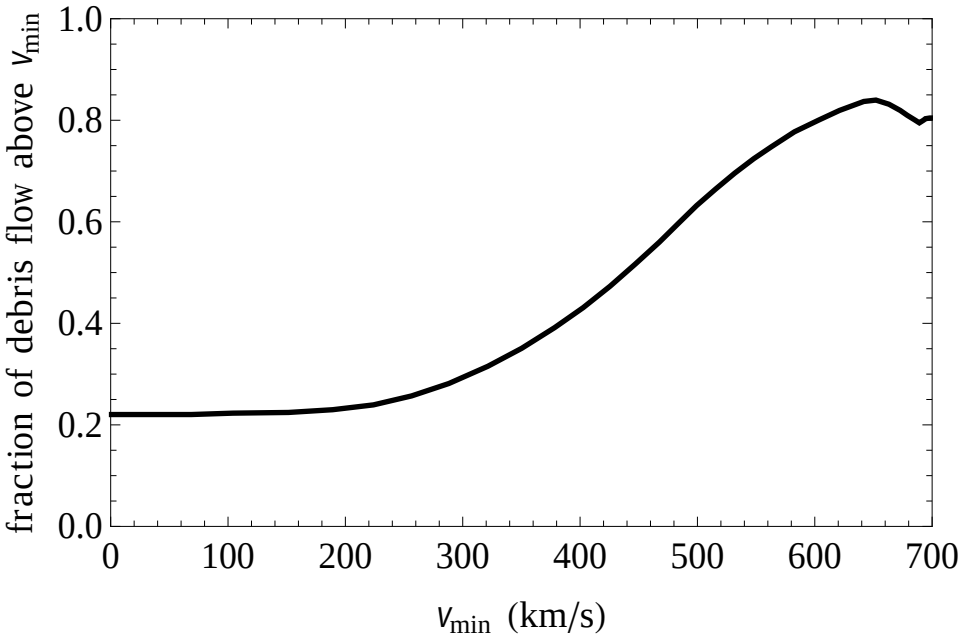

Figure 2.10: The fractional density of debris particles above some minimum velocity, v_{min}, in the Earth's rest frame (in summer) as found in Ref. [36].

The authors present a phenomenological description for the velocity distribution of the debris flow found in the Via Lactea simulation. They assume that in the halo rest frame, the debris flow is isotropic (no angular dependence) can be described by a delta function centered around one speed, v_{flow}. The velocity distribution in the halo rest frame will be given by

$$f_{debris}(\vec{u}) = \frac{1}{4\pi^2 v_{flow}^2}\delta(u - v_{flow})\,. \tag{2.57}$$

Substituting this distribution into Eq. 2.31 gives

$$g_{debris}(v_{min}, v_e) = \begin{cases} \frac{v_{flow}+v_e-|v_{flow}-v_e|}{2v_{flow}v_e}, & \text{if } v_{min} < |v_{flow} - v_e|\,, \\ \frac{v_{flow}+v_e-v_{min}}{2v_{flow}v_e}, & \text{if } |v_{flow} - v_e| < v_{min} < v_{flow} + v_e, \\ 0 & \text{if } v_{min} > v_{flow} + v_e, \end{cases} \tag{2.58}$$

The above expression differs slightly from the one given in Ref. [36]. This is because the authors were considering only the case of $v_{flow} > v_e$. The above expression indeed reduces to the result given in Ref. [36] for the case $v_{flow} > v_e$.

The results for the integral of the velocity distribution for the debris flow in a spherical shell of radii $7.5 - 9.5\,\text{kpc}$ found in the Via Lactea simulation are plotted in Fig. 2.11. The approximations for this integral as given in Eq. 2.58 are also shown for $v_{flow} = 340\,\text{km/s}$. We see that this phenonemological description of the debris flow does a decent job of capturing the main features of this type of substructure found in the Via Lactea simulation.

If a direct detection experiment is also sensitive to the annual modulation of a dark matter signal, then the above description is no longer sufficient. Fig. 2.12 shows the annual modulation signal for the configurations in Fig. 2.11 with the Via Lactea results shown as the solid, black line and the approximation of Eq. 2.58 shown as the red, dashed line. The approximate description for the debris flow does have a similar shape to the debris flow found in Via Lactea, but there is a large horizontal shift ($\sim$100 km/s). Additionally, the approximate description is overpredicting the maxmimum amplitude of the modulation by about a factor of 2.

Relaxing one of the assumptions that goes into the above approximation can yield significantly better results. Rather than having a δ-function in speed for the velocity distribution of the debris flow, we instead postulate an ansatz of a Gaussian with a non-zero dispersion. This is essentially a stream with a very large dispersion (see Eq. 2.57). The result for the

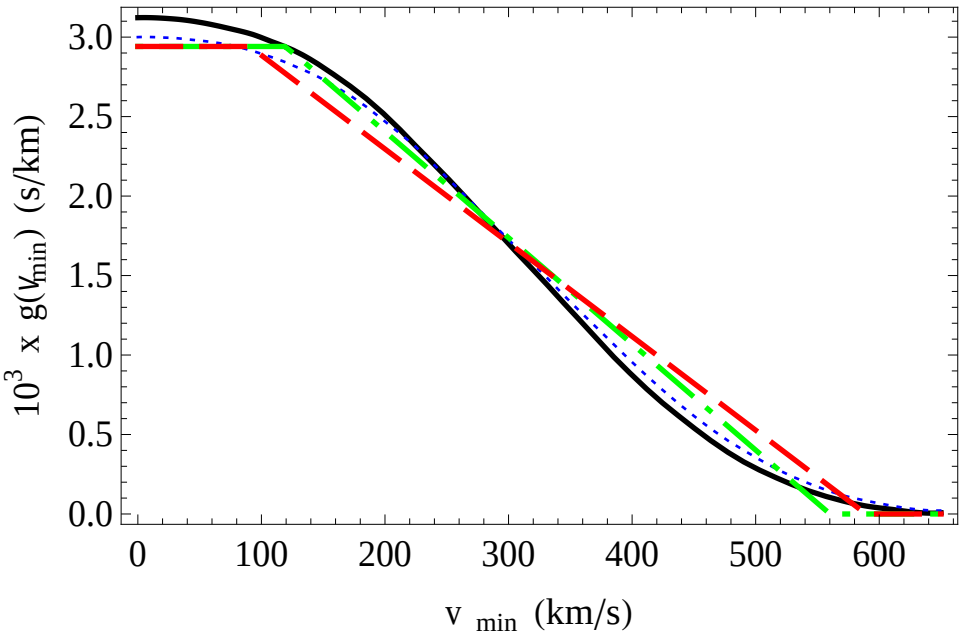

Figure 2.11: The blue, dotted (black,solid) line shows g_{debris} for the debris flow found in Via Lactea simulation in the summer (winter) [37]. The red, dashed (green, dot-dashed) line shows the approximate description for the debris as given in Eq. 2.58.

velocity integral can be taken directly from Eq. 2.51:

$$g_{debris}(v_{min}) = \frac{1}{2v_{e,str}}\left[\mathrm{erf}\left(\frac{v_{e,flow}+v_{min}}{v_{0d}}\right)+\mathrm{erf}\left(\frac{v_{e,flow}-v_{min}}{v_{0d}}\right)\right], \tag{2.59}$$

If we fit this function to the summer and winter velocity distributions from the Via Lactea simulations shown in Fig. 2.11, we find in the summer $v_{e,flow} = 323\,\mathrm{km/s}$ and $v_{0d} = 208\,\mathrm{km/s}$, while in the winter $v_{e,flow} = 311\,\mathrm{km/s}$ and $v_{0d} = 202\,\mathrm{km/s}$. The annual modulation for this fit to the debris flow is also plotted in Fig. 2.12 as the dashed, blue line. We see that this distribution provides a much better fit to annual modulation signal. Any analysis relating to debris flow in a direct detection experiment that will include an annual modulation aspect should thus use the better approximation given in Eq. 2.59.

To determine the effect the debris flow might have on the signal at a direct detection experiment, we plot the expected signal and annual modulation signal for a germanium

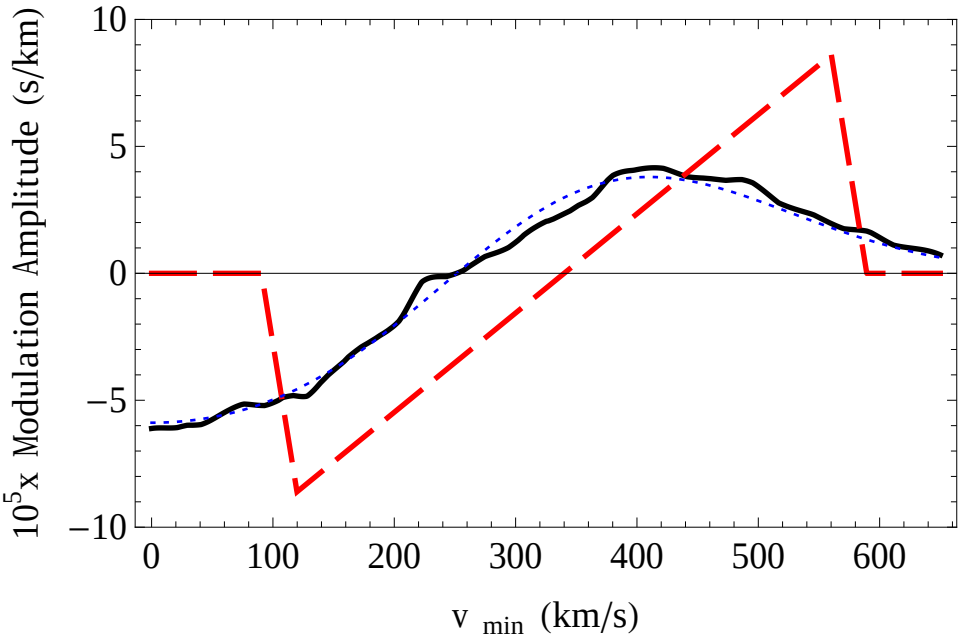

Figure 2.12: The annual modulation amplitude of g_{debris}. The Via Lactea results are shown as the black (solid) line, the approximation of Eq. 2.58 is shown as the red (dashed) line, and the improved approximation of Eq. 2.59 is shown as the blue (dotted) line.

detector in Fig. 2.13. We see that all three velocity distributions give quite similar spectra with the original approximation enhancing the signal a bit more at higher energies than the improved approximation. This enhancement is amplified when looking at the modulation signal. Using the original approximation, one could erroneously conclude the debris flow consistent with the Via Lactea simulation would predict a much larger annual modulation at higher energies than in the Maxwellian halo. We see that with the improved approximation, the actual enhancement of the higher energy annual modulation signal from the debris flow is actually quite small.

Overall, a Maxwellian halo provides a better description than one might have initially anticipated, especially considering the steady rise of the fraction of debris particles at large values of v_{min}, as shown in Fig 2.10. This is due in part to the fact that, although the fraction of debris particles is rising, the total number of dark matter particles is quite rapidly falling

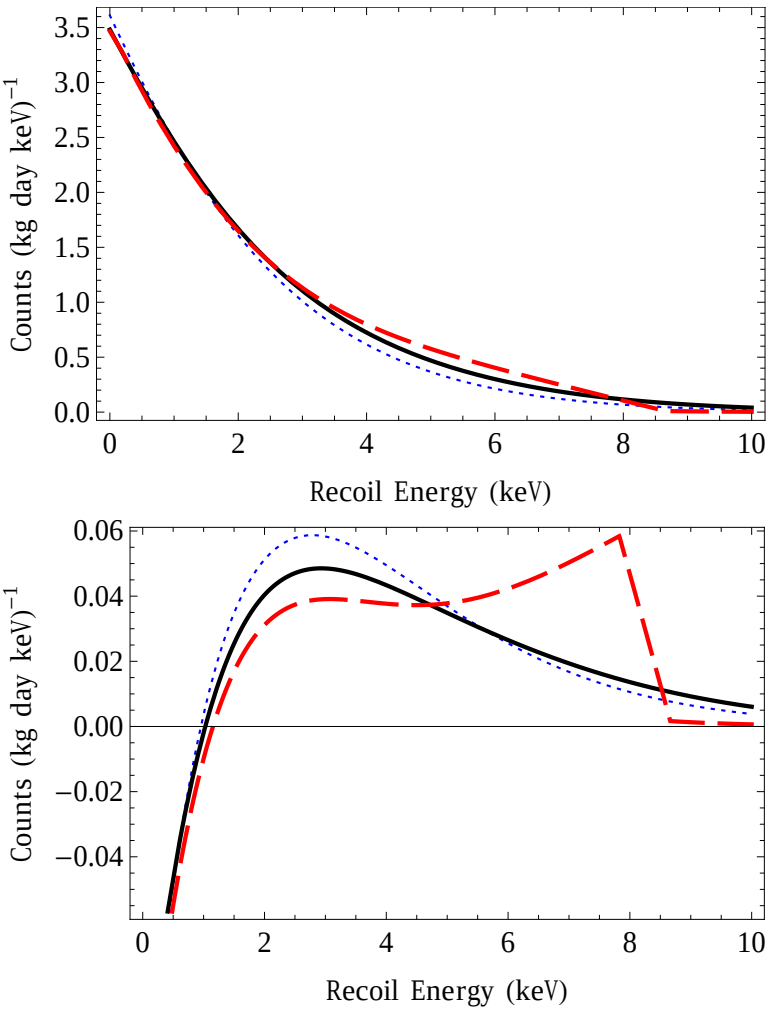

Figure 2.13: The upper frame plots the spectra in a germanium target for a dark matter particle with mass 10 GeV and cross section with nucleons of 10^{-41} cm^2 in the summer (June 1). The blue (dotted) line shows the signal from a Maxwellian halo with $v_0 = 220$ km/s and $v_{esc} = 544$ km/s. The black (solid) line shows the spectrum from both the Maxwellian halo and debris flow with the relative density of the debris flow given by the Via Lactea simulation shown in Fig. 2.10. The debris flow contribution to the spectrum is given by the improved approximation of Eq. 2.59. The red (dashed) line also line shows the spectrum from both the Maxwellian halo and debris flow but uses the original approximation given in Eq. 2.58. The lower frame plots the amplitude of the annual modulation signal in the same cases.

for these larger speeds. For example, above 450 km/s, more than 50% of the dark matter particles are debris flow. This would correspond to a recoil energy of 5 keV for a 10 GeV dark matter particle. As we see in Fig. 2.13, the signal above 5 keV is not very large because

there are not many dark matter particles with speeds large enough to produce nuclear recoils above this energy.

2.4.5 Astrophysics Independent Comparisons

As we have discussed in previous sections, features in v_{min} space (such as the cut-off in the spectrum for a stream) will occur at different energies for experiments that use different target nuclei. This can be traced to the fact that v_{min} is related to the energy scale through Eq. 2.4. Rearranging this relationship gives

$$E_r = \frac{2v_{min}^2}{m_N}\,. \tag{2.60}$$

In Ref.[38], the authors utilize this property to try and compare the results of two experiments without assuming a particular form for the halo. If there are nuclear recoil events in experiment 1 in the energy range $[E_{1,1}, E_{1,2}]$ that are definitively identified as dark matter in origin, there will be a corresponding signal in experiment 2 in the energy range $[E_{2,1}, E_{2,2}]$, with

$$E_{2,i} = \frac{\mu_2^2\, m_{N_1}}{\mu_1^2\, m_{N_2}} E_{1,i}\,. \tag{2.61}$$

The spectrum expected in the second experiment can be written in terms of the spectrum measured in the first experiment as

$$\frac{dR_2}{dE_{r,2}} = \frac{N_{T,2}\, m_{N,2}}{N_{T,1}\, m_{N,1}} \frac{\left[f_p Z_2 + f_n(A_2 - Z_2)\right]^2}{\left[f_p Z_1 + f_n(A_1 - Z_1)\right]^2} \frac{F_2^2(E_{r,2})}{F_1^2(E_{r,1})} \frac{dR_2}{dE_{r,2}}\,, \tag{2.62}$$

with $E_{r,1}$ related to $E_{r,2}$ by Eq. 2.61.

In essence, we are assuming that the true nature of the nuclear recoil spectrum is dark matter scattering and then treating $g(v_{min})$ as the "measureable" quantity. The additional assumptions that must be made to make the comparison, are only particle physics in nature:

the mass of the dark matter particle (to relate the two energy scales), and how the dark matter couples to protons and neutrons (f_p and f_n). In this way, astrophysical assumptions about the dark matter halo can be eliminated when comparing the results of two experiments. As shown in Ref. [38], this method can also be used determine whether a dark matter interpretation of a "signal" in one experiment is consistent with the non-observation of a signal in another experiment.

CHAPTER 3

DIRECT DETECTION EXPERIMENTS

3.1 Introduction

Among the techniques being pursued to identify the particle identity of dark matter are direct detection experiments, which are designed to observe particles of dark matter in the galactic halo through their elastic scattering with nuclei in a target material. Because the dark matter particles in our galaxy are only moving with speeds $\sim$100 km/s, the nuclei are expected to recoil with quite small energies, in the range of 10's to 100's of keV. The majority of the experiments apply (at least) one of three strategies for detecting nuclear recoils: ionization, heat, and scintillation.

A recoiling nucleus will ionize nearby electrons as it loses its energy. This charge can be collected and used to give a measure of how much energy the recoiling nucleus initially possessed. A recoiling nucleus will also bump into nearby nuclei in the crystal lattice. These collisions heat up the crystal as the nucleus loses energy. If the crystal is cryogenically cooled, the resulting phonon signal can be collected to give a measure of the original energy of the recoiling nucleus. Some materials have the interesting property that a recoiling nucleus will cause the material to produce light (scintillate). Using state-of-the-art photo-multiplier tubes allows experiments to measure the tiny amounts of light created by nuclear recoils in these scintillating materials. Table 3.1 presents many of the direct detection experiments that have run or are currently running right now.

As discussed in the Introduction, backgrounds are always at the heart of direct detection experiments. This is especially true for direct detection. Natural radioactivity of the detector

Experiment	Location	Readout (γ, ϕ, q)	T (K)	M (kg)	Target	Search Dates
NAIAD	Boulby	γ	300	50	NaI	2001–2005
DAMA/NaI	Gran Sasso	γ	300	87	NaI	1995–2002
DAMA/LIBRA	Gran Sasso	γ	300	233	NaI	2003–
ANAIS	Canfranc	γ	300	11	NaI	2000–2005
ANAIS	Canfranc	γ	300	100	NaI	2011–
KIMS	Yangyang	γ	300	35	CsI	2006–2007
KIMS	Yangyang	γ	300	104	CsI	2008–
CDMS II	Soudan	ϕ, q	< 1	1	Si	2001–2008
				3	Ge	2001–2008
EDELWEISS I	Modane	ϕ, q	< 1	1	Ge	2000–2004
EDELWEISS II	Modane	ϕ, q	< 1	4	Ge	2005–
CRESST II	Gran Sasso	ϕ, γ	< 1	1	$CaWO_4$	2000–
SIMPLE	Rustrel	Threshold	300	0.2	Freon	1999–
PICASSO	Sudbury	Threshold	300	2	Freon	2001–
COUPP	Fermilab	Threshold	300	2	Freon	2004–2009
COUPP	Fermilab	Threshold	300	60	Freon	2010–
TEXONO	Kuo-Sheng	q, $\beta\beta$	77	0.02	Ge	2006–
CoGeNT	Chicago	q, $\beta\beta$	77	0.3	Ge	2005–
CoGeNT	Soudan	q, $\beta\beta$	77	0.3	Ge	2008–
MAJORANA	Sanford	q, $\beta\beta$	77	60	Ge	2011–
ZEPLIN III	Boulby	γ, q	150	7	LXe	2004–
LUX	Sanford	γ, q	150	100	LXe	2010–
XMASS	Kamioke	γ, q	150	100	LXe	2010–
XENON10	Gran Sasso	γ, q	150	5	LXe	2005–2007
XENON100	Gran Sasso	γ, q	150	50	LXe	2009–
WArP	Gran Sasso	γ, q	86	3	LAr	2005–2007
WArP	Gran Sasso	γ, q	86	140	LAr	2010–
ArDM	CERN	γ, q	86	850	LAr	2009–
DEAP-1	SNOLAB	γ	86	7	LAr	2008–
MiniCLEAN	SNOLAB	γ	86	150	LAr	2012–
DEAP-3600	SNOLAB	γ	86	1000	LAr	2013–
DRIFT-I	Boulby	Direction	300	0.17	CS_2	2002–2005
DRIFT-2	Boulby	Direction	300	0.34	CS_2	2005–
NEWAGE	Kamioka	Direction	300	0.01	CF_4	2008–
MIMAC	Saclay	Direction	300	0.01	many	2006–
DMTPC	MIT	Direction	300	0.01	CF_4	2007–

Table 3.1: Characteristics of selected dark matter experiments [18], including fiducial mass M and whether scintillation light (γ), phonons (ϕ), ionization (q), or another form of energy is detected, and if the primary mission is neutrinoless double-beta decay ($\beta\beta$).

materials create nuclear recoils, the very signal that we are searching for. This means that detectors designs must take exhausting precautions to limit the amount of internal radiactivity as much as possible. Neutrons also produce nuclear recoils, so much effort is spent trying to minimize exposure to neutrons. For this reason, dark matter detectors are typically found deep underground so that the rock overburden can shield the detector from cosmic ray induced neutrons.

Dark matter is typically expected to interact primarily with an atom's nucleus, while many of the radioactive backgrounds interact primarily with electrons. If an experiment can discriminate between electron recoils and nuclear recoils, this knowledge can be used to reject these backgrounds. Many experiments try to take advantage of this fact by employing two of the detection strategies described above. This is because the ratio between the two signals (ionization to phonon, for example) is typically different for electron and nuclear recoils. In a threshold detector, such as COUPP, tuning thermodynamic parameters (like temperature and pressure) makes the detector insensitive to the low energy density deposited by a minimum-ionizing electron recoil. Only a dense energy deposition, such as from a nuclear recoil, will provide enough energy to cause nucleation.

In the following three sections, we will provide additional details about the three experiments upon which the majority of this work is based.

3.2 DAMA and DAMA/LIBRA

The DAMA/LIBRA experiment searches for the the annual modulation signature that is expected from elastically scattering dark matter. This experiment is located in Gran Sasso National Laboratory (Italy). The original DAMA apparatus consisted of nine, 9.70 kg, low-radioactive scintillating thallium-doped sodium iodide (NaI(Tl)) crystals. The detectors use photomultiplier tubes to collect scintillation light created by nuclear recoils. The DAMA

collaboration collected data over 7 annual cycles for a total exposure of 0.29 ton-year. The colloboration upgraded to the DAMA/LIBRA experiment, consisting of a total of 25 crystals for a total mass of $\sim$250 kg. The total exposure released to date is now 1.17 ton-year.

DAMA/LIBRA is the only direct detection experiment that has made a definitive claim of dark matter discovery. Their cumulative signal shows 8.9σ evidence for the presence of an annual modulation [39]. Although their backgrounds are relatively large, these backgrounds should not have the distinctive features of their claimed modulating dark matter signal. In particular, their annual modulation signature simultaneously satisfies all the following requirements:

1. the rate must contain a component modulated according to a cosine function
2. with one year period
3. a phase that peaks roughly around June 2
4. this modulation must only be found in a well-defined low energy range
5. it must apply only to those events in which just one detector registers a signal (singlehit events)
6. the modulation amplitude in the region of maximal sensitivity must be $\sim$7% for usually adopted halo distributions

The possibility that muons are the source for the DAMA signal has been extensively studied by many authors. The DAMA collaboration maintains muons as an explanation for their signal would fail in points 3, 4, and 5.

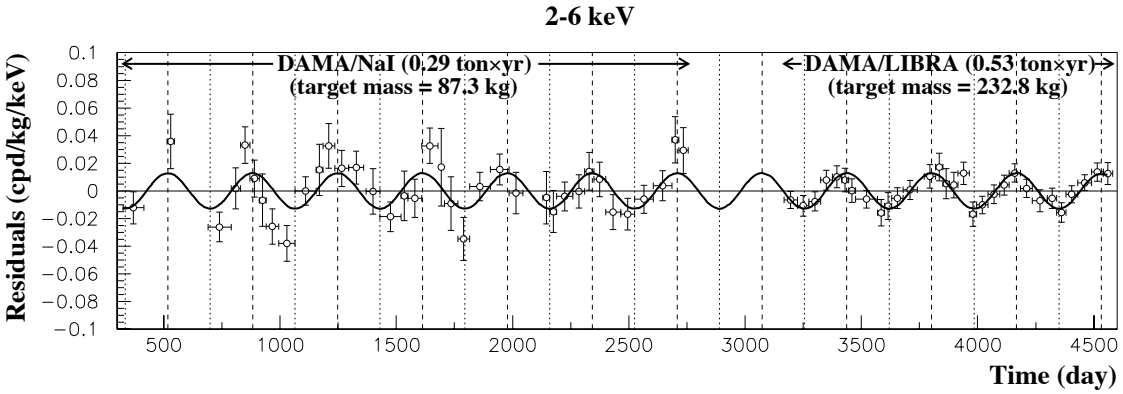

Figure 3.1: Sum of residuals of the single-hit scintillation events in the 2–6 keVee energy interval, after subtracting time-averaged rates in each energy bin in each detector, as a function of days since January 1, 1996, for the DAMA/NaI and DAMA/LIBRA experiments. The experimental errors are vertical bars, and the associated time bin widths are horizontal bars. The superimposed curve represents the cosinusoidal function $A\cos\omega(t-t_0)$ with modulation amplitude $A = (0.0129 \pm 0.0016)$ (keVee kg day)$^{-1}$ obtained by best fit over the whole data while constraining the period $T = 2\pi/\omega = 1$ yr and phase $t_0 = 152.5$ day (June 2^{nd}). The dashed vertical lines correspond to the maximum of the signal (June 2^{nd}), while the dotted vertical lines correspond to the minimum. Figure is taken from Ref. [40].

3.3 CoGeNT

CoGeNT, located in the Soudan Underground Laboratory in Northern Minnesota, consists of a 475 gram (a fiducial mass of 330 grams) target mass of p-type point contact germanium detector. The detector works by collecting the ionization charge created by a recoiling nucleus. Although this detector is considerably smaller mass than is employed by CDMS, XENON, and other direct detection experiments, CoGeNT's very low backgrounds and reduced electronic noise at low recoil energies make it exceptionally sensitive to low mass WIMPs. As the germanium isotopes which make up the CoGeNT detector contain little net spin, their experiment is searching for spin-independent dark matter-nucleus interactions.

In February 2010, the CoGeNT collaboration reported that they had observed approximately 100 events above expected backgrounds with ionization energies in the range of

approximately 0.4 to 1.0 keV [41]. In June 2011, the CoGeNT collaboration announced the results of their analysis of a full 15 months of data [42]. This larger data set was used to provide a much more detailed measurement of the spectrum of observed events. Furthermore, their analysis revealed a time variation in the rate of low energy nuclear recoil events, with a quoted significance of 2.8σ. We have performed extensive analyses of the publically available CoGeNT data in parallel and in addition to those performed by the CoGeNT collaboration. The results of these analyses are presented in Chapters 4-7.

3.4 CRESST II

The CRESST II experiment is also located in Gran Sasso National Laboratory. The detector is composed of modules that have a cylindrical shape (40mm in diameter and height) and are manufactured from about 300 g of very pure $CaWO_4$. The current experimental setup can accommodate up to 33 of these crystals, constituting a maximum target mass of about 10 kg. In Fig. 3.2, we plot the expected contribution of each element in the detector to a possible dark matter signal from a WIMP of a given mass. We see that for low-mass WIMPs, both oxygen and calcium will contribute to the signal, while tungsten recoils would be completely undetectable. For larger mass WIMPs, the A^2 enhancement leads to the signal being completely dominated by tungsten.

The detector is cryogenically cooled ($\sim$10 mK) so that the heat (phonon) signal created by a nuclear recoil can be measured. Additionally, the detector uses cryogenic light detectors to collect the scintillation light created by a nuclear recoil. The fact that CRESST II measures both phonon and scintillation allows them to define another handle to help reject backgrounds. The collaboration defines the light yield of an event as the ratio of energy measured with the light detector divided by the energy measured with the phonon detector. The typical backgrounds that are measured in the detector come from electron recoils

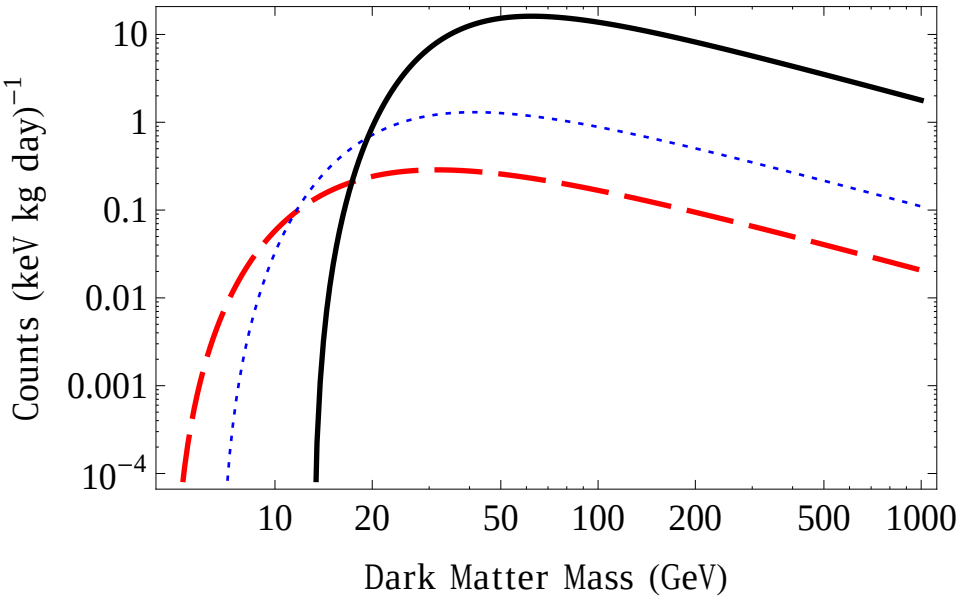

Figure 3.2: The expected signal at the CRESST II detector for a dark matter particle of the given mass and a scattering cross section with nucleons of $10^{-40}\,\mathrm{cm}^2$. The signal is obtained by integrating Eq. 2.1 over the energy range of 12 to 20 keV. The red (dashed) line is the signal from oxygen, the blue (dotted) line is from calcium, and the black (solid) line is from tungsten.

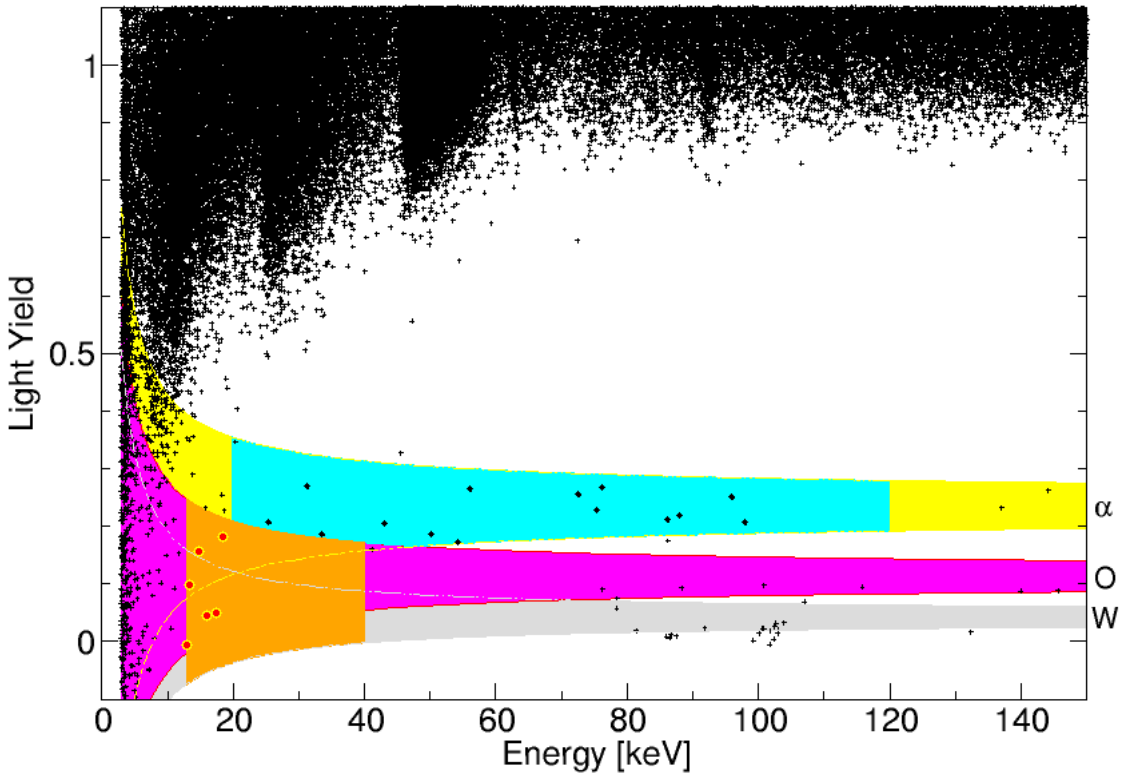

Figure 3.3: The data of one detector module (Ch20), shown in the light yield vs. recoil energy plane. The large number of events in the band around a light yield of 1 is due to electron and gamma background events. The shaded areas indicate the bands, where alpha (yellow), oxygen (violet), and tungsten (gray) recoil events are expected. Additionally highlighted are the acceptance region used in this work (orange), the reference region in the α-band (blue), as well as the events observed in these two regions. This plot is taken from [43].

induced either by β decay sources or by electron-gamma interactions and generally have a light yield of about 1. Nuclear recoils, on the other hand, typically have lower light yields.

If a signal event is plotted in the light yield, recoil energy plane, the different types of events tend to populate separated bands within the plane. Fig. 3.3 shows an example of the data obtained by one detector module, presented in the light yield-energy plane [43]. This allows the collaboration to select a signal region in the plane (shown in orange) to eliminate a large number of background events.

In September of 2011, the CRESST II collaboration reported their first results from

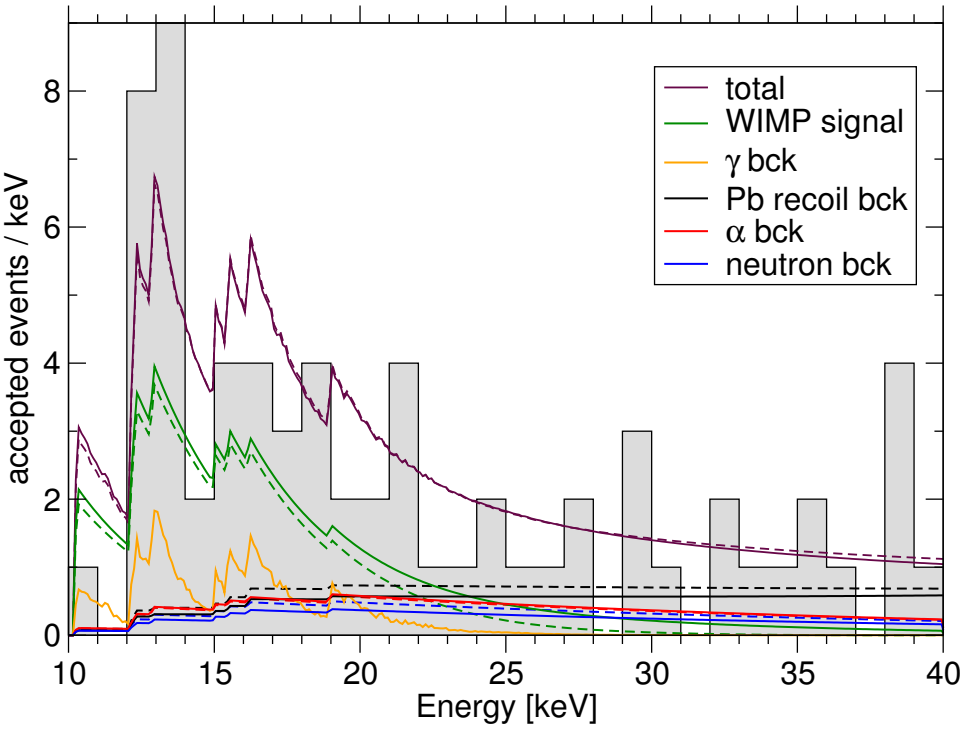

Figure 3.4: Energy spectrum of the accepted events from all detector modules, together with the expected contributions from the considered backgrounds and a WIMP signal, as inferred from the likelihood fit. The solid and dashed lines correspond to the fit results M1 and M2, respectively. This plot is taken from [43].

730 kg days in their detectors. They found an excess of ∼25 events that could not be accounted for by their background model [43]. Fig. 3.4 illustrates the fit result, showing an energy spectrum of all accepted events together with the expected contributions of backgrounds and WIMP signal. The solid lines correspond to the likelihood maximum M1, while the dashed lines belong to M2.

In Chapter 7, we examine the possibility that the excess events measured by DAMA/LIBRA, CoGeNT, and CRESST II could all be created by a single dark matter species.

CHAPTER 4

A CONSISTENT DARK MATTER INTERPRETATION OF COGENT & DAMA

4.1 Introduction

For nearly a decade, the DAMA collaboration (and more recently, the DAMA/LIBRA collaboration) has reported an annual modulation in their event rate and interpreted this signal as evidence for particle dark matter. According to their most recent results, which make use of over 1.17 ton-years of data, the DAMA/LIBRA collaboration observes a modulation with a significance of 8.9σ, and with a phase consistent with that predicted for elastically scattering dark matter [39]. When the null results from other dark matter searches [44, 45] are taken into account, one is forced to consider very light dark matter particles ($\lesssim 10$ GeV) to accommodate this signal [46, 47, 48].

Alternatively, one could also consider scenarios in which dark matter particles interact with nuclei through a resonance [49], interact with nuclei with a momentum dependence causing them to scatter more efficiently with NaI than other targets [50, 51], or which interact with nuclei largely through inelastic processes [52, 53, 54]; any of which could plausibly generate the DAMA/LIBRA signal while evading all relevant null results.

In February of 2010, the CoGeNT collaboration announced the observation of an excess of low energy events relative to expected backgrounds [41]. This excess, if interpreted as dark matter, implies the dark matter particles possess a mass in the range of 5-15 GeV and an elastic scattering cross section with nucleons on the order of 10^{-4} pb (10^{-40} cm^2). These implied values are remarkably similar to those needed to generate the annual modulation

reported by the DAMA/LIBRA collaboration. For theoretical work on dark matter particles in this mass range, see Refs. [55, 56, 57, 58, 59, 60, 61, 62].

Dark matter interpretations of the combined DAMA/LIBRA and CoGeNT signals have, however, been somewhat controversial. One reason for this is that it has been claimed that the regions of dark matter parameter space (mass vs. cross section) implied by CoGeNT and DAMA/LIBRA do not overlap, unless channeling occurs in the DAMA/LIBRA apparatus [41, 63, 64, 65, 66, 67]. This problem has been exacerbated by recent theoretical work which suggests that the effects of channeling in DAMA/LIBRA should be much smaller than previously considered [68] (even if some model-dependence remains). Another source of controversy has resulted from the null results of other dark matter searches, including XENON100, XENON10, and CDMS (Si) [63, 64, 45, 69].

In this section, we revisit these and related issues in an attempt to determine whether the signals reported by the DAMA/LIBRA and CoGeNT collaborations could potentially originate from the same dark matter particle without conflicting with the null results of other experiments. In Sec. 4.2, we calculate the regions of dark matter parameter space implied by DAMA/LIBRA and CoGeNT and determine that, if uncertainties in these experiments' quenching factors are taken into account, consistent regions do exist. In particular, the combination of DAMA/LIBRA and CoGeNT data can be well accommodated by a dark matter particle with a mass of approximately $\sim$7 GeV and an elastic scattering cross section with nucleons of $\sim 2\times10^{-4}$ pb (2×10^{-40} cm^2), even if no significant channeling is taking place. We also comment on the events observed in the oxygen band of the CRESST experiment. In Sec. 4.3, we discuss the null results of other dark matter experiments, including XENON 10, XENON 100, and CDMS (Si), and find that none currently exclude the region favored by the combination of DAMA/LIBRA and CoGeNT. We summarize our results in Sec. 4.4.

4.2 Consistency of CoGeNT and DAMA/LIBRA

Since the first presentation of the original CoGeNT results [41], several groups [63, 64, 65, 66, 67] have fit the observed spectrum of events to elastically scattering dark matter scenarios and compared these fits to those implied by the annual modulation observed by DAMA/LIBRA [39]. While these studies find that the CoGeNT and DAMA/LIBRA signals point to similar regions of dark matter parameter space, the regions were found to overlap only if the effects of channeling are significant within the DAMA/LIBRA detectors.

In channeled events, the crystal nature of the detector enables the total recoil energy to be detected, in contrast to ordinary nuclear recoil events in which only a fraction (known as the quenching factor) of the energy is deposited in observable forms (scintillation light, heat, and/or ionization) relative to that in electron recoils [70, 71]. Recent theoretical work, however, appears to disfavor the possibility that channeling plays an important role in an experiment such as DAMA/LIBRA [68, 69]. In particular, ions recoiled by a dark matter particle originate in lattice sites and will not approach the channels of the crystal, but instead are expected to be efficiently blocked by the crystal lattice. In light of these findings, we will assume throughout this study that the fraction of events that are channeled at DAMA/LIBRA (or in other direct detection experiments) is negligible.

The question we wish to address in this section is whether, without channeling, the CoGeNT and DAMA/LIBRA signals could both originate from the same dark matter particle species. With this goal in mind, we consider the systematic uncertainties involved in these experiments' results, in particular those pertaining to the germanium and sodium quenching factors.

The calculation of the spectrum (in nuclear recoil energy) of dark matter induced elastic scattering events is given in Chapter 2. We use a Maxwellian halo as the velocity distribution of the dark matter (see sec. 2.4.2) with $v_0 = 230$ km/s and limit the velocity distribution with

a galactic escape velocity of 600 km/s [34, 22]. Throughout our analysis, we take $\rho_{DM} = 0.3$ GeV/cm^3. We will assume that $f_p = f_n$ so that the scattering cross section is given by Eq. 2.17. We also adopt the Helm form factor as described in Sec. 2.3.

Note that other commonly used parameterizations of the form factor can lead to modest but not insignificant (on the order of 10 to 20%) variations in the region of dark matter parameter space that provide a good fit to the CoGeNT (and to a lesser extent DAMA/LIBRA) signal.

While variations in the velocity distribution of dark matter particles could also significantly affect the quality of the fits found to the CoGeNT and/or DAMA/LIBRA data (see, for example, Ref. [72]), such changes tend to affect the fits to each data set in a similar way. Increasing v_0 and/or v_{esc}, for example, will tend to move the acceptable regions of dark matter parameter space toward lighter masses (and smaller cross sections) for both CoGeNT and DAMA/LIBRA. Since both regions will be moved in approximate unison, we do not consider such variations further. Similarly, we do not contemplate any deviations from a standard isothermal dark matter halo, another source of possible uncertainty affecting the comparison of DAMA/LIBRA to other experiments [73].

Over the energy range of the CoGeNT signal (approximately 0.4 to 2 keVee, where keVee denotes the equivalent electron energy), a number of measurements have been made of the relevant quenching factors (*i.e.* the ratio of ionization energy to total recoil energy) [74, 75, 76, 77, 78]. These are summarized in Fig. 4.1. The solid line in this figure represents the best fit to the data shown, assuming a parametrization chosen to follow the Lindhard theory (using $k = 0.20$). The dashed lines reflect the 2σ statistical upper and lower limits. In our fits, we will adopt a quenching factor for germanium given by $Q_{\rm Ge}(E_{\rm Recoil} = 3\,{\rm keV}) = 0.218 \pm 0.0058$, and with the energy dependence predicted by the Lindhard theory. Note that this neglects any systematic errors; the inclusion of which would further enlarge the region of dark matter parameter space potentially capable of accommodating the CoGeNT signal.

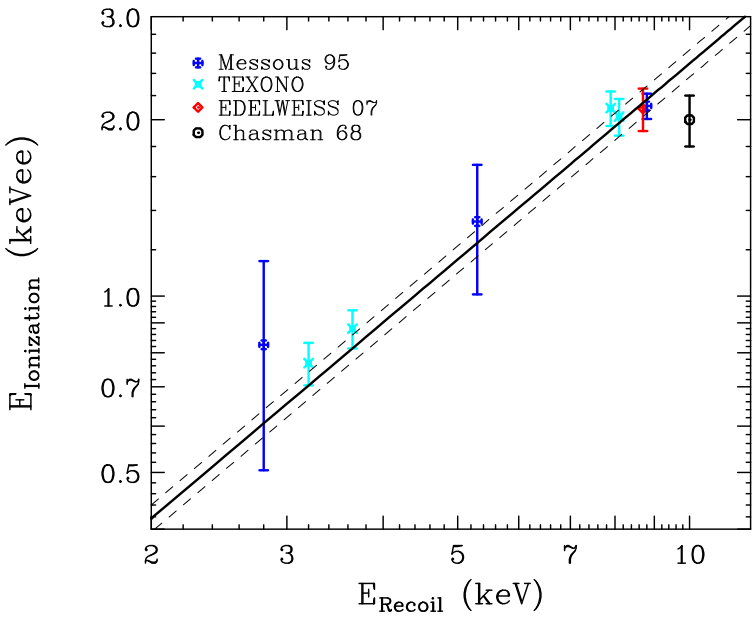

Figure 4.1: Measurements of the germanium quenching factor ($Q_{\rm Ge} \equiv E_{\rm ionization}/E_{\rm Recoil}$) over the energy range of the excess events observed by CoGeNT. The solid line denotes the best fit normalization to these measurements, assuming the slope predicted by Lindhard theory ($k = 0.20$). The dashed lines represent the upper and lower 2σ normalizations, accounting only for statistical errors. For the measurements used, see Ref. [74, 75]. Additional measurements by the CoGeNT collaboration span down to $E_{\rm Recoil} = 0.7$ keV [76, 77, 78].

For DAMA/LIBRA, measurements of the NaI(Tl) quenching factors are often averaged over large ranges of energy, hindering efforts to quantify the uncertainties in the narrow energy range of interest for light dark matter particles. In particular, the DAMA/LIBRA collaboration reports a measurement of their sodium (in the form of NaI, doped with thallium) quenching factor to be $Q_{\rm Na} = 0.30 \pm 0.01$ averaged over the energy recoil range of 6.5 to 97 keV [79]. Other groups have reported similar values: $Q_{\rm Na} = 0.25 \pm 0.03$ (over 20-80 keV), 0.275 ± 0.018 (over 4-252 keV), and 0.4 ± 0.2 (over 5-100 keV) [80]. As the sodium quenching factor is generally anticipated to vary as a function of energy, it is very plausible that over the range of recoil energies relevant for light (5-10) GeV dark matter (approximately 5 to 20 keV) the quenching factor could be somewhat higher than the av-

erage values reported from these measurements [81, 82] (see, for example, Ref. [83] and discussion in Ref. [84, 85, 86]). For recoil energies below approximately 20 keV, Ref. [87] reports a measurement of $Q_{\rm Na} = 0.33 \pm 0.15$, whereas Ref. [88] reports a somewhat smaller value of $Q_{\rm Na} = 0.252 \pm 0.064$ near 10 keV. A failure to account for the non-proportionality in electron response at low energy [89] appears in the energy calibration of several of these measurements, including those of Ref. [88]: the need for additional precision measurements of quenching factor near DAMA/LIBRA's threshold of 2 keVee seems evident. Some recent measurement of the quenching factor are shown in Fig. 4.2 taken from Ref. [90]. In our fits, we conservatively adopt a sodium quenching factor of $Q_{\rm Na} = 0.3 \pm 0.13$ over the energy range of interest ($E \approx 2 - 6$ keVee), which we deem representative of present experimental uncertainties.

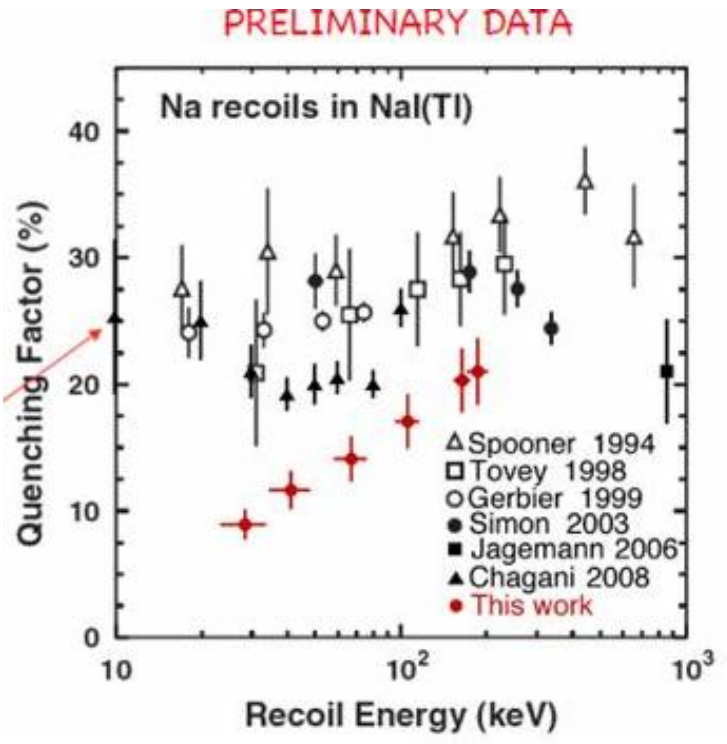

Figure 4.2: Measurements of the sodium quenching factor ($Q_{\rm Na} \equiv E_{\rm ionization}/E_{\rm Recoil}$) presented in Ref. [90].

In Fig. 4.3, we show the regions of dark matter parameter space which provide a good fit to the DAMA/LIBRA and CoGeNT data separately (upper frame) and combined (lower frame). In performing our fits, we have used the (13) DAMA/LIBRA bins below 8.5 keVee and the (28) CoGeNT bins between 0.4 and 1.8 keVee. The data at higher energies will not include any events from dark matter particles in the mass range considered here, and the inclusion of higher energy bins would not affect our results in any significant way.

From Fig. 4.3, we see that there exists a range of masses and cross sections for which both DAMA/LIBRA and CoGeNT can potentially be accommodated. In the range of $m_{\rm DM}$ $\sim$7-8 GeV and $\sigma_{\rm DM-N} \approx (1-3) \times 10^{-4}$ pb, quite good fits can be found for both experiments.[1] The overlapping region requires fairly large values of the sodium quenching factors, $Q_{\rm Na} \approx 0.45$ or greater throughout the 99% CL region and $Q_{\rm Na} \approx 0.50 - 0.55$ in the 90% CL region; considerably larger than the measurements presented in Ref. [88]. In the upper frame of Fig. 4.4, we show the spectrum of events in CoGeNT for the case of $m_{\rm DM} = 6.8$ GeV and $\sigma_{\rm DM-N} = 1.58 \times 10^{-4}$ pb. The dashed line shows our background model, which consists of a flat spectrum combined with a well understood double gaussian peak (see Ref. [41] for details). In the lower frame of Fig. 4.4, we show the prediction for the same dark matter model compared to the spectrum of DAMA/LIBRA's annual modulation. From these plots, it is clear that both the CoGeNT and DAMA/LIBRA signals could potentially result from a $\sim$7-8 GeV dark matter particle with an elastic scattering cross section of $\sigma_{\rm DM-N} \approx (1-3) \times 10^{-4}$ pb.

Lastly, we briefly consider the spectrum of events reported in talks by the CRESST collaboration [92, 93]. In the data from 9 $CaWO_4$ crystals, with a total exposure of 333 kg-days, a larger than anticipated number of events has been observed in the oxygen band of their experiment with recoil energies below $\sim$20 keV. In Fig. 4.5, we show the spectrum of

[1] An eventual stripping of L-shell electron capture peaks in the low-energy CoGeNT spectrum, based on high-statistics measurements of their K-shell counterparts and the known L/K capture ratio [91], is expected to favor precisely this same dark matter mass and cross section.

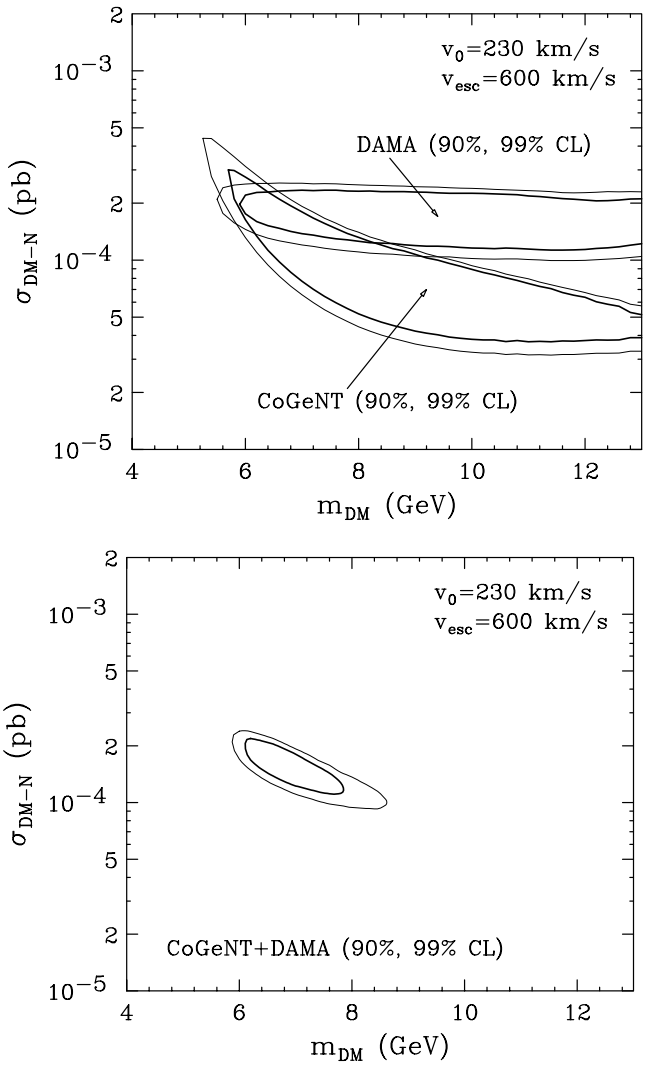

Figure 4.3: The regions in the elastic scattering cross section (per nucleon), mass plane in which dark matter provides a good fit to the excess CoGeNT events and to the annual modulation reported by DAMA/LIBRA (upper frame), as well as the region in which the combination of CoGeNT+DAMA/LIBRA is well fit (lower frame). We have assumed that any effects of channeling are negligible and have adopted $v_0 = 230$ km/s and $v_{\rm esc} = 600$ km/s. No errors associated with uncertainties in the form factors have been taken into account. If these and other systematics were fully included, the allowed region would be expected to increase considerably. See text for more details.

the oxygen band events reported in Ref. [92, 93] and compare this to the spectrum predicted for a dark matter particle consistent with both CoGeNT and DAMA/LIBRA ($m = 6.8$ GeV, $\sigma_{\rm DM-N} = 2 \times 10^{-4}$ pb). Note that as the total exposure of the observation is not completely

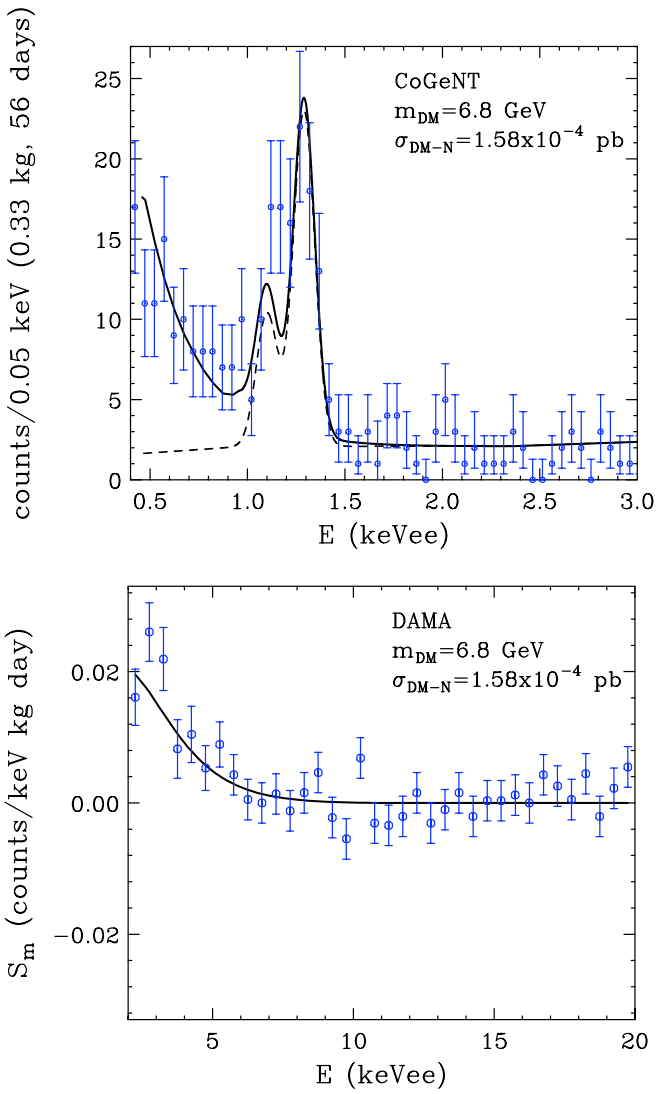

Figure 4.4: The spectrum of events in CoGeNT (upper frame) and the spectrum of the annual modulation in DAMA/LIBRA (lower frame) for overall best fit dark matter parameters of $m_{\rm DM} = 6.8$ GeV and $\sigma_{\rm DM-N} = 1.58 \times 10^{-4}$ pb. In the upper frame, the solid black line is the predicted result for signal plus background (with triggering and signal acceptance efficiency built into the model), whereas the dashed line is the background alone and points denote the measured values. In the lower frame, the solid line is the predicted signal and the points denote the measurements reported by DAMA/LIBRA. We have assumed that any effects of channeling are negligible and have adopted $v_0 = 230$ km/s and $v_{\rm esc} = 600$ km/s. See text for more details.

specified in Ref. [92, 93], we have normalized the predicted curve (the solid line) to the data, which corresponds to an exposure (times efficiency) of 210 kg-days. Remarkably good

agreement is found. For heavier dark matter particles, most of the dark matter events are expected to result from scattering with tungsten rather than oxygen nuclei. In the case of a very light dark matter particle, however, scattering with tungsten produces events with recoil energies below the threshold of the experiment. For this dark matter mass and cross section, we predict only one event in the tungsten band above 3.7 keV, and about ten events between 3.0 and 3.7 keV. We would like to emphasize the preliminary nature of these results, and recognize that, until the CRESST collaboration publishes their final distribution of events, fits to these data should be assessed with caution. In particular, we emphasize that some fraction of the events observed in the oxygen band could be spillage from CRESST's alpha or tungsten bands, neutron backgrounds, or be the result of radioactive backgrounds. Further information from the CRESST collaboration will be essential for understanding these results.

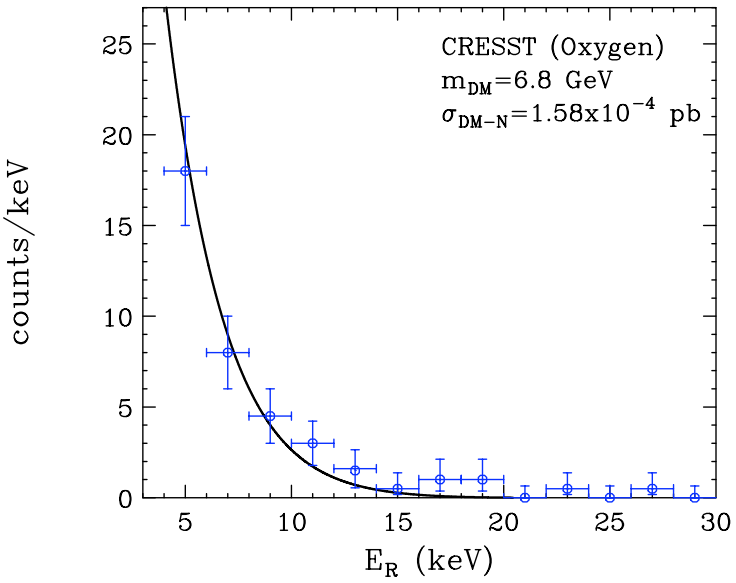

Figure 4.5: The preliminary spectrum of events in the oxygen band of the CRESST experiment, compared to the spectral shape predicted for the case of $m_{\rm DM} = 6.8$ GeV and $\sigma_{\rm DM-N} = 1.58 \times 10^{-4}$ pb (which provides good fit to both CoGeNT and DAMA/LIBRA). The solid line is the predicted signal and the error bars denote the preliminary spectrum of events reported by the CRESST collaboration. We have adopted $v_0 = 230$ km/s and $v_{\rm esc} = 600$ km/s. See text for more details.

4.3 Consistency With Null Results

In this section, we discuss whether a dark matter interpretation of the combined CoGeNT and DAMA/LIBRA signals is consistent with the null results reported by other direct detection experiments. In particular, recent claims have been made that a dark matter interpretation of the CoGeNT and DAMA/LIBRA data is inconsistent with the measurements of the XENON 100 experiment [45]. This conclusion, however, depends critically on the scintillation efficiency of liquid xenon, $L_{\rm eff}$ that is adopted [84, 85, 86, 69]. In particular, while both theoretical arguments and measurements of $L_{\rm eff}$ lead one to expect this quantity to decrease at low energies, no measurements exist below $\sim$ 4 keV, forcing one to speculate or extrapolate at lower energies. Unless quite optimistic values for these quantities are adopted, the range of masses and cross sections best fit by DAMA/LIBRA and CoGeNT are not significantly constrained by XENON 100 [84, 85, 86]. In fact, stronger constraints than those from XENON 100 can be derived from the data of XENON 10, due to its lower energy threshold [69] (see also Ref. [94, 95]). The recent work of Manzur *et al.* provides measurements of $L_{\rm eff}$ over the range of approximately 4 to 70 keV [96]. By not taking into account Poisson fluctuations from dark matter signals below 4 keV, and thus not making any assumptions regarding the values of $L_{\rm eff}$ below this range, it is possible to arrive at the constraints shown in the upper frame of Fig. 4.6. These constraints yield only a mild tension (less than $\sim 1\sigma$) with the parameter space region favored by DAMA/LIBRA and CoGeNT. If we instead assume that $L_{\rm eff}$ drops linearly below 4 keV, slightly stronger limits are found (Fig. 4.6, lower frame). Again, however, this constraint conflicts with the region favored by DAMA/LIBRA and CoGeNT at only about $\sim 1\sigma$. We emphasize that other existing measurements and extrapolations of $L_{\rm eff}$ lead to a complete absence of constraints on the region of DAMA/LIBRA and CoGeNT compatibility, even when sub-threshold Poisson fluctuations are assumed [84, 85, 86].

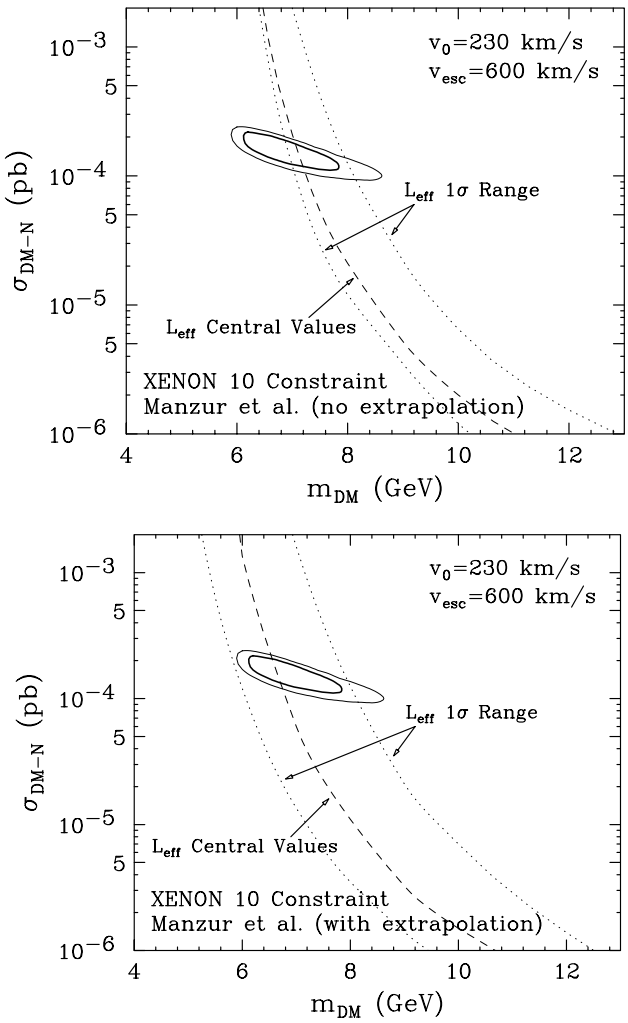

Figure 4.6: Constraints from the XENON 10 experiment [69]. In each frame, the dashed line denotes the limit when using the central values of the scintillation efficiency, $L_{\rm eff}$, as measured by Manzur *et al.* [96], whereas the dotted lines are derived using $\pm 1\sigma$ values of $L_{\rm eff}$. In the upper frame, no assumptions are made regarding the values of $L_{\rm eff}$ at energies below 4 keV (for which no measurements exist). In the lower frame, $L_{\rm eff}$ is assumed to fall linearly below 4 keV. Considerably more relaxed constraints are obtained from other existing measurements of $L_{\rm eff}$ [84, 85, 86]. See text for more details.

For typical dark matter masses, the null results from CDMS-II's germanium detectors provide the strongest constraints on the dark matter-nucleon elastic scattering cross-section [44]. Below ∼10 GeV, however, the CDMS-II silicon detectors provide better constraints [97, 98] due to the favorable kinematics of the lighter target nucleus. In Fig. 4.7, we compare

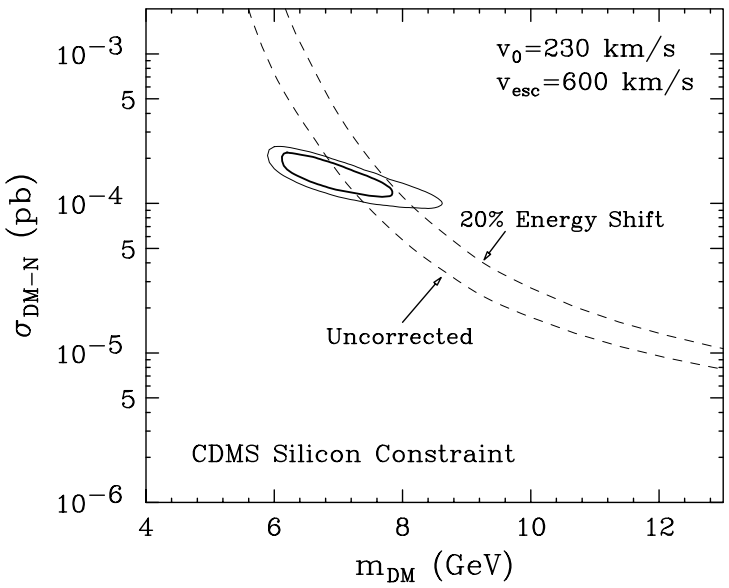

Figure 4.7: Constraints from the CDMS experiment's silicon analysis. The lower dashed curve denotes the results as presented in Ref. [97, 98], whereas the upper dashed curve shows the result with a 20% shift in CDMS's silicon recoil energy scale, a conservative correction that alleviates concerns expressed in the discussion surrounding Fig. 3.20 of Ref. [97]. See text for more details.

these contraints to the regions favored by the dark matter interpretation of the combined DAMA/LIBRA and CoGeNT results. Taken as published (after accounting for the different velocity distribution used in Refs. [97, 98]), we find that this constraint covers most of the 2σ range of masses and cross sections found to fit the DAMA/LIBRA and CoGeNT signals.

As noted in Ref. [97] (and as shown in their Fig. 3.20), however, the observed CDMS-II silicon nuclear recoil quenching is not reproduced by Lindhard theory, and is also markedly discrepant with previous measurements [99]. In contrast, an excellent agreement is observed for CDMS germanium detectors.[2] It is possible to attribute this disagreement to a systematic error in the absolute energy scale in the silicon detectors. The energy scale of the silicon detectors is more complicated than the germanium detectors to calibrate, since the silicon

[2]We remark without undue emphasis that a rough analysis of the CDMS germanium data in the relevant 2-5 keV recoil energy region exists [100].

detectors are not thick enough to contain the full energy deposition from barium gamma rays used for calibration. Additionally, large corrections affecting the recoil energy scale are applied to the CDMS detectors to remove position dependances (see the discussion surrounding Fig. 3.18 of Ref. [97]). The discrepancy between the observed quenching and Lindhard theory could indicate a $\sim$20-30% error in the low energy calibration, larger if other existing experimental data [99] are taken as the reference. In Fig. 4.7, we show how a corrected energy scale can change the constraints derived from the CDMS-II experiment, for the case of a linear 20% correction.[3] This shows that, while the CDMS-II silicon exposure could potentially constrain the region favored by DAMA/LIBRA and CoGeNT, this constraint is weakened due to the energy scale uncertainty and does not rule out the region favored by these experiments.

4.4 Summary and Discussion

In this paper, we have studied the excess of low energy events recently reported by the CoGeNT collaboration and the annual modulation signal reported by DAMA/LIBRA and conclude that these two signals could arise from an elastically scattering dark matter particle with a mass in the approximate range of $\sim$7 GeV and a cross section (with nucleons) of $\sigma \sim 2 \times 10^{-4}$ pb (2×10^{-40} cm^2). This conclusion is reached even if channeling is assumed to be negligible. The concordance between these two signals, which has not been found in previous studies, is made possible in large part by our choice of nuclear form factors and our accounting for uncertainties in the quenching factors of germanium and sodium. We also point out that the preliminary events observed in the oxygen band of the CRESST experiment are consistent with being the result of such a dark matter particle.

[3]Note that a non-linear energy correction would be needed to reconcile the Lindhard theory with the energies observed at CDMS-II. In particular, Fig 3.20 of Ref. [97] shows the observed nuclear recoil band crossing the prediction from Lindhard theory. The linear 20% correction used here, however, represents a reasonable estimate for the range of energies relevant for the detection of $\lesssim$ 10 GeV dark matter.

We have also considered in these sections the constraints from null results of other direct detection experiments, including XENON 10, XENON 100, and CDMS (Si). After taking into account the uncertainties in the scintillation efficiency of liquid xenon and the recoil energy scale of silicon events at CDMS, we find that the region of dark matter parameter space favored by CoGeNT and DAMA/LIBRA is consistent with all current constraints.

In the future, it may become possible for the CoGeNT or CRESST experiments to observe an annual modulation in their rate. In particular, we calculate that if CoGeNT is observing dark matter interactions, their event rate should be approximately 20% higher in the summer than it is in the winter, for a particle of this mass and CoGeNT's energy threshold. To detect this effect with a significance of 3σ, an approximate exposure of 40 kg-days would be required in each of the summer and winter seasons. This goal appears to be attainable for the CoGeNT experiment, which is operating continuously since December of 2009 with an active target mass of 0.33 kg. If observed, this would provide an important confirmation of the hypothesis that these experiments are in fact detecting dark matter.

CHAPTER 5

PROSPECTS FOR IDENTIFYING DARK MATTER WITH COGENT

5.1 Introduction

In February 2010, the CoGeNT collaboration reported that they had observed on the order of 100 events above expected backgrounds with ionization energies in the range of approximately 0.4 to 1.0 keV [41]. While the origin of these events is not yet certain, it has been shown that they could be accounted for with dark matter with a mass in the range of 5-15 GeV and an elastic scattering cross section with nuclei of $\sim 10^{-4}$ pb ($\sim 10^{-40}$ cm^2) [63, 64, 65, 66].

The CoGeNT excess is particularly intriguing when compared to other signals potentially resulting from dark matter. For nearly a decade, the DAMA collaboration (and more recently, the DAMA/LIBRA collaboration) has reported an annual modulation of their event rate, and has interpreted this behavior as evidence for particle dark matter. According to the most recent DAMA/LIBRA results, which make use of over 1.17 ton-years of data, they observe a modulation with a significance of 8.9σ, and with a phase consistent with that predicted for elastically scattering dark matter [39]. The simplest interpretation of this signal which does not conflict with the null results of other dark matter searches [44, 45] introduces light dark matter particles ($\lesssim 10$ GeV) with an elastic scattering cross section with nuclei on the order of $\sim 10^{-4}$ pb [46, 47, 48]. After all constraints [44, 45, 101, 94, 95, 69] and uncertainties [14, 84, 85, 86] are taken into account, a region of dark matter parameter space exists in which both the CoGeNT and DAMA/LIBRA signals can be accommodated [102].

In October of 2010, an anomalous component of gamma rays from the inner 0.5° around the Galactic Center was identified in the first two years of data from the Fermi Gamma Ray Space Telescope (FGST) [103]. The spectrum of this signal peaks at 2-4 GeV (in E^2 units) and is highly concentrated around the Galactic Center (but is not point-like). Although no known astrophysical sources or mechanism can account for this emission, annihilating dark matter can provide a good fit to the observed spectrum and morphology of the signal. If interpreted as dark matter annihilation products, the observed gamma rays imply a dark matter mass in the range of 7.3 to 9.2 GeV, very similar to that required to accommodate both CoGeNT and DAMA/LIBRA.

Although the evidence collectively provided by CoGeNT, DAMA/LIBRA, and FGST has become fairly compelling, more information will be needed before a confident and conclusive claim of discovery can be made. The annual modulation reported by DAMA/LIBRA, however, is based on data taken over 13 years, and little new information is expected from DAMA/LIBRA in the foreseeable future. Similarly, the gamma ray signal from the Galactic Center was extracted from two full years of FGST data (August 2008-August 2010). In contrast, the excess reported by CoGeNT was observed over a period of only 56 days in late 2009. With the currently existing data that has been collected over the past year, the CoGeNT collaboration will be able to dramatically improve upon their measurement on the nuclear recoil spectrum. Furthermore, if elastically scattering dark matter is responsible for their observed excess, CoGeNT will likely be sensitive to the predicted annual modulation. Looking further into the future, a planned expansion of CoGeNT (four 0.9 kg detectors, with an estimated combined fiducial mass of $\sim$2.5 kg) will not only be capable of detecting the presence of a modulation, but will be sensitive to the energy spectrum of the modulation, providing an irrefutable confirmation that their excess originates from dark matter.

The remainder of this Chapter is structured as follows. In Sec. 5.2, we calculate the spectrum of events from elastically scattering dark matter in the CoGeNT detector and

describe the current status of the CoGeNT excess. In Sec. 5.3, we will project the ability of CoGeNT to constrain the mass and cross section of the dark matter using their first full year of data, and with the planned CoGeNT upgrade, focusing on the ability of CoGeNT to detect the annual modulation of the dark matter signal. We argue that this will provide an essential confirmation of the dark matter origin of the observed excess. In Sec. 5.4, we discuss the role that other direct detection experiments will likely play in studying dark matter in the region implied by CoGeNT and DAMA/LIBRA. In Sec. 5.5 we summarize our results and conclusions.

5.2 CoGeNT and Elastically Scattering Dark Matter

CoGeNT, located in the Soudan Underground Laboratory in Northern Minnesota, consists of a 475 gram target mass of Germanium (a fiducial mass of 330 grams). Although this is considerably smaller mass than is employed by CDMS, XENON, and other direct detection experiments, CoGeNT's very low backgrounds at low recoil energies make it exceptionally sensitive to low mass WIMPs.

The spectrum (in nuclear recoil energy) of dark matter induced elastic scattering events is calculate in Chapter 2. We use the the standard Maxwell-Boltzmann distribution for the galactic halo as described in Sec. 2.4.2. We will consider values of v_0 over a range of 180 to 320 km/s and values of the galactic escape velocity between 460 and 640 km/s [11, 104, 105, 72, 38]. Throughout our analysis, we take $\rho_{DM} = 0.3$ GeV/cm^3. We will assume that $f_p = f_n$ resulting in the scattering cross section given by Eq. 2.17. We also adopt the Helm form factor as described in Sec. 2.3.

To convert from nuclear recoil energy to the measured ionization energy, we have to scale the results by the appropriate quenching factor. Over the energy range of the CoGeNT signal (approximately 0.4 to 2 keVee, where keVee denotes keV electron equivalent), the quenching

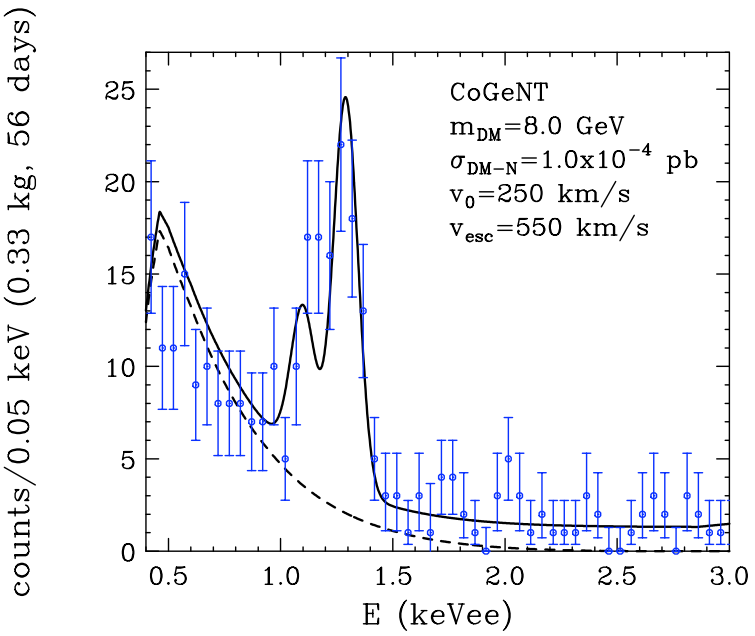

Figure 5.1: The current spectrum of events reported by CoGeNT compared to the spectrum predicted for an elastically scattering dark matter particle. The dashed line denotes the spectrum of dark matter events alone, while the solid line is the dark matter spectrum plus backgrounds.

factors for germanium have been well measured [74, 75, 76, 77, 78] and are described by $Q_{\rm Ge}(E_{\rm Recoil} = 3\,{\rm keV}) = 0.218$, and with the energy dependence predicted by the Lindhard theory (see Ref. [102]).

In Fig. 5.1, we show the current results from CoGeNT, compared to the spectrum predicted for an 8 GeV dark matter particle with an elastically scattering cross section with nucleons of 10^{-4} pb and a velocity distribution described by $v_0 = 250$ km/s and $v_{\rm esc} = 550$ km/s. For the background spectrum, we consider a simple flat distribution of events, and Gaussian peaks at 1.1 and 1.29 keV with widths given by the resolution of the detector, which arise from well understood physics (see Ref. [41]). We multiply the overall spectrum by the efficiency factors as described in Ref. [41].

Even with the relatively little exposure that went into this measurement (56 days, and 330 grams of target mass after cuts) CoGeNT has observed approximately $\sim$100 events between

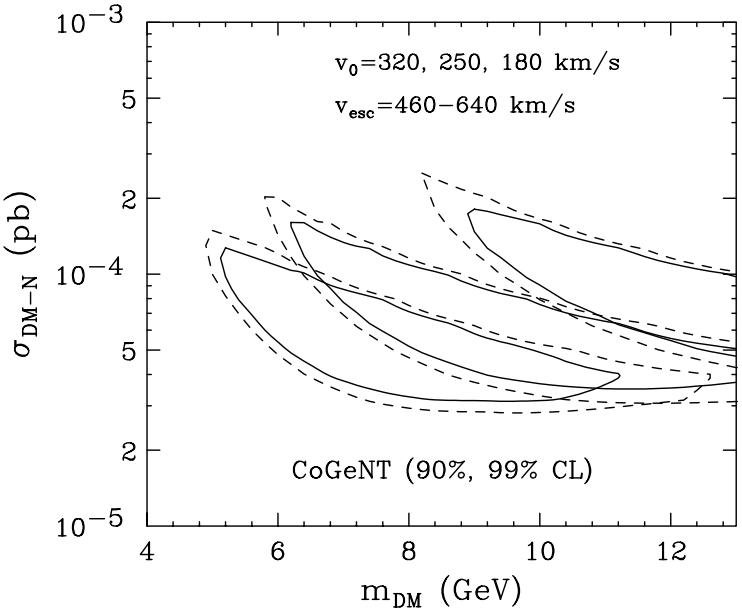

Figure 5.2: The range of dark matter parameter space that provides a good fit to the current CoGeNT data. The three overlapping regions correspond to $v_0 = 320$, 250 and 180 km/s, from left-to-right. Each region has been marginalized over escape velocities between 460 and 640 km/s. The solid and dashed lines denote the 90% and 99% confidence level contours.

0.4 and 1.0 keVee which cannot be accounted for by known backgrounds. In Fig. 5.2, we show the range of dark matter masses and cross sections that provide a good fit to the current CoGeNT excess, for various choices of the velocity distribution parameters. The three overlapping regions represent the range of mass and cross section that can fit the current data for values of $v_0 = 320, 250$ and 180 km/s, respectively (in each region, the escape velocity is marginalized over the range of 460 to 640 km/s).

5.3 Future Projections For CoGeNT

If the excess events reported by CoGeNT is the result of elastically scattering dark matter particles, then we should expect a degree of seasonal variation in the event rate. Due to the Earth's motion around the Sun, the rate of dark matter recoil events is predicted to vary throughout the year, peaking at or around June 2nd (see Sec. 2.4.2).

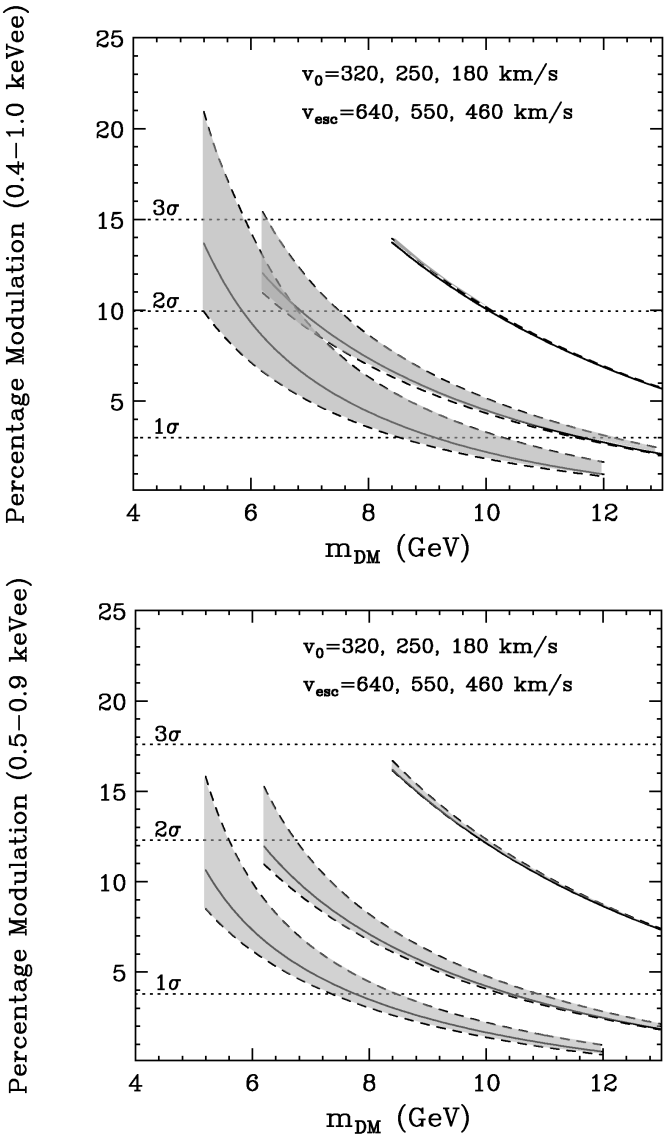

Figure 5.3: The predicted degree of annual modulation in the event rate of CoGeNT. The top (bottom) frame shows the modulation over the range of 0.4 to 1.0 keVee (0.5 to 0.9 keVee). The horizontal dotted lines denote the projected confidence levels at which CoGeNT will be able to identify a modulation with one full year of data. The three solid lines in each frame correspond to $v_0 = 320, 250$, and 180 km/s, from left-to-right, each with $v_{\rm esc} = 550$ km/s. The dashed lines above and below each solid line correspond to $v_{\rm esc} = 640$ and 460 km/s, respectively.

In Fig. 5.3, we show the predicted degree of modulation for dark matter within the parameter space region capable of generating the observed CoGeNT excess. The percentage

modulation that is plotted is defined as $(R_{\rm summer} - R_{\rm winter})/(2R_{\rm ave})$, where $R_{\rm summer}$ and $R_{\rm winter}$ denote the maxima and minima of the rate. The top frame of Fig. 5.3 shows the modulation over the range of 0.4 to 1.0 keVee, while the bottom frame considers a more narrow (and more conservative) range of 0.5 to 0.9 keVee. In each frame, the horizontal dotted lines denote the projected confidence levels at which CoGeNT will be able to identify a modulation after one year.

The additional data collected by CoGeNT over its first year will also considerably improve its ability to measure the spectrum of events, and place corresponding constraints on the underlying dark matter parameter space. In Fig. 5.4, we show the spectrum projected to be measured by CoGeNT after one year (top) and the corresponding regions of dark matter parameter space that provide a good fit to this spectrum (bottom). In calculating these regions, we considered only the spectrum between 0.4 and 1.0 keVee.

In Fig. 5.5, we show similar results, but projected for the planned upgrade of CoGeNT, with a fiducial mass of 2.5 kg. In addition to improving upon the spectral constraints, such an upgrade will also make it possible to measure the energy spectrum of the modulation amplitude. We illustrate this in Fig. 5.6. The solid curves shown in Fig. 5.6 denote the prediction for our central model ($m_{\rm DM}$ =8 GeV, $\sigma_{\rm DM-N} = 10^{-4}$ pb, $v_0 = 250$ km/s, $v_{\rm esc} = 550$ km/s) including backgrounds, whereas the upper (lower) dotted curve represents the prediction for parameters in the left (right) island-region in the bottom frame of Fig. 5.5. Note that this projection is somewhat conservative, as the 1.1 and 1.29 keV backgrounds are due to cosmogenic activation and will become steadily depleted with time.

5.4 The Role of Other Experiments

In this section, we will briefly discuss the ability of other direct detection experiments to study dark matter particles with the characteristics needed to generate the signals reported

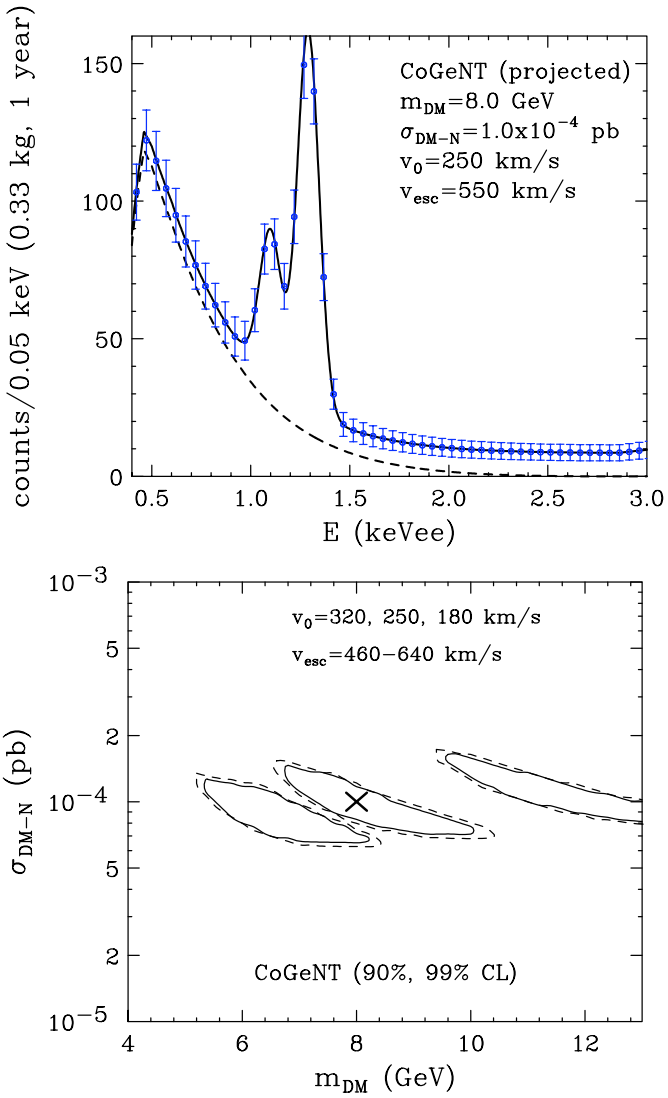

Figure 5.4: Top: The projected spectrum of events with one year of CoGeNT data, for an underlying dark matter model with a mass of 8 GeV, an elastic scattering cross section of 10^{-4} pb, $v_0 = 250$ km/s, and $v_{\rm esc} = 550$ km/s (the "true model"). Again, the dashed line denotes the spectrum of dark matter events alone, while the solid line is the dark matter spectrum plus backgrounds. Bottom: The range of dark matter parameter space that provides a good fit to the projected CoGeNT data. The three regions shown correspond to $v_0 = 320$, 250 and 180 km/s, from left-to-right. Each region has been marginalized over escape velocities between 460 and 640 km/s. The solid and dashed lines denote the 90% and 99% confidence level contours. The X denotes location of the true model.

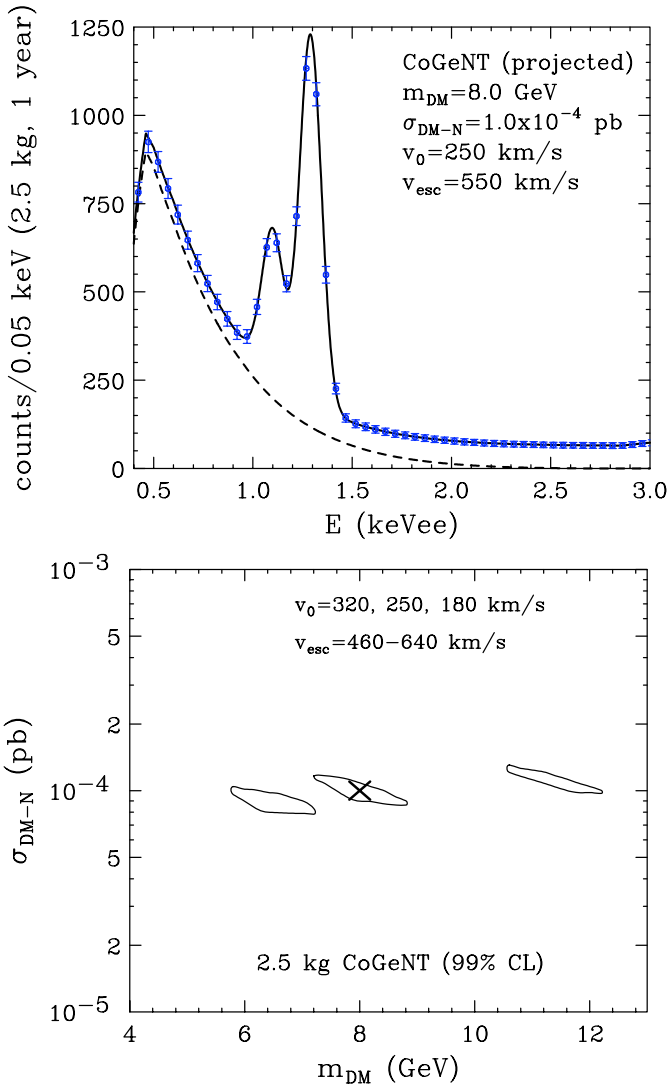

Figure 5.5: As shown in Fig. 5.4, but for an upgraded CoGeNT with a fiducial mass of 2.5 kg.

by CoGeNT and DAMA/LIBRA. Starting with DAMA/LIBRA, we note that although its comparatively enormous target mass (250 kg) has enabled it to make a very high significance measurement of the annual modulation amplitude, sizable uncertainties in the low energy behavior of its quenching factor limit the precision with which its data can be used to constrain the underlying dark matter parameter space. We also emphasize that, unlike CoGeNT, DAMA/LIBRA is capably only of measuring the amplitude of the modulation of

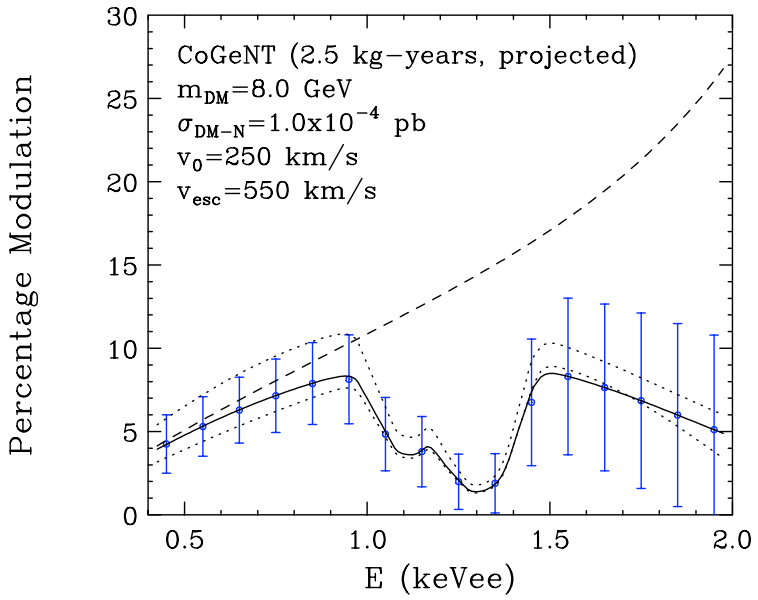

Figure 5.6: The measurement of the energy spectrum of the modulation, as projected for an upgraded CoGeNT with a 2.5 kg fidicial mass. The dashed line denotes the modulation for dark matter events alone, whereas the solid line represent the modulation in the total (signal plus background) rate. The upper (lower) dotted curve represents the prediction for parameters in the left (right) island-region in the bottom frame of Fig. 5.5.

their signal, and not the amplitude of the signal itself. The detection of a modulated rate by CoGeNT will provide the first combined measurement of modulation and signal amplitudes (the ratio of which is the percentage modulation shown in our figures), and will thus provide an important way of discriminating dark matter events from backgrounds. For an unknown background to modulate with a fractional amplitude that is similar to that predicted for dark matter would require an unfortunate and unlikely conspiracy of nature.

There are a number of other existing direct detection experiments that may be sensitive to 5-10 GeV dark matter particles. The CDMS collaboration has used low-threshold data from their shallow Stanford site to place constraints on light dark matter particles [101]. At such low energies, however, the backgrounds observed by CDMS are not well understood, somewhat limiting their ability to probe the region implied by CoGeNT and DAMA/LIBRA. Dark matter experiments which use liquid Xenon as their target suffer from sizable uncer-

tainties in the scintillation efficiency ($L_{\rm eff}$) and recoil energy scale (Q_i) at low recoil energies [14, 84, 85, 86], making it difficult to interpret their results within the context of light dark matter.

Experiments with relatively light elements in their detectors, such as CRESST ($CaWO_4$) and COUPP (CF_3I) are potentially well suited for studying light dark matter. Throughout 2010, the CRESST collaboration described in talks an excess of events in their oxygen band [106, 107, 92, 108] which could potentially arise from the elastic scattering of a dark matter particle in the CoGeNT/DAMA region [102]. We eagerly await further details pertaining to this observation. The COUPP collaboration has very recently begun operation of their 4 kg chamber at SNOLAB. A dark matter particle near the center of the region preferred by CoGeNT and DAMA/LIBRA is predicted to generate $\sim$1 event at COUPP per day (running with a recoil energy threshold of $\sim$7 keV). If their backgrounds are as low as anticipated, they could rapidly accumulate a significant excess of events.

5.5 Summary and Outlook

The excess of low energy events reported by the CoGeNT collaboration (as well as the annual modulation reported by DAMA/LIBRA and the gamma ray emission observed from the Galactic Center) have generated a great deal of interest in 5-10 GeV dark matter particles. In this paper, we have studied the ability of current and future CoGeNT data to further elucidate this situation. Results from the first year of CoGeNT data are anticipated to be presented shortly. This data will not only enable the recoil energy spectrum of dark matter events to be measured with much greater precision, but will also likely be able to identify (or rule out) the presence of an annual modulation with a significance of 1-3σ. If observed, this would represent a major confirmation that CoGeNT's excess arises from dark matter. In the less immediate future, the planned upgrade for CoGeNT (with a fiducial mass of

approximately 2.5 kg) will further improve upon these measurements, and will provide a measurement of the energy spectrum of the modulation amplitude.

The CDMS collaboration released a low threshold analysis of their Soudan data [109], which appears to conflict with the dark matter interpretation of the CoGeNT excess. Their data set, however, contains a large number of events classified as "zero-charge" background which overlap with the region of nuclear recoil candidates. A modest uncertainty or systematic error in the energy scale calibration at energies near their threshold could plausibly shift this exclusion contour above the region being considered here [110].

CHAPTER 6

IMPLICATIONS OF COGENT'S NEW RESULTS FOR DARK MATTER

6.1 Introduction

Many of the technologies and target materials currently used in direct detection experiments are most sensitive to dark matter particles with masses greater than $\sim$10 GeV. By virtue of their very low electronic noise, however, the P-type point contact germanium detectors employed by the CoGeNT collaboration are able to detect very low energy scattering events and thus, despite their modest target mass of 475 grams (330 grams fiducial), are quite sensitive to low mass WIMPs.

In Februaru 2010, the CoGeNT collaboration reported the observation of $\sim$100 events above expected backgrounds over a period of 56 days, with ionization energies in the range of approximately 0.4 to 1.0 keV [41]. One possible interpretation of these events is the elastic scattering of dark matter particles with a mass in the range of approximately 5-10 GeV and a cross section with nucleons on the order of $\sim 10^{-40}$ cm^2 [63].

In June 2011, the CoGeNT collaboration announced the results of their analysis of a full 15 months of data [42]. This larger data set has been used to provide a much more detailed measurement of the spectrum of observed events. Furthermore, their analysis has revealed a time variation in the rate of low energy nuclear recoil events, with a quoted significance of 2.8σ. As a result of the Earth's motion around the Sun and relative to the rest frame of the dark matter halo, the rate of dark matter elastic scattering events is predicted to vary with an annual cycle (see Sec. 2.4.2 and Ref. [111]). The modulation reported by the CoGeNT

collaboration is consistent in amplitude, phase, and period with that predicted to arise from elastically scattering dark matter [112].

The only other direct detection experiment to report the observation of an annual modulation in their event rate is DAMA/LIBRA. In particular, the DAMA/LIBRA collaboration reports a high significance (8.9σ) detection of annual modulation with a phase and period consistent with elastically scattering dark matter [39]. The spectrum of the signals reported by DAMA/LIBRA and CoGeNT each point toward a similar range of dark matter parameter space [102]. Furthermore, the range of dark matter mass implied by CoGeNT and DAMA/LIBRA is very similar to that required to explain the spectrum of gamma rays observed by the Fermi Gamma Ray Space Telescope (FGST) from the the inner 0.5° around the Galactic Center [103], and for the observed synchrotron emission known as the WMAP Haze [113].

In this Chapter, we present an independent analysis of the data recently provided by CoGeNT and discuss the implications of this data for particle dark matter. In Sec. 6.2, we calculate the spectrum of events predicted to result from elastically scattering dark matter particles and compare this prediction to that reported by CoGeNT. In doing so, we find that for a reasonable range of dark matter velocity distributions, the spectrum of the CoGeNT excess is consistent with a dark matter particle with a mass in the range of 4.5 to 12 GeV. In Sec. 6.3, we discuss the properties of CoGeNT's annual modulation. In Sec. 6.4, we consider the constraints on a dark matter interpretation of the CoGeNT signal from other direct detection experiments and discuss the implications of the CoGeNT result for other dark matter searches currently being conducted. In Sec. 6.5 we summarize our results and conclusions.

6.2 CoGeNT's Spectrum and Elastically Scattering Dark Matter

The CoGeNT detector, located in Northern Minnesota's Soudan Underground Laboratory, observes nuclear recoil events as ionization. In the left frame of Fig. 6.1, we show the raw spectrum of events (between 0.5 and 3.2 keVee) observed by CoGeNT as a function of ionization energy (in keV-electron equivalent, keVee). Some of these events are the result of cosmogenically-activated radioisotopes decaying via electron capture. Most apparent are peaks appearing near 1.1 and 1.3 keVee, which result from Zn^{65} and Ge^{68}, respectively. These backgrounds correspond to the L-shell peaks associated with the isotopes listed in Table 6.1. By measuring the magnitude of the corresponding K-shell peaks (which appear at higher energies), the rate of these backgrounds can be reliably predicted. In Table 6.1, the total number of events predicted in each L-shell peak is given (over all time after the beginning of the current CoGeNT data set), along with the fractional uncertainty in this quantity. The half-life of each decay is also listed, along with the central energy of each peak (the width of each peak is determined by the energy resolution of the detector, and varies between 0.0728 and 0.0777 keVee over the relevant energy range).

In the bottom frame of Fig. 6.1, we show the spectrum of events reported by CoGeNT along with their error bars, after subtracting the L-shell peaks and correcting for the detector efficiency. Above approximately 1.5 to 2.0 keVee, the spectrum of events observed by CoGeNT is approximately flat and displays no obvious features. At lower energies, however, the rate climbs rapidly. These events appearing below 1.5 keVee are not associated with any known backgrounds [41].

To assess the hypothesis that the excess events reported by CoGeNT are the product of the elastic scattering of dark matter particles, we will compare CoGeNT's event spectrum to that predicted from dark matter. The spectrum (in nuclear recoil energy) of dark matter induced elastic scattering events is calculated in Chapter 2. We use the the standard

Isotope	Total Events	Uncertainty (%)	Energy (keV)	Half-Life (days)
As^{73}	12.74	33.48	1.414	80
Ge^{68}	639.0	1.35	1.298	271
Ga^{68}	52.83	5.11	1.194	271
Zn^{65}	211.2	2.23	1.096	244
Ni^{56}	1.53	23.46	0.926	5.9
$Co^{56,58}$	9.44	44.9	0.846	71
Co^{57}	2.59	8.0	0.846	271
Fe^{55}	44.94	11.63	0.769	996
Mn^{54}	21.09	9.34	0.695	312
Cr^{51}	2.94	15.29	0.628	28
V^{49}	14.91	12.26	0.564	330

Table 6.1: Characteristics of the backgrounds from cosmogenically-activated radioisotopes decaying via electron capture (EC). By measuring the corresponding K-shell peaks, the properties of these L-shell peaks can be well constrained. Listed here are the total number of events predicted in each L-shell peak (over all time after the beginning of the current CoGeNT data set), along with the fractional uncertainty in this quantity. The half-life of each decay is also given, along with the central energy of each peak.

Maxwell-Boltzmann distribution for the galactic halo as described in Sec. 2.4.2. We will consider values of v_0 over a range of 180 to 320 km/s and values of the galactic escape velocity between 460 and 640 km/s [11, 104, 105, 72, 38]. Departures from a Maxwellian velocity distribution are not unexpected and could non-negligibly impact the spectrum of dark matter induced events, as well as the degree of seasonal variation in the rate (see Secs. 2.4.3 ans 2.4.4 and Refs. [33, 15]). Throughout our analysis, we take $\rho_{DM} = 0.3$ GeV/cm^3. Unless stated otherwise, our results have been calculated under the assumption that $f_p = f_n$ so that the scattering cross section is given by Eq. 2.17. We also adopt the Helm form factor as described in Sec. 2.3. To convert from nuclear recoil energy to the measured ionization energy, we have scaled the results by the quenching factor for germanium as described in Refs. [74, 75, 76, 77, 78] ($Q_{\rm Ge} = 0.218$ at E_R =3 keV, and with the energy dependence predicted by the Lindhard theory [102]).

In the right frame of Fig. 6.1, we compare the prediction from dark matter to the spectrum

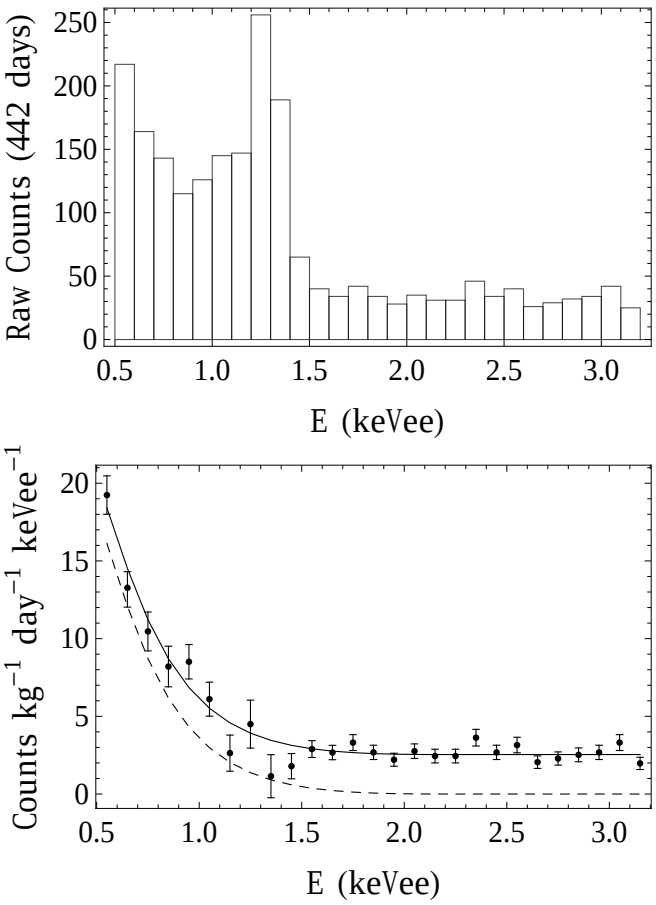

Figure 6.1: In the top frame, we show the raw spectrum of events reported by CoGeNT. In the bottom frame, the spectrum is shown after subtracting the predicted contribution from L-shell electron capture peaks and correcting for the detector efficiency. For comparison, we show the spectrum predicted for a dark matter particle with a mass of 7 GeV, an elastic scattering cross section with nucleons of 1.2×10^{-40} cm^2, a local density of 0.3 GeV/cm^3, and with a velocity distribution described by $v_0 = 250$ km/s and $v_{\rm esc} = 550$ km/s. The dashed line represents the spectrum of dark matter events alone, while the solid line is the dark matter spectrum plus a flat background.

of events observed by CoGeNT. In particular, we show the result for the case of a 7 GeV WIMP with an elastic scattering cross section with nucleons of $\sigma_{\rm DM-N} = 1.2 \times 10^{-40}$ cm^2, with a velocity distribution described by $v_0 = 250$ km/s and $v_{\rm esc} = 550$ km/s. The dashed line denotes the contribution from dark matter alone, while the solid line also includes a flat background.

Considering a wider range of dark matter masses, cross sections and velocity distributions, we show in Figs. 6.2 and 6.3 the range of parameter space that provides a good fit to the spectrum observed by CoGeNT. We find that for a reasonable range of velocity distributions, the CoGeNT spectrum can be well fit by dark matter particles with masses in the range of approximately 4.5 to 12 GeV. Here, we have allowed the normalization of the flat background to float, but have removed the L-shell peaks according to the parameters listed in Table 6.1. Also shown in these figures are contours which denote the fractional annual modulation (as a percentage of the average rate) that is predicted to be observed by CoGeNT over an energy range of 0.5-3.0 keVee (Fig. 6.2) and 0.5 to 0.9 keVee (Fig. 6.3). In the next section, we will compare the predicted and observed annual modulations in more detail.

6.3 CoGeNT's Annual Modulation

If the excess of events reported by CoGeNT is in fact the result of elastically scattering dark matter particles, then we should expect a degree of seasonal variation in the event rate. Due to the Earth's motion around the Sun, the rate of dark matter recoil events is predicted to vary throughout the year, peaking within several weeks of late May or early June (see Sec. 2.4.2). In Chapter 5, we predicted that if CoGeNT's excess is the result of dark matter, the signal rate (not including backgrounds) should modulate at a level of between 1% and 21% over the energy range of 0.4 to 1.0 keVee (and between 1% and 16% over 0.5 to 0.9 keVee) [112]. This fractional modulation is defined as $(R_{\rm summer} - R_{\rm winter})/(2R_{\rm ave})$, where $R_{\rm summer}$ and $R_{\rm winter}$ denote the maxima and minima of the rate. If non-modulating backgrounds are included, the predicted fractional modulation will be diluted accordingly.

From the contours shown in Figs. 6.2 and 6.3, we see that the newly reported CoGeNT spectrum leads to an anticipated annual modulation at the level of 5% to 16% between 0.5 and 0.9 keVee and between 4% to 10% between 0.5 and 3.0 keVee. If the rate observed by

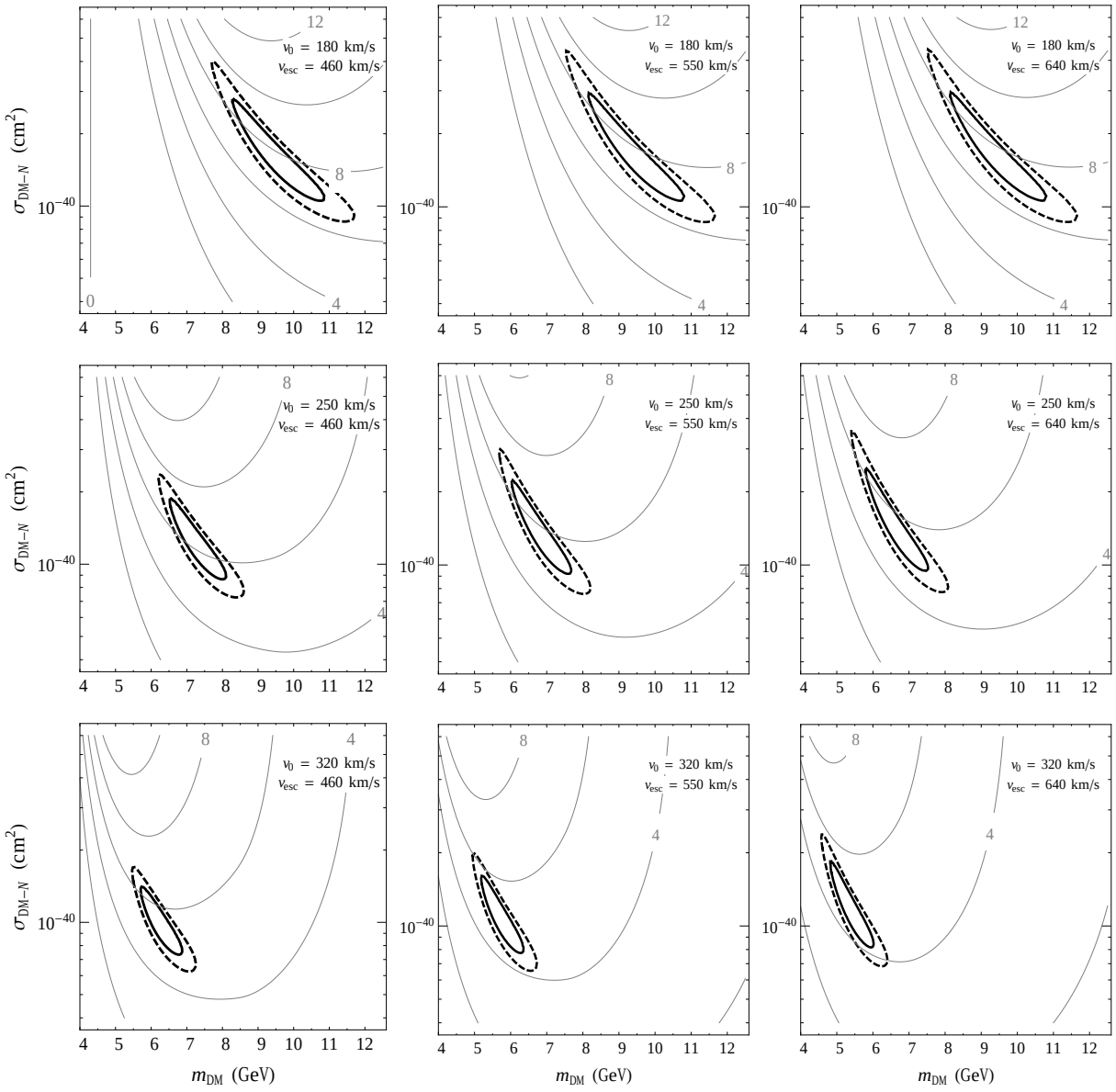

Figure 6.2: The 90% (solid) and 99% (dashed) confidence level contours for the spectrum of events observed by CoGeNT, for 9 choices of the velocity distribution parameters (v_0 and $v_{\rm esc}$). Also shown are contours for the predicted fractional modulation (given as a percentage of the overall rate) over the energy range of 0.5 to 3.0 keVee.

CoGeNT did not demonstrate an annual modulation at approximately this magnitude, it would be difficult to interpret their excess events as a product of elastically scattering dark matter.

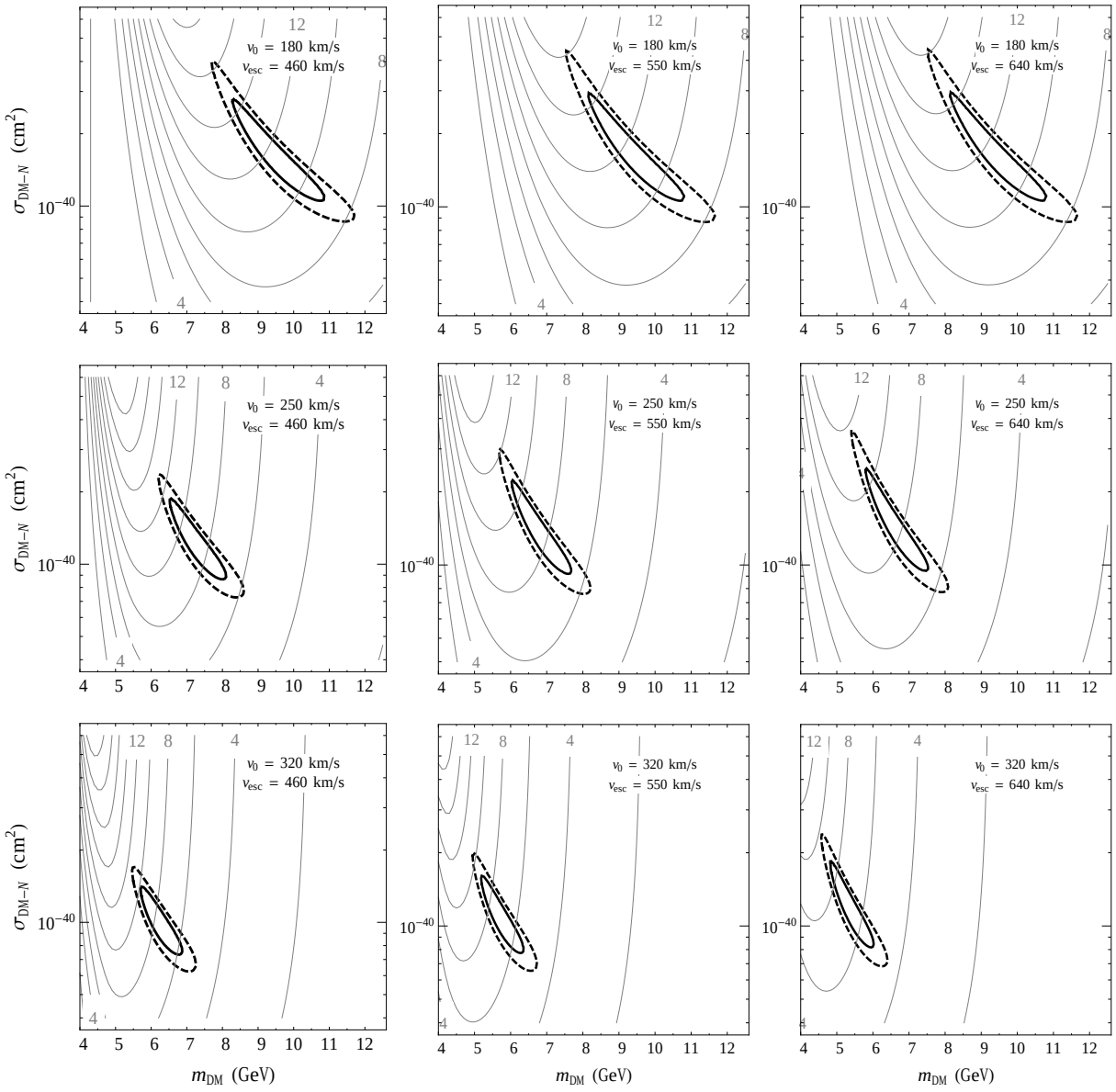

Figure 6.3: The same as Fig. 6.2, except that the contours for the predicted fractional modulation (given as a percentage of the overall rate) correspond to the energy range of 0.5 to 0.9 keVee.

In Fig. 6.4, we plot the rate of events observed by CoGeNT with energies between 0.5 and 3.2 keVee as a function of time, after subtracting the contribution from L-shell peaks. Based on our analysis of this data, we find that the presence of an annual modulation is favored over a flat event rate at a confidence level corresponding to 2.7σ (the CoGeNT

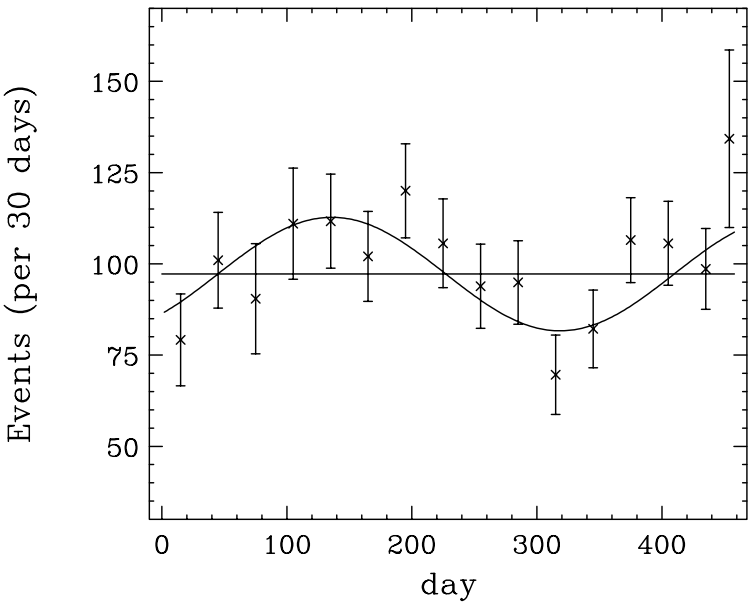

Figure 6.4: The rate of events between 0.5 and 3.2 keVee observed by CoGeNT, as a function of time, after the subtraction of L-shell peaks. Times are given in units of days since the beginning of CoGeNT's data taking (Dec. 4, 2009). The solid curve represents the best fit annual modulation (16%, peaking at April 18), while the flat line is the constant rate with the best fit normalization.

collaboration, in their own analysis, finds a similar significance of 2.8σ for events between 0.5 and 3.0 keVee [42]). In particular, we find a modulation of 16±5% (including the flat background, but after the subtraction of L-shell peaks), and with a phase that peaks at April 18±16 days. Again, the CoGeNT collaboration's analysis yields very similar conclusions (16.6±3.8%, peaking at April 16±12 days).

Comparing the phase of this observed modulation to that reported by the DAMA/LIBRA collaboration, we find that both CoGeNT and DAMA/LIBRA prefer a peak rate that occurs somewhat earlier than the late May/early June region typically expected from dark matter (the phase of DAMA/LIBRA modulation between 2 and 4 keV and between 2 and 6 keV, has been reported as May 16±7 days and May 26±7 days, respectively). The combination of CoGeNT and DAMA data collectively favor a modulation that peaks in early May. Studies based on N-body simulations find that 68% of all realizations feature a peak rate that is

within ± 20 days from late May/early June [33]. Thus we conclude that the phase of the modulation favored by CoGeNT is consistent with that reported by DAMA/LIBRA, and with that expected from elastically scattering dark matter.

Although the statistics provided by CoGeNT are limited, we can begin to study the spectrum of the observed modulation amplitude. In Fig. 6.5, we show the observed modulation amplitude, for three choices of the phase (peaking at April 18, May 9, and May 26). We find the presence of modulation in each of the three energy bins below 3.2 keVee, but no statistically significant modulation at higher energies. We also show in each of these frames the modulation spectrum that is predicted for two dark matter scenarios: $m_{\rm DM} = 7$ GeV, $v_0 = 250$ km/s (solid) and $m_{\rm DM} = 11$ GeV, $v_0 = 180$ km/s (dashed); each with $\sigma_{{\rm DM}-N} = 1.2 \times 10^{-40}$ cm^2 and $v_{\rm esc} = 550$ km/s. At this point, we note that there appears to be somewhat more modulation observed at 1.4-3.2 keVee than is predicted, although more data will be needed to evaluate this issue with satisfactory statistical significance. The modulation in this energy range could be enhanced if the dark matter's velocity distribution were to depart significantly from the Maxwellian form that we have assumed (see Sec.2.4.3.

6.4 Results Of and Prospects For Other Direct Detection Experiments

In this section, we discuss the implications of the results of other direct detection experiments on a dark matter interpretation of the CoGeNT spectrum and modulation. We will also discuss the prospects for other direct detection experiments which may be sensitive to dark matter in the $\sim$5-10 GeV mass range.

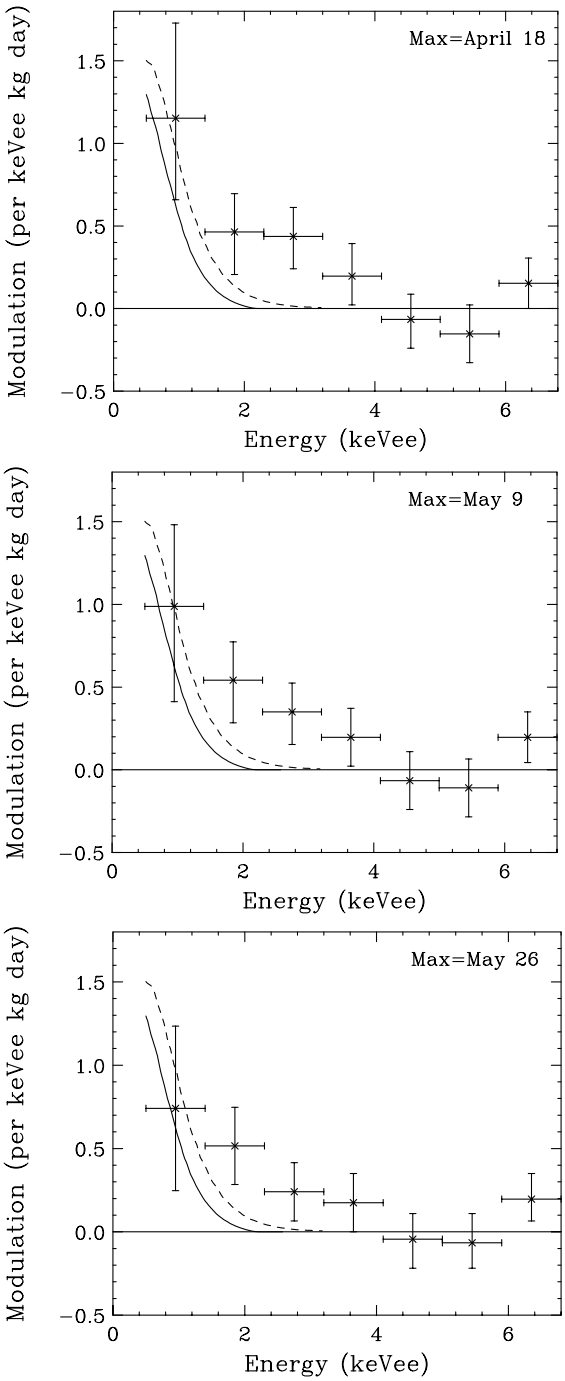

Figure 6.5: The spectrum of the annual modulation amplitude observed by CoGeNT for three choices of the phase. Also shown for comparison is the modulation spectrum predicted for two dark matter scenarios: $m_{\rm DM} = 7$ GeV, $v_0 = 250$ km/s (solid) and $m_{\rm DM} = 11$ GeV, $v_0 = 180$ km/s (dashed); each with $\sigma_{{\rm DM}-N} = 1.2 \times 10^{-40}$ cm^2 and $v_{\rm esc} = 550$ km/s.

6.4.1 Comparison With Results From DAMA/LIBRA

The only direct detection experiment other than CoGeNT to report the observation of an annual modulation is DAMA/LIBRA [39]. The statistical significance of DAMA's modulation is very high (8.9σ), and demonstrates a phase which is compatible with that measured by CoGeNT (peaking at May 16$\pm$7 days between 2 and 4 keV and May 26$\pm$7 days between 2 and 6 keV, compared to April 18$\pm$16 days for CoGeNT). The combination of CoGeNT and DAMA/LIBRA data favor a modulation that peaks in early May, which is consistent with expectations from dark matter simulations [33].

In Fig. 6.6, we compare the regions of the dark matter parameter space favored by the CoGeNT spectrum to those favored by the modulation spectrum reported by DAMA/LIBRA (the DAMA region has been taken from Ref. [102], and we have used the velocity distribution parameters from that study for comparison). The agreement is clearly very good, but requires the quenching factors for low energy nuclear recoils on sodium to be somewhat larger than are often assumed ($Q_{\rm Na} \sim 0.40 - 0.45$ rather than $Q_{\rm Na} \sim 0.3$, see also Ref. [83]) [102]. We have not included any effects of channeling [114] in these results. If significant channeling occurs in DAMA's NaI crystals, the favored range of masses and cross sections would be modified.

6.4.2 Constraints From CDMS and XENON

The CDMS and XENON100 collaborations have each presented results which they interpret to exclude or strongly constrain dark matter interpretations of the CoGeNT signal (see Fig. 6.7). Here, we will briefly review these results and discuss means by which they could potentially be reconciled with CoGeNT.

In April of 2011, the XENON100 collaboration presented the result of their first 100 live days of data [12], and conclude that (for a velocity distribution given by $v_0 = 220$ km/s,

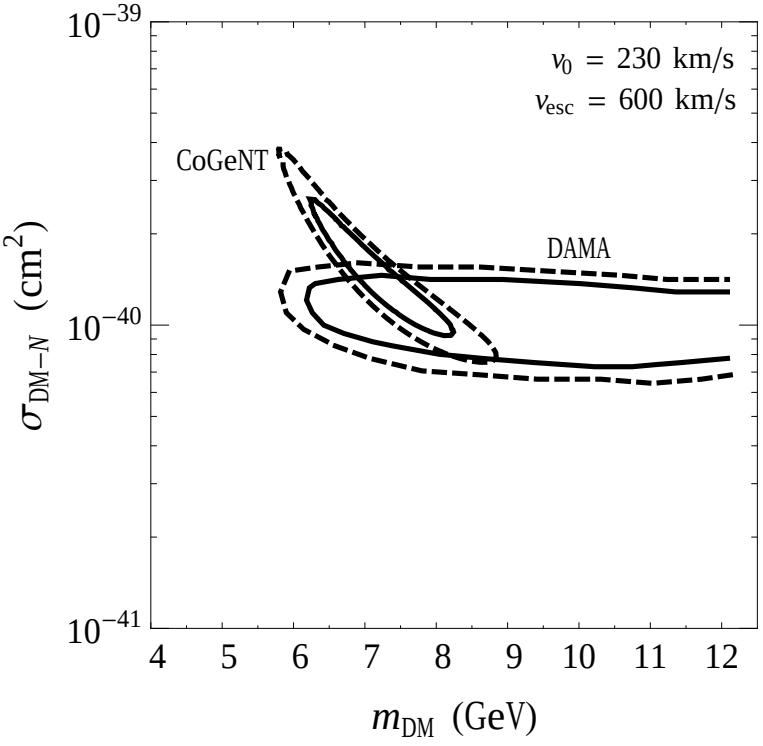

Figure 6.6: A comparison of the parameter space favored by the CoGeNT spectrum with that favored by the modulation spectrum reported by DAMA/LIBRA [102]. Good agreement is found, but somewhat large quenching factors for low energy nuclear recoils on sodium are required ($Q_{\rm Na} \sim 0.40 - 0.45$) [102].

$v_{\rm esc} = 544^{+64}_{-46}$ km/s) a dark matter particle with a mass of 7 GeV is required to possess a nucleon-level cross section less than $\sim 3 \times 10^{-41}$ cm^2. The constraint falls off quickly with the mass of the dark matter, however; for a 6 GeV mass, for example, the quoted constraint is weaker by a factor of five, to $\sim 1.5 \times 10^{-40}$ cm^2 (see Fig. 6.7). At face value, this result appears to exclude the region of parameter space consistent with the spectrum reported by CoGeNT. There are a number of ways, however, in which this constraint could be significantly weaker than it appears. Firstly, any uncertainties in the scintillation efficiency of liquid xenon, $L_{\rm eff}$, and/or in the quenching factor of germanium, could impact the corresponding constraints for dark matter particles with mass in the range of interest. The XENON100 constraints have been derived using measurements of $L_{\rm eff}$ as described in Refs. [116, 96], which have

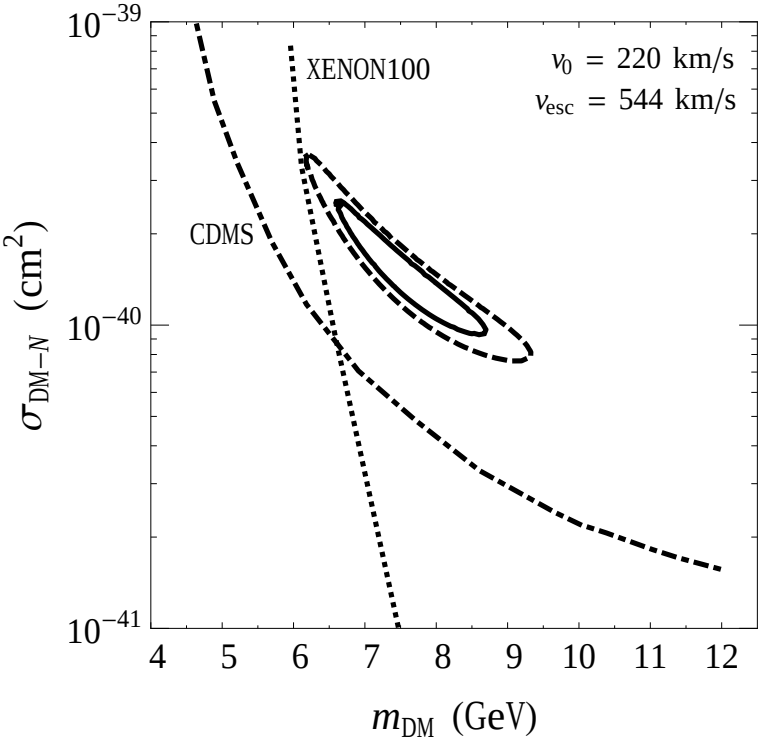

Figure 6.7: Constraints on light dark matter particles as presented by the CDMS (dot-dash) [109] and XENON100 (dotted) [12] collaboration. For a discussion of these constraints and their implications for CoGeNT, see the text and Refs. [14, 13, 115].

been criticized in Refs. [14, 13]. Even modest changes to these values at the lowest measured energies ($\sim$3-4 keV) can lead to much weaker constraints on light dark matter particles. It has been been argued that the relatively large (9.3 eV) band-gap in liquid xenon should lead to suppression of xenon's sensitivity to nuclear recoils in the energy range of interest (see Ref. [14] and references therein). Many of these issues also apply to constraints on light dark matter making use of only the ionization signal in liquid xenon detectors [117].

Alternatively, any apparent conflict between CoGeNT and XENON100 could be resolved if dark matter particles couple differently to protons and neutrons [63, 118]. In particular, for a ratio of these couplings given by $f_n/f_p \approx -0.7$, the constraint from xenon-based experiments is weakened by a factor of $\sim$20 relative to that found in the $f_n = f_p$ case.

The rate of low energy events reported by the CDMS collaboration is also somewhat lower than those observed by CoGeNT [109, 101]. The degree to which these spectra are discrepant has been discussed elsewhere, and depends on issues such as the precise calibration of the CDMS energy scale, and on the choice of basing the CDMS measurement on the single detector with the lowest rate, or on the average of the eight detectors (see Ref. [115] and the appendix of Ref. [109] for opposing viewpoints on this and related issues).

As both CDMS and CoGeNT use germanium (along with silicon in the case of CDMS) as their dark matter target, differences in their relative rates cannot be accounted for by varying the ratio of f_n and f_p. One possibility is that the relatively warm temperature of CoGeNT compared to CDMS ($T \approx 90$ K vs. 0.040 K) leads to a fraction of events to be channeled at CoGeNT, but not at CDMS. Although theoretical estimates suggest that the probability of channeling is too low to account for this discrepancy [68], the non-occurrence of channeling in germanium crystals is yet to be experimentally confirmed.

6.4.3 Predictions For COUPP and CRESST

Experiments which make use of relatively light elements, such as CRESST ($CaWO_4$) and COUPP (CF_3I) are potentially well suited to detect and study light dark matter particles. If CoGeNT is in fact observing the elastic scattering of dark matter particles, these experiments should also be capable of observing such events.

In a number of conference talks given since late 2010, members of the CRESST collaboration have reported an excess of events which appears to be consistent with the elastic scattering of dark matter [106, 107, 92, 108]. More specifically, based on approximatley 700 kg-days of data, CRESST observes a rate of events in their oxygen band (events which are consistent with the recoil of an oxygen nucleus) which is in excess of their expected backgrounds at the level of 4.6σ. For dark matter particles with a mass in the range favored by

CoGeNT, spin-independent scattering is expected to occur mostly with oxygen nuclei (rather than with CRESST's tungsten or calcium). Although more details of this analysis will be needed before any firm conclusions can be drawn, the preliminary results from CRESST appear to favor dark matter particles with a mass and elastic scattering rate similar to that implied by CoGeNT [106, 107, 92, 108, 102]. In particular, it was recently reported that the spectrum of CRESST's events is best fit by a dark matter particle with a mass of 13 GeV and a cross section with nucleons of 3×10^{-41} cm^2, although the confidence contours around this best fit model have not been reported [106, 107, 92, 108]. We eagerly await further details pertaining to the CRESST analysis.

The COUPP collaboration has begun operation of their 4 kg chamber at SNOLAB (3.3 kg fiducial). A dark matter particle near the center of the region preferred by CoGeNT and DAMA/LIBRA is predicted to generate $\sim$0.7 events at COUPP per day, when running with a recoil energy threshold of $\sim$7 keV. If their backgrounds are as low as anticipated, COUPP could rapidly accumulate a significant excess of events.

Over the past several months, the 4 kg COUPP chamber has been operated at temperatures and pressures corresponding to three different recoil energy thresholds, estimated at 7, 10 and 15 keV. In Fig. 6.8, we show the event rate predicted at COUPP for a CoGeNT-like dark matter particle, as a function of the recoil energy threshold. From this figure, it is clear that this variation of threshold is predicted to result in a dramatic variation in the rate of dark matter induced events. The approximately 20 live days of data taken at each of 7 and 10 keV thresholds [119] should be anticipated to contain $\sim$14 and $\sim$4 events, respectively, from dark matter scattering. In contrast, less than one event per month is anticipated when running with a threshold of 15 keV. With a sufficiently large exposure, it may also be possible for COUPP to observe season variations in their event rate. The predicted rate with a 15 keV threshold, in particular, can vary by a factor of 2-3 between summer and winter.

Both COUPP and CRESST could enhance their event rate from light dark matter par-

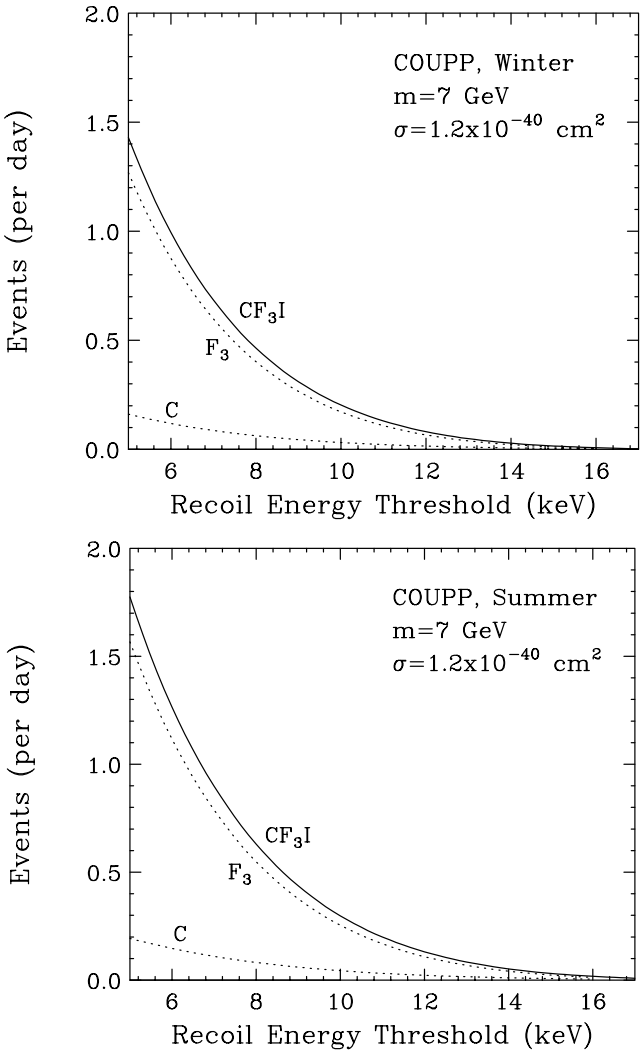

Figure 6.8: The event rate (with a fidicual mass of 3.3 kg) at COUPP from a CoGeNT-like dark matter particle as a function of the recoil energy threshold and in the winter (left) and summer (right). The overall rate is predicted to vary dramatically with threshold.

ticles per target mass by adopting a target material which does not contain heavy nuclei. The COUPP collaboration, for example, has considered replacing their CF_3I target with C_3F_8, resulting in a roughly 50% higher event rate from light dark matter particles (after accounting for the lower density). Similarly, the CRESST collaboration is considering using Al_2O_3 as a target more favorable for low mass dark matter [106, 107, 92, 108].

6.5 Summary and Conclusions

The possibility that the excess of low energy events as originally reported by the CoGeNT collaboration in February of 2010 [41] is the result of elastically scattering dark matter particles has received a great deal of attention [120, 121, 122, 123, 124, 125, 126, 127, 128, 129, 130, 131, 65, 64, 132, 112, 102, 15, 63, 118]. The most clear and straightforward test of this hypothesis was to observe whether or not the rate of this excess modulated with time, and if so whether its modulation was consistent in amplitude, phase, and period with the annual modulation predicted for elastically scattering dark matter [111, 102, 112, 38]. With the most recent results from CoGeNT, based on 15 months of data taking, we have learned that such a modulation does in fact appear to be present (with a statistical significance of 2.7-2.8σ), and is consistent with a simple interpretation as a relatively light dark matter particle ($m \approx$5-12 GeV) with a sizeable elastic scattering cross section with nucleons ($\sigma_{\rm DM-N} \sim 10^{-40}$ cm^2).

In this paper, we have independently analyzed the CoGeNT data (as made available by the CoGeNT collaboration) and reached similar conclusions to those presented by the CoGeNT collaboration [42]. In particular, we find that over the energy range of 0.5 to 3.2 keVee, the overall rate (after the substraction of L-shell peaks) modulates with an amplitude of $16 \pm 5\%$, with a period consistent with one year, and with a phase that peaks at April 18 ± 16 days. If the true phase peaks in early May, this would represent a modulation consistent with that reported by the DAMA/LIBRA collaboration [39].

Looking forward, it is clear that more data will be required to better explore the dark matter interpretation of the CoGeNT signal. Although the current data set is sufficient to identify a modestly statistically signficant annual modulation, the energy spectrum of this modulation can not yet be studied in much detail. The existing CoGeNT detector has recommenced its operation following the fire in the Soudan Mine, and the additional

exposure will certainly be valuable in further efforts to the characterize the signal in question. Furthermore, the first of four detectors to make up the CoGeNT-4 (C4) experiment is planned to be deployed soon. Each of these four detectors will offer a fiducial mass two to three times larger than in the current CoGeNT detector. Approximately 17 months of data taken with the first of the C4 detectors is projected to identify the presence of annual modulation with a significance of 5σ. The entire C4 experiment will offer the ability to measure the spectrum of this modulation in considerable detail, allowing us to begin to disentangle the mass and cross section of the dark matter particle from the dark matter's velocity distribution.

If the excess CoGeNT events and their modulation is the result of an elastically scattering dark matter particle, then the CRESST and COUPP experiments should also be capable of observing a signficant rate of dark matter induced events. The CRESST collaboration has reported the observation of an excess of events roughly consistent with that anticipated from a CoGeNT-like dark matter particle. We eagerly await further details from CRESST, and the presentation of the first results from COUPP at SNOLAB.

CHAPTER 7

TOWARD A CONSISTENT PICTURE FOR CRESST, COGENT AND DAMA

7.1 Introduction

Recently, a great deal of attention has been given to a number of dark matter experiments which have reported signals that do not appear to be consistent with any known backgrounds. The longest standing of these claims is from the DAMA (and more recently the DAMA/LIBRA) collaboration, which has reported annual variation in the event rate at their lowest observed energies, in keeping with the predictions from dark matter scattering [39]. In early 2011, the CoGeNT collaboration reported that their previously observed excess of low-energy events also exhibits seasonal variation [41, 42], similar to the signal reported by DAMA/LIBRA. The CRESST-II collaboration has reported an excess of events potentially attributable to dark matter [43].

A casual comparison of these results can be confusing or even misleading. Conventionally, both experimentalists and theorists in the field of dark matter direct detection report their constraints and other results as derived using specific astrophysical assumptions and estimates of detector response. Adopting a single choice for each of these characteristics (even if that choice represents a reasonable estimate), rather than marginalizing over the possible or plausible range of those choices, can lead to regions of compatibility that are artificially small, and to constraints which are artificially stringent.

In this Chapter, we revisit the signals reported by the CRESST-II, CoGeNT and DAMA/LIBRA collaborations, and attempt to determine whether they can be consistently

explained with dark matter. In particular, in Sec. 7.2, we study and directly compare the spectra of excess events reported by CoGeNT and CRESST-II, and from this conclude that (for reasonable astrophysical assumptions) a dark matter particle with a mass of roughly 10-20 GeV and an elastic scattering cross section with nucleons of approximately $(1-3)\times10^{-41}$ cm^2 could account for the excess events reported by each of these collaborations. We also note that a sizable fraction of this parameter space is consistent with the constraints placed by the CDMS-II collaboration. The constraints presented by the XENON-100 and XENON-10 collaborations, however, remain in conflict, unless either the response of liquid xenon to very low-energy nuclear recoils is lower than previously claimed, or the dark matter's couplings to protons and neutrons destructively interfere for a xenon target. In Sec. 7.3, we compare the annual modulation signals reported by the DAMA/LIBRA and CoGeNT collaborations. Again, we find good agreement between the results of these two experiments, but point out that under common assumptions (Maxwellian velocity distributions and velocity independent scattering cross sections), the amplitude of the observed modulation requires the dark matter to possess a significantly larger (by a factor of approximately 3–10) elastic scattering cross section than would be inferred from the spectra reported by CoGeNT and CRESST-II. In Sec. 7.4.1, we explore how this apparent discrepancy between the observed event rate and modulation amplitude could potentially be resolved by the presence of streams or other non-Maxwellian velocity structures in the local distribution of dark matter, or by dark matter with a velocity-dependent scattering cross section with nuclei. In Sec. 7.5, we summarize our results and draw conclusions.

7.2 The Nuclear Recoil Spectrum

The CoGeNT and CRESST-II collaborations have each reported an excess of nuclear recoil candidate events, difficult to attribute to known backgrounds. In this section, we discuss the

energy spectra of these events and the dark matter parameter space which could potentially account for these signals.

7.2.1 CoGeNT's Event Spectrum

CoGeNT is a P-type point contact germanium detector with very low levels of electronic noise, enabling sensitivity to very low-energy nuclear recoils, and thus very low mass dark matter particles. Located in Northern Minnesota's Soudan Underground Laboratory, CoGeNT observes nuclear recoil events as ionization, and has thus far reported the results of 15 months of data collection, taken between December 2009 and March 2011 [41, 42].

In the upper-left frame of Fig. 7.1, we show the spectrum of events reported by CoGeNT as a function of ionization energy (in keV-electron equivalent, keVee), after subtracting the L-shell electron capture peaks (as described in Ref. [133]). Above about 1.5 keVee, the spectrum observed by CoGeNT is approximately flat and featureless, and is thought to be dominated by Compton scattering events. At lower energies, the observed rate climbs rapidly. While contamination from (non-rejected) surface events is expected to contribute significantly near threshold, it does not appear to be possible to account for the observed low-energy rate with this or other known backgrounds.

To assess the hypothesis that the excess events reported by CoGeNT are the product of the elastic scattering of dark matter particles, we compare CoGeNT's event spectrum to that predicted from dark matter. The spectrum (in nuclear recoil energy) of dark matter induced elastic scattering events is calculated as described in Chapter 2. We use the the standard Maxwell-Boltzmann distribution for the galactic halo as described in Sec. 2.4.2. As a default choice, we adopt the commonly used values of $v_0 = 220\,\mathrm{m/s}$ and a Galactic escape velocity of $544\,\mathrm{km/s}$. This function should be thought of as a reasonable, but approximate, parametrization of the dark matter's true velocity distribution. Departures

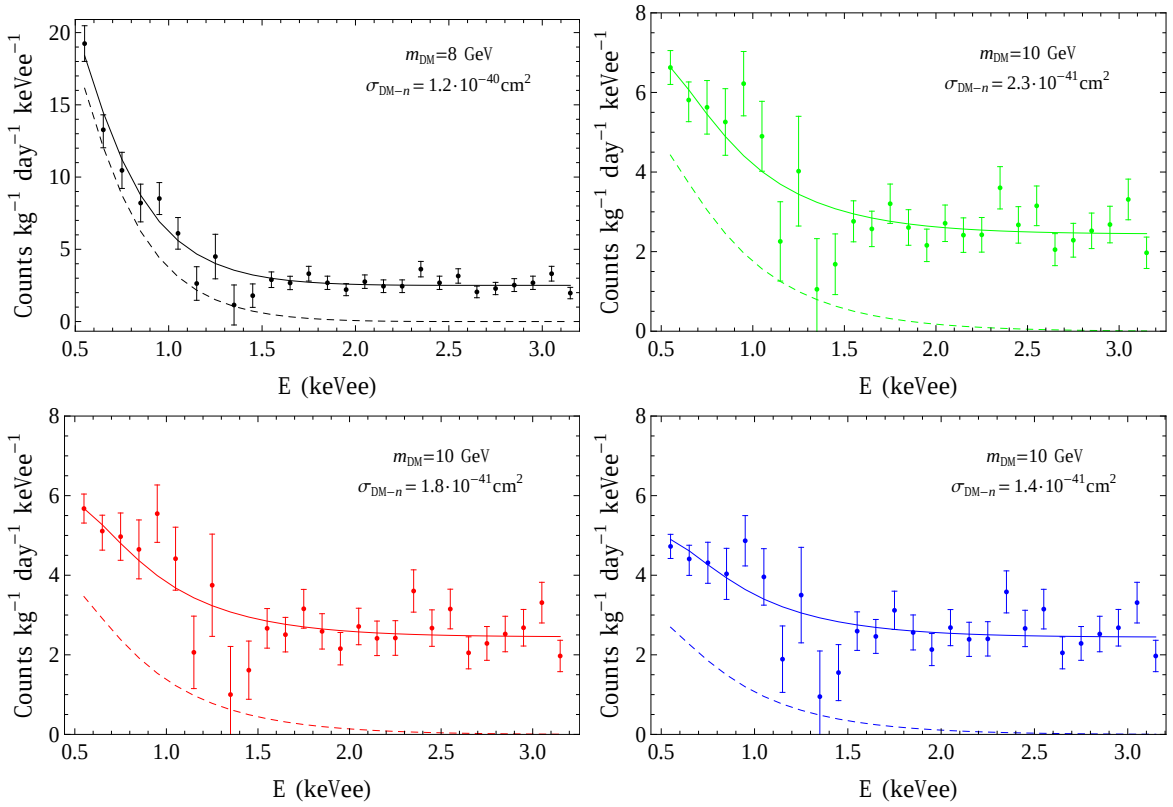

Figure 7.1: In the upper-left frame, we show the raw spectrum of nuclear recoil candidate events as observed by CoGeNT, as originally presented in Ref. [133]. In the other three frames, this spectrum has been corrected using three different estimates for CoGeNT's surface event correcton factor, as shown in Fig. 7.2. In each frame, a spectrum of events from dark matter is shown (dashed line), along with this signal plus a flat background from Compton scattering (solid line).

from a Maxwellian velocity distribution are in fact required for consistency with observed (and simulated) halo density profiles (see, for example, Ref. [15] and references therein). Such departures can non-negligibly impact the spectrum of dark matter induced events, and can significantly modify the degree of seasonal variation in the rate [15, 33]. In Sec. 7.4.1, we will return to this issue and examine the extent to which non-Maxwellian structures in the velocity distribution could potentially impact the signals reported by direct detection experiments.

Throughout our analysis, we take $\rho_{DM} = 0.3$ GeV/cm^3. Unless stated otherwise, our

results have been calculated under the assumption that $f_p = f_n$ so that the scattering cross section is given by Eq. 2.17. We also adopt the Helm form factor as described in Sec. 2.3. To convert from nuclear recoil energy to the measured ionization energy, we have scaled the results by the quenching factor for germanium as described in Refs. [74, 75, 76, 77, 78] ($Q_{\rm Ge} = 0.218$ at E_R =3 keV, and with the energy dependence predicted by the Lindhard theory [102]).

Although the majority of surface events have been removed from the spectrum presented by the CoGeNT collaboration through the application of a rise-time cut, this spectrum does not take into account any inefficiencies in their surface event rejection algorithm. While it was initially estimated that the signal would suffer only a minor degree of contamination from non-rejected surface events [41], the CoGeNT collaboration has recently reported a somewhat higher estimate for the rate of non-rejected surface events near their energy threshold [134]. This (preliminary) estimate of the fraction of the event spectrum which consists of non-surface events (*i.e.* nuclear recoil candidate events) is shown in Fig. 7.2. Any unidentified surface events constitute an additional background that should be accounted for when attempting to identify a dark matter signal from the CoGeNT detector. As can be observed from Fig. 7.2, this new measurement significantly reduces the estimate of the number of low-energy events that could potentially be attributed to dark matter. The precision of this measurement is expected to improve over time as more statistics are accumulated.

In Fig. 7.1, we show the spectrum events at CoGeNT, for several different choices of the surface event correction factor. As mentioned previously, the upper-left frame of Fig. 7.1 depicts the spectrum of events assuming a perfect surface event rejection efficiency (100% of all surface events are identified as such, at all energies). The other three frames show the remaining spectrum of events after applying the most mild (green), central (red), and most stringent (blue) correction factor, as shown in Fig. 7.2, to the raw spectrum. For each of these choices of the surface event correction factor, we find that the resulting spectrum

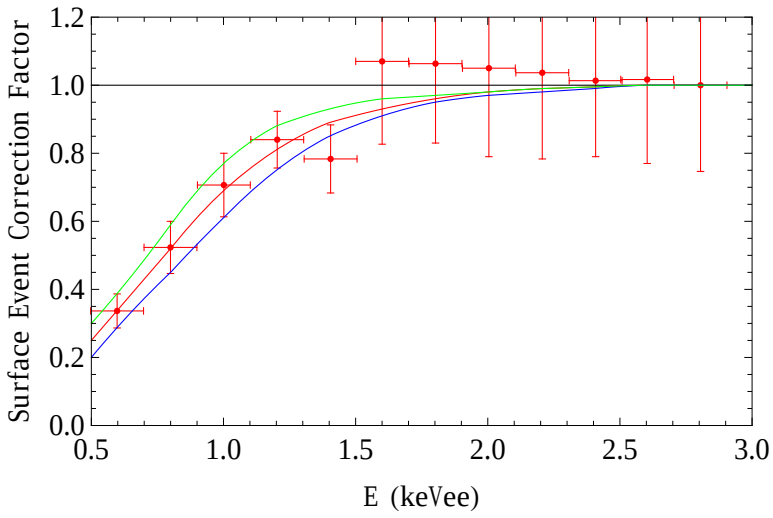

Figure 7.2: CoGeNT's surface event rejection correction factor (the fraction of nuclear recoil candidate events that are not surface events) as recently presented in Ref. [134]. The four curves shown (including the horizontal line) correspond to the correction factors used to generate the corresponding spectra in Fig. 7.1.

can be explained by an elastically scattering dark matter particle, although with slightly differing ranges of masses and cross sections. In each frame, we show an example of a good fit, with the dashed line denoting the signal from the dark matter alone and the solid line also including a flat background from Compton scattering events, in each case correcting for the detector efficiency, as described in Ref. [41].

In Fig. 7.3 we plot the regions of dark matter parameter space that provide a good fit to the efficiency corrected spectra shown in Fig. 7.1. In each case, we have allowed the normalization of the flat background to float. As expected, the inclusion of the non-rejected surface event background shifts the preferred region towards smaller cross sections, as there is now less dark matter signal then expected previously. The range of dark matter masses favored also shifts upward somewhat as a result of the additional surface event background.

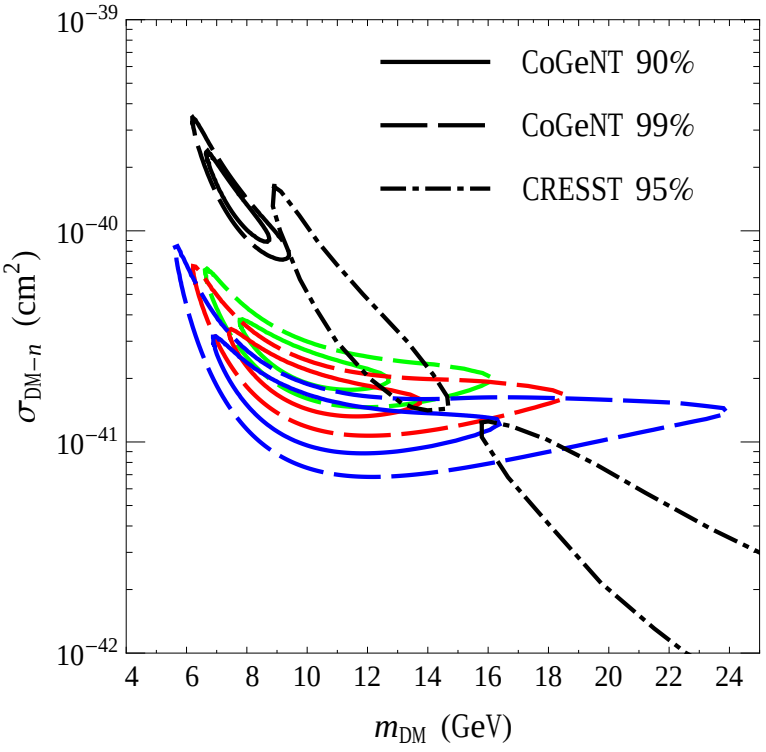

Figure 7.3: The 90% (solid) and 99% (dashed) confidence level contours for the spectrum of events observed by CoGeNT, with each color matching the corresponding correction factors shown in Fig. 7.2. The CRESST contours (dot-dashed) denote the 95% confidence level regions. A dark matter particle with a mass of approximately 10-20 GeV and an elastic scattering cross section with nucleons of approximately $(1-3)\times 10^{-41}$ cm^2 can account for the excess events reported by each of these experiments.

7.2.2 CRESST's Event Spectrum

The CRESST-II collaboration makes use of eight 300 gram cryogenic $CaWO_4$ detectors, operating in Italy's Laboratori Nazionali del Gran Sasso. Due to the relatively light oxygen and calcium nuclei in their target, CRESST is quite sensitive to dark matter particles in the mass range favored by CoGeNT. CRESST observes events through both scintillation and heat (phonons), enabling them to discriminate nuclear recoil candidate events from a variety of backgrounds.

The CRESST-II collaboration released an analysis of their first 730 kg-days of data,

taken over a period between 2009 and 2011 [43]. The analysis identified 67 low-energy nuclear recoil candidate events, which is at least 30% more than can be accounted for with known backgrounds. The CRESST-II collaboration has assessed the statistical significance of this excess to be greater than 4σ.

The CRESST-II analysis identified two distinct regions of dark matter parameter space which are compatible with the observed excess (see Fig. 7.3). In the high mass region (referred to as M1), the majority of the excess events arise from dark matter recoils with tungsten nuclei. Within the low mass (M2) region, in contrast, the excess events are dominated by recoils on both oxygen and calcium. In an independent analysis based on the publicly available portions of the CRESST data, Ref. [135] identified a similar, but somewhat larger, region of compatible dark matter parameter space.

As can be seen in Fig. 7.3, the dark matter parameter space favored by CRESST-II is compatible with the region implied by CoGeNT's spectrum, after correcting for surface event contamination. In particular, a dark matter particle with a mass of roughly 10-20 GeV and an elastic scattering cross section with nucleons of $(1-3)\times10^{-41}$ cm^2 could account for the excess events reported by both collaborations.

7.2.3 Constraints From Other Experiments

A number of direct detection experiments have produced constraints which are relevant to the interpretation of the events reported by CoGeNT and CRESST-II. In particular, the impact of the constraints presented by the CDMS-II, XENON-100, and XENON-10 collaborations are significant for the regions of low-mass dark matter parameter space favored by CoGeNT and CRESST-II.

The CDMS-II collaboration has presented the results of two analyses searching for dark matter particles in the mass range collectively favored by CoGeNT and CRESST [109, 101].

Before taking into account the updated estimates of CoGeNT's surface event rejection efficiency, these constraints appeared to be in conflict with a dark matter interpretation of CoGeNT's excess (see, however, Ref. [115]). As both CDMS and CoGeNT make use of germanium detectors, and thus are sensitive to similar systematic factors such as quenching factors for low-energy nuclear recoils, it was generally considered difficult to reconcile CDMS's constraints with a dark matter interpretation of CoGeNT. In light of the CoGeNT collaboration recent estimate for their surface event rejection efficiency, however, this apparent conflict seems to be largely resolved. In Fig. 7.4, we compare the spectrum at CoGeNT (after subtracting the flat, Compton scattering, component, and applying the central estimate for the surface event correction factor) to that reported by the low-threshold analysis of CDMS-II. While the spectrum below 1.2 keVee from CDMS's T1Z5 detector is slightly lower than that observed by CoGeNT, the all-detectors spectrum reported by CDMS is in good agreement with CoGeNT's.

The XENON-100 [12] and XENON-10 [117] collaborations have also each reported rather strong constraints on the parameter space of low-mass dark matter particles. As presented, these constraints appear to largely rule out the dark matter parameter space collectively favored by CoGeNT and CRESST. There are a number of ways, however, in which these constraints could be significantly weaker than they might appear. Firstly, any uncertainties in the response of liquid xenon to very low-energy nuclear recoils (as encapsulated in the functions $L_{\rm eff}$ and/or Q_y) could significantly impact the corresponding constraints for dark matter particles with a mass in the range of interest. The constraints from the XENON-100 collaboration were derived using measurements of the scintillation efficiency, $L_{\rm eff}$, as described in Refs. [116], which have been criticized in Ref. [13] (see also Ref. [14]). Even modest changes to these values at the lowest measured energies ($\sim$3-4 keV) can lead to much weaker constraints on light dark matter particles. It has also been argued that the relatively large (9.3 eV) band-gap of xenon is expected to lead to a suppression of the response to

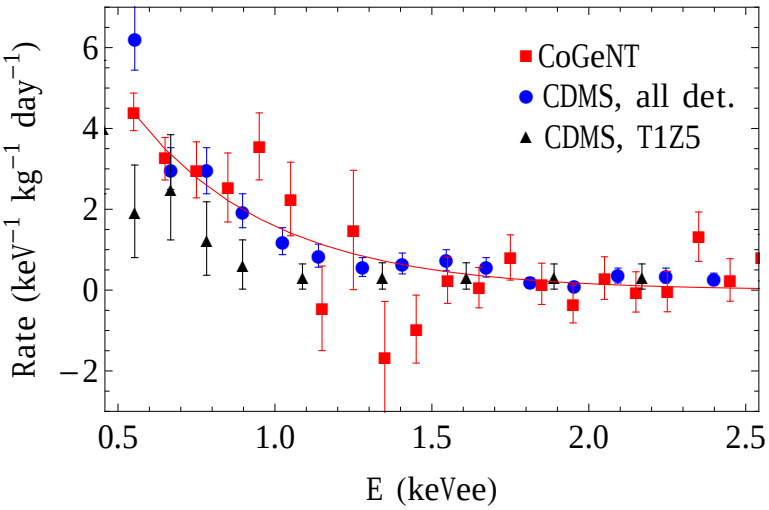

Figure 7.4: A comparison of CoGeNT's spectrum (using the central estimate for the surface event correction factor, as shown in Fig. 7.2) with that reported by the CDMS-II collaboration [109]. We have subtracted the flat (Compton scattering) component from CoGeNT's spectrum, and corrected for CoGeNT's efficiency. The solid curve represents the prediction for a 10 GeV dark matter particle with an elastic scattering cross section of $\sigma_n = 1.8 \times 10^{-41}$ cm^2. The spectrum observed by the combination of all of CDMS's detectors is in good agreement with that observed by CoGeNT, although the spectrum from the single detector, T1Z5, is slightly lower than CoGeNT's below 1.2 keVee.

nuclear recoils in the energy range of interest (see Ref. [14] and references therein). Many of these issues also apply to constraints on light dark matter making use of only the ionization signal in liquid xenon detectors [117].

Alternatively, the constraints from XENON-100 and XENON-10 could be modified if dark matter particles do not have identical couplings to protons and neutrons [63, 118]. In particular, for a ratio of couplings given by $f_n/f_p \approx -0.7$, the constraint from xenon-based experiments is weakened by a factor of $\sim$20 relative to that found in the $f_n = f_p$ case [118]. For this ratio of couplings, the cross section favored by CRESST-II would also be moved down by a factor of $\sim$7 relative to that observed by CoGeNT. Alternatively, a ratio of $f_n/f_p \approx -0.6$ would reduce the strength of the XENON-100 and XENON-10 constraints by a factor of 3-4, while also lowering the CRESST-II region (relative to that of CoGeNT) by a similar factor.

Lastly, we note that a constraint has also been placed by making use of the CRESST commissioning run data [136]. These results appear to be in mild tension with the upper range (in cross section) of the parameter space reported to be favored by the analysis of the CRESST-II collaboration.

7.3 Annual Modulation

If a population of events observed in a detector are in fact the result of elastically scattering dark matter particles, then we should expect the Earth's motion around the Sun to induce a degree of seasonal variation in the rate of those events. For most commonly assumed velocity distributions of dark matter particles, the rate is predicted to follow a roughly sinusoidal behavior, with a peak that occurs within several weeks of late May or early June (see Sec. 2.4.2 and Ref.[111]).

The CoGeNT and DAMA/LIBRA collaborations have each reported the observation of annual modulation of their event rates. In this section, we characterize and compare the modulation signals reported by these collaborations, and discuss whether these signals could be the result of dark matter.

7.3.1 DAMA/LIBRA's Modulation

The DAMA/LIBRA experiment makes use of a large mass detector (242.5 kg in its current form) consisting of high purity NaI(Tl) crystals, located at Gran Sasso. DAMA/LIBRA observes nuclear recoil events as scintillation, and is designed to search for time variations in their event rate, rather than to identify individual dark matter candidate events.

Based on the data collected over a period of 13 annual cycles, the DAMA/LIBRA collaboration reports evidence of an annual modulation with a statistical significance of 8.9σ. The variation of their rate is consistent with a sinusoid peaking at May 16$\pm$7 days at energies

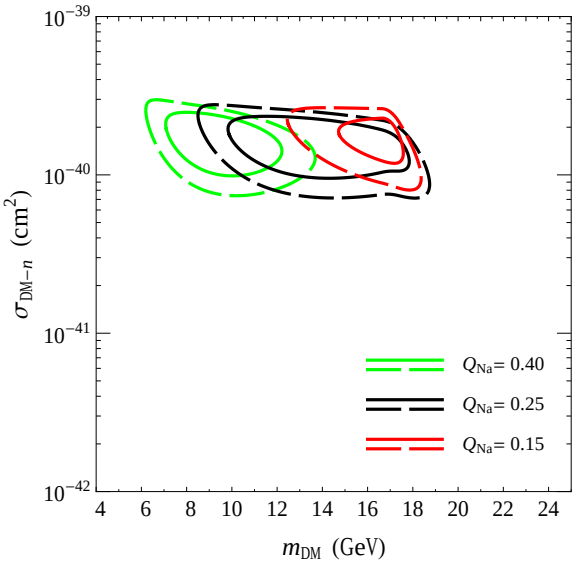

Figure 7.5: The 90% (solid) and 99% (dashed) confidence level contours for the spectrum of the amplitude of the annual modulation observed by DAMA/LIBRA, assuming a simple Maxwellian velocity distribution with $v_0 = 220\,\mathrm{km/s}$ and $v_{\mathrm{esc}} = 544\,\mathrm{km/s}$. Contours are shown for three choices of the low-energy sodium quenching factor, Q_{Na}.

between 2 and 4 keV, May 22±7 days between 2 and 5 keV, and May 26±7 days between 2 and 6 keV, consistent with that predicted for dark matter with a roughly Maxwellian velocity distribution.

While DAMA/LIBRA's strategy of looking for an annual modulation in their rate can be successfully used to separate a dark matter signal from many possible backgrounds, one might worry about sources of background which could also exhibit seasonal variation. For example, the underground muon flux is known to modulate as a result of temperature variations in the stratosphere (although with a later phase and lower rate than is observed by DAMA/LIBRA [137]). Observed variations in the radon-induced background rate are also out-of-phase with the signal reported by DAMA/LIBRA. To date, no background has been identified with a phase, spectrum and rate compatible with DAMA/LIBRA's signal.

The regions of dark matter parameter space in which the DAMA/LIBRA modulation can be accounted for depends strongly on the highly uncertain low-energy sodium quench-

ing factor (the fraction of recoil energy of an elastic scattering event which is manifest as scintillation). In their analysis, the DAMA/LIBRA collaboration has adopted a canonical value of $Q_{\rm Na} = 0.3 \pm 0.01$ for this quantity, which they report to be the measured value averaged over the recoil energy range of 6.5 to 97 keV [79]. Other groups have reported similar values: $Q_{\rm Na} = 0.25 \pm 0.03$ (over 20-80 keV), 0.275 ± 0.018 (over 4-252 keV), and 0.4 ± 0.2 (over 5-100 keV) [80]. As the sodium quenching factor is generally anticipated to vary as a function of energy, it is very plausible that over the range of recoil energies relevant for light (5-20 GeV) dark matter particles (approximately 5 to 30 keV) the quenching factor could be quite different from the average values reported from these measurements. For recoil energies below approximately 20 keV, Ref. [87] reports a measurement of $Q_{\rm Na} = 0.33 \pm 0.15$, whereas Ref. [88] reports a somewhat smaller value of $Q_{\rm Na} = 0.252 \pm 0.064$ near 10 keV. The results of a very recent and preliminary measurement favor values of $Q_{\rm Na} \approx 0.15 - 0.2$ at similarly low energies [134, 110]. At this time, we choose to keep an open mind regarding the relevant low-energy quenching factor for sodium, and will consider a range of values between $Q_{\rm Na} \sim 0.15$ and 0.40. Based on theoretical considerations [68, 69] and recently experimental evidence [134], we do not consider the possibility that channeling plays an important role at DAMA/LIBRA.

For a quenching factor of $Q_{\rm Na} \approx 0.25$ (0.15, 0.4), elastically scattering dark matter with a mass in the range of approximately 8-19 GeV (12-19 GeV, 6-14 GeV) can accommodate the spectrum of the modulation amplitude reported by DAMA/LIBRA (see Fig. 7.5), assuming a Maxwellian velocity distribution with typical parameters (for earlier fits of DAMA data to light dark matter particles, see Refs. [138, 139]). The allowed regions do not extend to masses above about 18-20 GeV, where scattering with iodine nuclei begins to dominate. Under these same assumptions, an elastic scattering cross section of $\sigma_n \approx (0.7 - 3) \times 10^{-40}$ cm^2 is required to produce the observed magnitude of DAMA/LIBRA's modulation, which is significantly larger than the cross section implied by the spectra reported by CoGeNT

and CRESST. Departures from a Maxwellian velocity distribution, however, could strongly impact (and potentially enhance) the observed modulation amplitude. We will return to this issue in Sec. 7.4.1.

7.3.2 CoGeNT's Modulation

The CoGeNT collaboration has also reported evidence of an annual modulation in their event rate, although with a modest statistical significance of 2.8σ. Despite the lower statistical significance of this signal, it is interesting to compare the features of CoGeNT's time variation with that observed by DAMA/LIBRA. The peak of CoGeNT's phase is May 18$\pm$16 days, which is slightly earlier (at the 1.6σ level) than that favored by DAMA/LIBRA. If the modulation signals reported by DAMA/LIBRA and CoGeNT both arise from dark matter, a common phase that peaks in early May seems most likely [133], in concordance with expectations for dark matter based on results from numerical simulations [33].

In comparing the spectra of the modulation amplitudes reported by DAMA/LIBRA and CoGeNT, it is possible to remove the dependence on the dark matter's velocity distribution, following the approach of Ref. [38] (see also Ref. [16]). This method maps the events in a certain energy range in an experiment with one type of target to events in a different energy range in another experiment with a different target without making any assumptions about the velocity distribution of the dark matter. In Figs. 7.6 and 7.7, we present such a comparison. Although this comparison does not depend on the velocity distribution of the dark matter particles, it does rely on assumptions pertaining to the mass of the dark matter particle, on the ratio of the elastic scattering cross sections with germanium and sodium, and on the relevant quenching factors. Based on the shape of the CoGeNT and CRESST-II event spectra, we choose here to consider masses of 10 and 15 GeV, and assume a cross section which scales with A^2 of the target nucleus, as predicted for generic spin-independent

scattering. In each of the three frames, we show the results for a different value of the low-energy sodium quenching factor. The spectrum of CoGeNT's modulation amplitude was determined using the (publically available) 15 month CoGeNT data set [42], as described in Ref. [133].

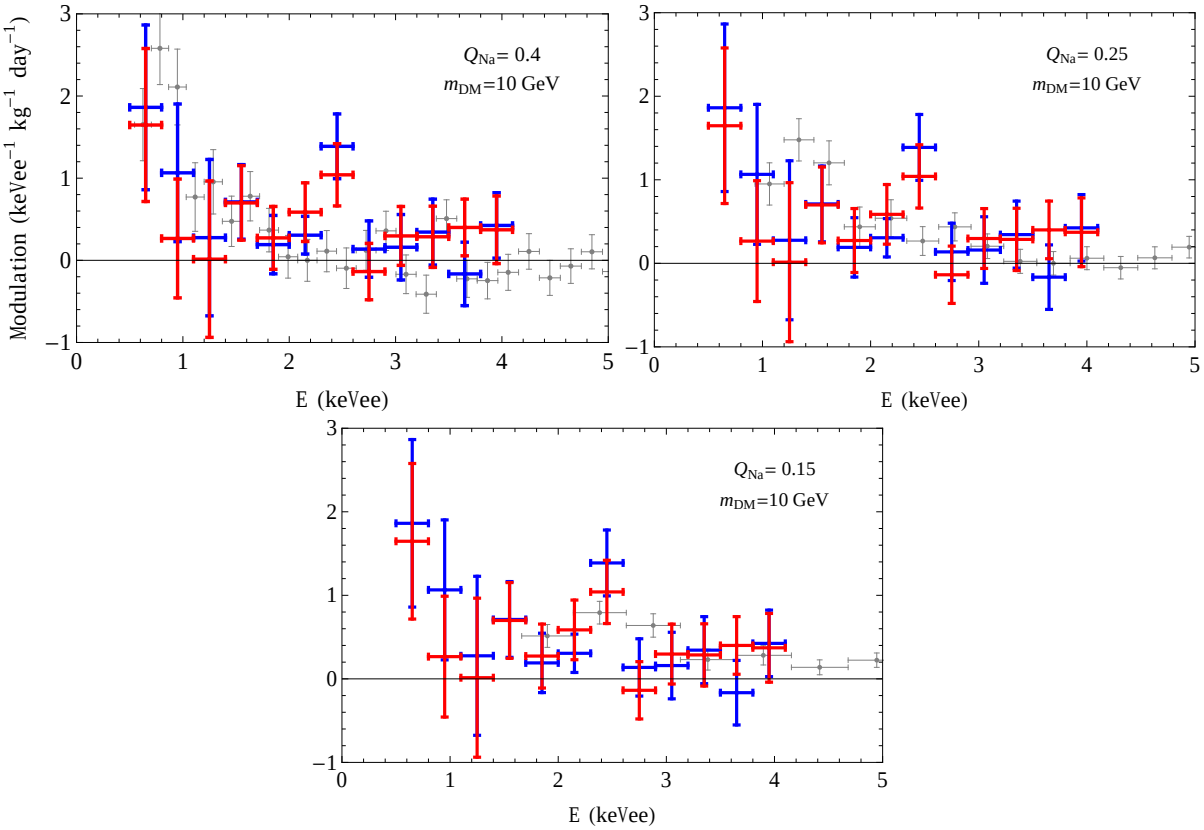

Figure 7.6: A comparison between the modulation amplitude spectrum observed by DAMA/LIBRA and CoGeNT, independent of the dark matter's velocity distribution, following the approach of Ref. [38]. The comparison is done for dark matter masses of 10 and 15 GeV, and for three choices of the low-energy sodium quenching factor. The blue (red) error bars denote the CoGeNT modulation amplitude assuming a phase that peaks on April 18th (May 26th). The grey error bars denote the expected DAMA/LIBRA modulation spectrum mapped onto the CoGeNT detector. In normalizing the results, we have assumed the dark matter's elastic scattering cross section to scale with the square of the target's atomic number, A^2.

From Fig. 7.6, it is immediately evident that the spectrum and overall normalization of the modulation amplitudes reported by CoGeNT and DAMA/LIBRA are quite similar.

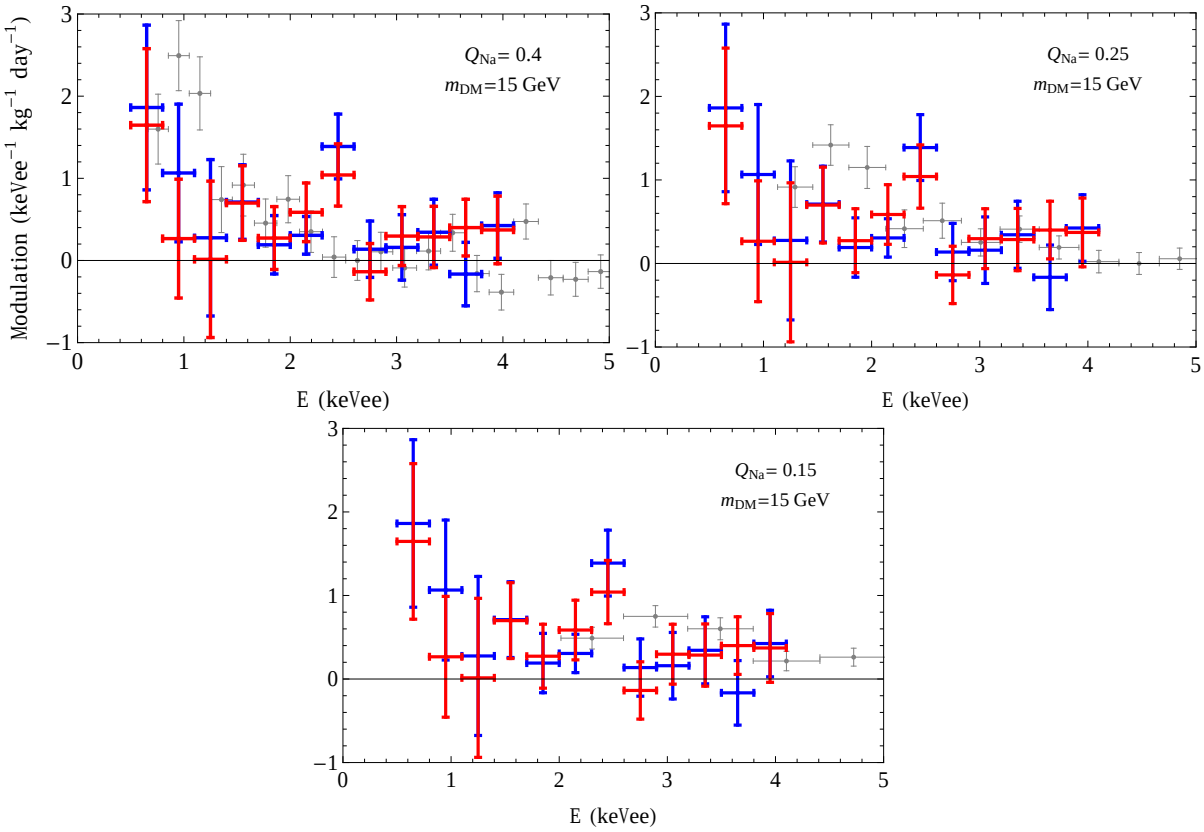

Figure 7.7: The same as Fig. 7.6 but for a dark matter mass of 15 GeV.

In fact, if the modulation reported by DAMA/LIBRA is the product of spin-independent elastic scattering with dark matter, then one should expect CoGeNT to observe a modulation with broad features very much like that they report, and vice versa. The details of this comparison, however, depend significantly on the value of the low-energy sodium quenching factor that is adopted. For a larger value ($Q_{\rm Na} \approx 0.3-0.4$) the steadily increasing modulation amplitude at low energies is seen by both experiments, while CoGeNT's high modulation bin at $\sim$2.5 keVee is not confirmed by DAMA/LIBRA. As this feature is apparent only in one bin with a sizable error bar, we consider it possible that this bin represents a statistical fluctuation which may disappear with further data from CoGeNT. Alternatively, if a lower sodium quenching factor is adopted ($Q_{\rm Na} \approx 0.15-0.2$, as favored by Ref. [134, 110]), the modulation reported by DAMA/LIBRA can overlap with CoGeNT's 2.5 keVee bin, while

CoGeNT's lower energy modulation falls below the energy threshold of DAMA/LIBRA. In this case, one could consider the possibility that this narrow feature results from a velocity stream of dark matter present in the local halo.

7.4 Why Is The Observed Modulation Amplitude So Large?

In the previous sections, we found that the event spectra observed by CoGeNT and CRESST-II are compatible with arising from the same dark matter particle. Similarly, the modulation amplitudes reported by DAMA/LIBRA and CoGeNT appear to be mutually consistent. Under the standard assumptions of a Maxwellian velocity distribution and velocity-independent scattering cross sections, however, the spectrum and rate of events reported by CoGeNT and CRESST-II would lead one to expect a signficantly smaller (by a factor of 3–10) modulation amplitude than is observed by DAMA/LIBRA and CoGeNT. In this section, we discuss how departures from these assumptions could explain why DAMA/LIBRA and CoGeNT have observed more modulation than would be naively predicted.

7.4.1 Streams and Other Non-Maxwellian Velocity Distributions

In Fig. 7.8, we show an example of how streams might impact the spectrum of the modulation amplitude, as observed by CoGeNT. In the upper left frame, the results from a simple Maxwellian distribution are shown for a dark matter mass of 10 GeV and an elastic scattering cross section of $\sigma_n = 1.5 \times 10^{-41}$ cm^2. As previously emphasized, the overall normalization of the predicted modulation is a factor of a few smaller than is observed. In the upper right frame, we add an additional tidal stream of dark matter, with a velocity of 160 km/s, a local density of 0.06 GeV/cm^3 (20% of the density of the smooth halo), and a dispersion of 15 km/s. The lower frame shows the spectrum that this model would produce along with spectrum of events measured at CoGeNT using the central value for the surface event

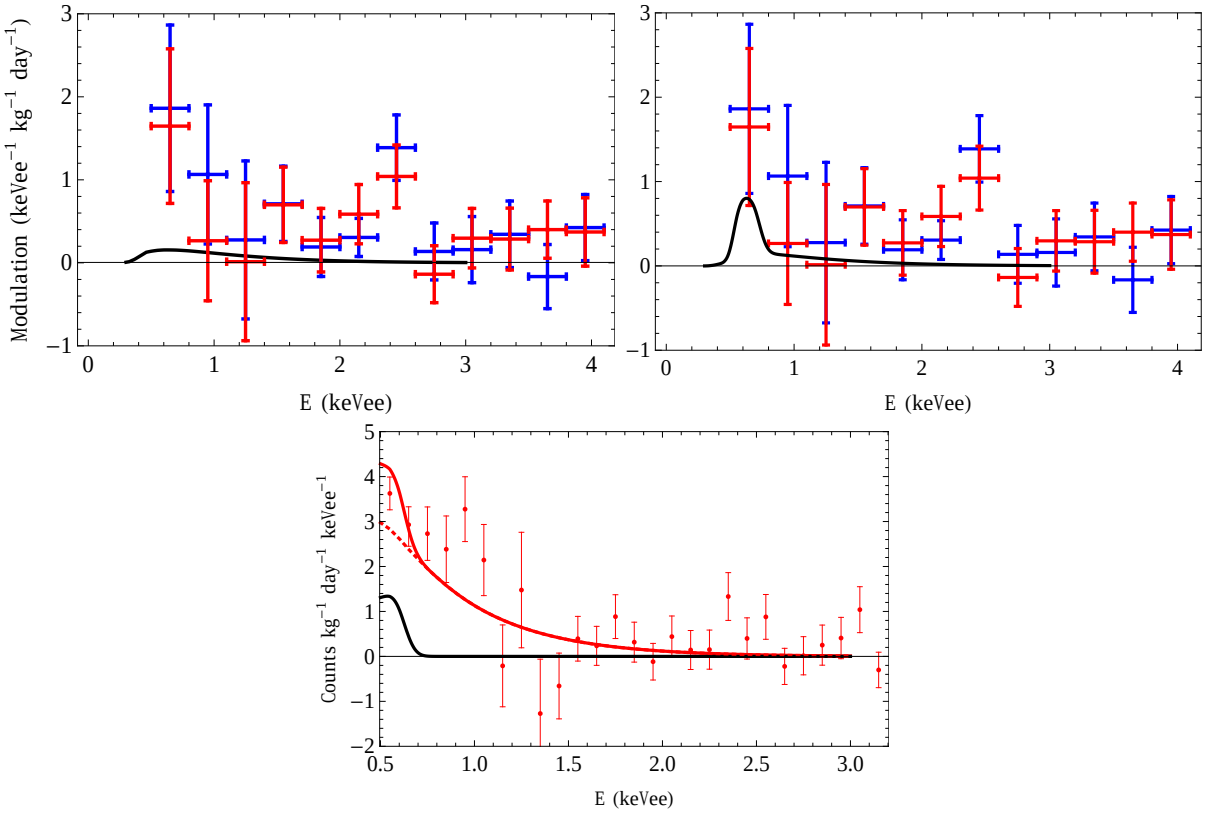

Figure 7.8: The impact of tidal streams on the modulation spectrum measured at CoGeNT. In the upper left frame, the result of a simple Maxwellian distribution is shown for a dark matter mass of 10 GeV and an elastic scattering cross section of $\sigma_n = 1.5 \times 10^{-41}$ cm^2. In the upper right frame, we add a tidal stream of dark matter with a velocity of 160 km/s, a local density of 0.06 GeV/cm^3 (20% of the density of the smooth halo), and a dispersion of 15 km/s. The lower frame shows the stream (solid black), smooth halo (dashed red), and total (solid red) spectra that this model would produce along with the spectrum measured at CoGeNT using the central value for the surface event correction factor and subtracting the constant background (red error bars).

correction factor and subtracting the constant background.

We find that this tidal stream can significantly enhance the modulation signal while still providing a reasonable fit to the overall spectrum at CoGeNT. One might postulate another stream to explain the rather high error bar at 2.5 keVee (and, for the appropriate choice of the sodium quenching factor, the peak in the DAMA/LIBRA spectrum as well; see the bottom frame of Fig. 7.6). In examining CoGeNT's data, we have become increasingly

convinced that this high error bar is due to a downward fluctuation in the winter rather than an enhancement in the summer. We predict that if dark matter is the source of the CoGeNT excess, then this error bar will come back down as more statistics are added.

Given the presently limited resolution of numerical simulations, it is difficult to assess the probability of significant tidal streams being present in our local neighborhood. Relatively small streams many orders of magnitude below the length scales that can be currently resolved could be very important. As an approximate lower limit, we note that current simulations [27, 23, 28, 29, 30] find significant streams to be present at our location of the Milky Way in roughly a few percent of realizations [33].

7.4.2 Velocity-Dependent Dark Matter Scattering

If the dark matter's scattering cross section with nuclei increases with the velocity of the dark matter particle, the degree of seasonal variation in the observed rate can be larger than is predicted in the standard (velocity-independent) case. Inelastic dark matter scenarios are a well known example of models in which the dark matter possesses velocity-dependent cross sections. In such models, the dark matter can only scatter with nuclei by being excited into a slightly heavier (typically on the order of 100 keV) state [52, 53, 54]. This requirement suppresses the rate of low energy events, and can increase the degree of annual modulation.

Inelastic dark matter, however, does not appear help in reconciling the spectra observed by CoGeNT and CRESST-II with the modulation of DAMA/LIBRA and CoGeNT. In particular, the spectrum of events from inelastically scattering dark matter is predicted to be quite flat at low energies, unlike that observed by CoGeNT and CRESST-II.

Other models which introduce a velocity dependent scattering cross section include form factor dark matter [50, 51] and resonant dark matter models [49] (see also Refs. [132, 140]). Each of these classes of models hold promise for potentially explaining the large degree of

modulation observed by DAMA/LIBRA and CoGeNT. In the first case, a new form factor is introduced which induces a momentum dependence in the interaction between dark matter and nuclei, enhancing the cross section for higher velocity dark matter particles. While this feature can boost the observed modulation amplitude, it will also distort the spectrum of events. In the case of resonant dark matter, the interaction cross section is significantly enhanced near a particular center-of-mass energy, leading to large (and potentially narrow in energy) modulation amplitudes.

As the CoGeNT collaboration collects more data, the spectrum of the modulation amplitude will become rapidly better measured, making it possible to begin to discriminate between the various options described in this section. By the summer of 2012, CoGeNT will have doubled the size of its data set, and with less background contamination from L-shell electron capture peaks than was present in earlier data. In addition, the CoGeNT collaboration plans to deploy the first of four CoGeNT-4 (C4) detectors in early 2012, roughly quadrupling their effective target mass. If streams or resonances are responsible for a significant fracton of the observed modulation, these features will become increasingly apparent as this data set grows.

7.5 Summary and Discussion

In this Chapter, we have compared the signals reported by the DAMA/LIBRA, CoGeNT, and CRESST-II collaborations. We summarize our finding as follows:

- The spectra of events reported by CoGeNT and CRESST-II are in good agreement, and (for a typical Maxwellian velocity distribution) are consistent with a dark matter particle with a mass of approximately 10-20 GeV and an elastic scattering cross section of $\sigma_n \approx (1-3) \times 10^{-41}$ cm^2. This range of parameter space is roughly consistent with the constraints from CDMS-II, but is in tension with the constraints of xenon-based

experiments unless the response of liquid xenon to very low-energy nuclear recoils is lower than previously claimed, or the dark matter's couplings to protons and neutrons destructively interfere for a xenon target.

- The spectra of the modulation amplitudes reported by DAMA/LIBRA and CoGeNT are also consistent with each other. Under the assumption of a typical Maxwellian velocity distribution, these modulation signals favor dark matter particles with masses of 8-19 GeV and an elastic scattering cross section of $\sigma_n \approx (0.7 - 3) \times 10^{-40}$ cm^2.

- The apparent mismatch between the elastic scattering cross sections required to produce the event spectra observed by CoGeNT and CRESST-II and those needed to produced the modulations reported by DAMA/LIBRA and CoGeNT could be potentially resolved if the local dark matter distribution contains streams or other highly non-Maxwellian features, or if the dark matter's scattering cross section with nuclei is velocity-dependent.

Taken together, these data appear to favor a dark matter particle with a mass of approximately 10-15 GeV, and an elastic scattering cross section of roughly $\sigma_n \sim 2 \times 10^{-41}$ cm^2. This mass range is of particular interest in light of recent indirect detection results. In particular, the spatial morphology and spectrum of gamma-rays observed from the Galactic Center can be explained by the annihilations of a 7-12 GeV dark matter particle, annihilating primarily to leptons, and with an annihilation cross section approximately equal to the value required to generate the observed cosmological abundance of dark matter in the early Universe ($\sigma v \sim 3 \times 10^{-26}$ cm^3/s) [141, 103]. The same dark matter model (mass, annihilation cross section, annihilation channels, and halo profile) has also been shown to lead to the production of a diffuse haze of synchrotron emission consistent with that observed by WMAP [113, 142, 143]. It also appears that the excess radio emission observed at higher galactic longitudes by the ARCADE 2 experiment [144, 145] possesses a spectral

shape and overall intensity consistent with originating from dark matter with the same mass, cross section, dominant channels, and distribution [146, 147]. Lastly, we mention that $\sim$10 GeV dark matter particles with the same distribution and annihilation cross section would be capable of depositing the required energetic electrons into the Milky Way's non-thermal radio filaments [148], providing an explanation for their peculiar spectral features. Comparing these results to the CRESST-II, CoGeNT, and DAMA/LIBRA signals discussed in this paper, it may be the case that these experiments are each observing different facets of the same species of dark matter.

REFERENCES

[1] F. Zwicky, "Die Rotverschiebung von extragalaktischen Nebeln," *Helvetica Physica Acta* **6** .

[2] S. W. Allen, A. E. Evrard, and A. B. Mantz, "Cosmological Parameters from Observations of Galaxy Clusters," *Ann.Rev.Astron.Astrophys.* **49** (2011) 409–470, arXiv:1103.4829 [astro-ph.CO].

[3] D. Clowe, M. Bradac, A. H. Gonzalez, M. Markevitch, S. W. Randall, *et al.*, "A direct empirical proof of the existence of dark matter," *Astrophys.J.* **648** (2006) L109–L113, arXiv:astro-ph/0608407 [astro-ph].

[4] A. Borriello and P. Salucci, "The Dark matter distribution in disk galaxies," *Mon.Not.Roy.Astron.Soc.* **323** (2001) 285, arXiv:astro-ph/0001082 [astro-ph].

[5] H. Hoekstra, H. Yee, and M. Gladders, "Current status of weak gravitational lensing," *New Astron.Rev.* **46** (2002) 767–781, arXiv:astro-ph/0205205 [astro-ph].

[6] L. A. Moustakas, K. Abazajian, A. Benson, A. S. Bolton, J. S. Bullock, *et al.*, "Strong gravitational lensing probes of the particle nature of dark matter," arXiv:0902.3219 [astro-ph.CO].

[7] N. Jarosik, C. Bennett, J. Dunkley, B. Gold, M. Greason, *et al.*, "Seven-Year Wilkinson Microwave Anisotropy Probe (WMAP) Observations: Sky Maps, Systematic Errors, and Basic Results," *Astrophys.J.Suppl.* **192** (2011) 14, arXiv:1001.4744 [astro-ph.CO].

[8] K. A. Olive, G. Steigman, and T. P. Walker, "Primordial nucleosynthesis: Theory and observations," *Phys.Rept.* **333** (2000) 389–407, arXiv:astro-ph/9905320 [astro-ph].

[9] **SDSS Collaboration** Collaboration, M. Tegmark *et al.*, "The 3-D power spectrum of galaxies from the SDSS," *Astrophys.J.* **606** (2004) 702–740, arXiv:astro-ph/0310725 [astro-ph].

[10] D. Hooper, "TASI 2008 Lectures on Dark Matter," arXiv:0901.4090 [hep-ph].

[11] M. C. Smith, G. Ruchti, A. Helmi, R. Wyse, J. Fulbright, *et al.*, "The RAVE Survey: Constraining the Local Galactic Escape Speed," *Mon.Not.Roy.Astron.Soc.* **379** (2007) 755–772, arXiv:astro-ph/0611671 [astro-ph].

[12] **XENON100 Collaboration** Collaboration, E. Aprile *et al.*, "Dark Matter Results from 100 Live Days of XENON100 Data," *Phys.Rev.Lett.* **107** (2011) 131302, arXiv:1104.2549 [astro-ph.CO].

[13] J. Collar, "A Realistic Assessment of the Sensitivity of XENON10 and XENON100 to Light-Mass WIMPs," arXiv:1106.0653 [astro-ph.CO].

[14] J. Collar, "Light WIMP Searches: The Effect of the Uncertainty in Recoil Energy Scale and Quenching Factor," arXiv:1010.5187 [astro-ph.IM].

[15] M. Lisanti, L. E. Strigari, J. G. Wacker, and R. H. Wechsler, "The Dark Matter at the End of the Galaxy," *Phys.Rev.* **D83** (2011) 023519, arXiv:1010.4300 [astro-ph.CO].

[16] P. J. Fox, G. D. Kribs, and T. M. Tait, "Interpreting Dark Matter Direct Detection Independently of the Local Velocity and Density Distribution," *Phys.Rev.* **D83** (2011) 034007, arXiv:1011.1910 [hep-ph].

[17] D. G. Cerdeno and A. M. Green, "Direct detection of WIMPs," arXiv:1002.1912 [astro-ph.CO].

[18] R. Schnee, "Introduction to dark matter experiments," arXiv:1101.5205 [astro-ph.CO].

[19] R. H. Helm, "Inelastic and Elastic Scattering of 187-Mev Electrons from Selected Even-Even Nuclei," *Phys.Rev.* **104** (1956) 1466–1475.

[20] G. Duda, A. Kemper, and P. Gondolo, "Model Independent Form Factors for Spin Independent Neutralino-Nucleon Scattering from Elastic Electron Scattering Data," *JCAP* **0704** (2007) 012, arXiv:hep-ph/0608035 [hep-ph].

[21] G. Fricke, C. Bernhardt, K. Heilig, L. Schaller, L. Schellenberg, *et al.*, "Nuclear Ground State Charge Radii from Electromagnetic Interactions," *Atom.Data Nucl.Data Tabl.* **60** (1995) 177.

[22] C. Savage, K. Freese, and P. Gondolo, "Annual Modulation of Dark Matter in the Presence of Streams," *Phys.Rev.* **D74** (2006) 043531, arXiv:astro-ph/0607121 [astro-ph].

[23] J. Diemand, M. Kuhlen, and P. Madau, "Dark matter substructure and gamma-ray annihilation in the Milky Way halo," *Astrophys.J.* **657** (2007) 262–270, arXiv:astro-ph/0611370 [astro-ph].

[24] R. Wojtak, E. L. Lokas, S. Gottloeber, and G. A. Mamon, "Radial velocity moments of dark matter haloes," *Mon.Not.Roy.Astron.Soc.* **361** (2005) L1, arXiv:astro-ph/0503391 [astro-ph].

[25] S. H. Hansen, B. Moore, M. Zemp, and J. Stadel, "A Universal velocity distribution of relaxed collisionless structures," *JCAP* **0601** (2006) 014, arXiv:astro-ph/0505420 [astro-ph].

[26] S. H. Hansen and B. Moore, "A Universal density slope - velocity anisotropy relation for relaxed structures," *New Astron.* **11** (2006) 333, arXiv:astro-ph/0411473 [astro-ph].

[27] J. Diemand, M. Kuhlen, P. Madau, M. Zemp, B. Moore, *et al.*, "Clumps and streams in the local dark matter distribution," *Nature* **454** (2008) 735–738, arXiv:0805.1244 [astro-ph].

[28] J. Stadel, D. Potter, B. Moore, J. Diemand, P. Madau, *et al.*, "Quantifying the heart of darkness with GHALO - a multi-billion particle simulation of our galactic halo," arXiv:0808.2981 [astro-ph].

[29] V. Springel, J. Wang, M. Vogelsberger, A. Ludlow, A. Jenkins, *et al.*, "The Aquarius Project: the subhalos of galactic halos," *Mon.Not.Roy.Astron.Soc.* **391** (2008) 1685–1711, arXiv:0809.0898 [astro-ph].

[30] M. Zemp, J. Diemand, M. Kuhlen, P. Madau, B. Moore, *et al.*, "The Graininess of Dark Matter Haloes," *Mon.Not.Roy.Astron.Soc.* **394** (2009) 641–659, arXiv:0812.2033 [astro-ph].

[31] B. Moore, C. Calcaneo-Roldan, J. Stadel, T. R. Quinn, G. Lake, *et al.*, "Dark matter in draco and the local group: implications for direct detection experiments," *Phys.Rev.* **D64** (2001) 063508, arXiv:astro-ph/0106271 [astro-ph].

[32] J. Vergados, S. Hansen, and O. Host, "The impact of going beyond the Maxwell distribution in direct dark matter detection rates," *Phys.Rev.* **D77** (2008) 023509, arXiv:0711.4895 [astro-ph].

[33] M. Kuhlen, N. Weiner, J. Diemand, P. Madau, B. Moore, *et al.*, "Dark Matter Direct Detection with Non-Maxwellian Velocity Structure," *JCAP* **1002** (2010) 030, arXiv:0912.2358 [astro-ph.GA].

[34] J. Lewin and P. Smith, "Review of mathematics, numerical factors, and corrections for dark matter experiments based on elastic nuclear recoil," *Astropart.Phys.* **6** (1996) 87–112.

[35] A. Natarajan, C. Savage, and K. Freese, "Probing dark matter streams with CoGeNT," *Phys.Rev.* **D84** (2011) 103005, arXiv:1109.0014 [astro-ph.CO].

[36] M. Kuhlen, M. Lisanti, and D. N. Spergel, "Direct Detection of Dark Matter Debris Flows," arXiv:1202.0007 [astro-ph.GA].

[37] M. Lisanti. Personal communication.

[38] P. J. Fox, J. Liu, and N. Weiner, "Integrating Out Astrophysical Uncertainties," *Phys.Rev.* **D83** (2011) 103514, arXiv:1011.1915 [hep-ph].

[39] **DAMA Collaboration, LIBRA Collaboration** Collaboration, R. Bernabei *et al.*, "New results from DAMA/LIBRA," *Eur.Phys.J.* **C67** (2010) 39–49, arXiv:1002.1028 [astro-ph.GA].

[40] **DAMA Collaboration** Collaboration, R. Bernabei *et al.*, "First results from DAMA/LIBRA and the combined results with DAMA/NaI," *Eur.Phys.J.* **C56** (2008) 333–355, arXiv:0804.2741 [astro-ph].

[41] **CoGeNT collaboration** Collaboration, C. Aalseth *et al.*, "Results from a Search for Light-Mass Dark Matter with a P-type Point Contact Germanium Detector," *Phys.Rev.Lett.* **106** (2011) 131301, arXiv:1002.4703 [astro-ph.CO].

[42] C. Aalseth, P. Barbeau, J. Colaresi, J. Collar, J. Diaz Leon, *et al.*, "Search for an Annual Modulation in a P-type Point Contact Germanium Dark Matter Detector," *Phys.Rev.Lett.* **107** (2011) 141301, arXiv:1106.0650 [astro-ph.CO].

[43] G. Angloher, M. Bauer, I. Bavykina, A. Bento, C. Bucci, *et al.*, "Results from 730 kg days of the CRESST-II Dark Matter Search," *Eur.Phys.J.* **C72** (2012) 1971, arXiv:1109.0702 [astro-ph.CO].

[44] **CDMS-II Collaboration** Collaboration, Z. Ahmed *et al.*, "Dark Matter Search Results from the CDMS II Experiment," *Science* **327** (2010) 1619–1621, arXiv:0912.3592 [astro-ph.CO].

[45] **XENON100 Collaboration** Collaboration, E. Aprile *et al.*, "First Dark Matter Results from the XENON100 Experiment," *Phys.Rev.Lett.* **105** (2010) 131302, arXiv:1005.0380 [astro-ph.CO].

[46] F. Petriello and K. M. Zurek, "DAMA and WIMP dark matter," *JHEP* **0809** (2008) 047, arXiv:0806.3989 [hep-ph].

[47] C. Savage, K. Freese, P. Gondolo, and D. Spolyar, "Compatibility of DAMA/LIBRA dark matter detection with other searches in light of new Galactic rotation velocity measurements," *JCAP* **0909** (2009) 036, arXiv:0901.2713 [astro-ph].

[48] C. Savage, G. Gelmini, P. Gondolo, and K. Freese, "Compatibility of DAMA/LIBRA dark matter detection with other searches," *JCAP* **0904** (2009) 010, arXiv:0808.3607 [astro-ph].

[49] Y. Bai and P. J. Fox, "Resonant Dark Matter," *JHEP* **0911** (2009) 052, arXiv:0909.2900 [hep-ph].

[50] B. Feldstein, A. L. Fitzpatrick, and E. Katz, "Form Factor Dark Matter," *JCAP* **1001** (2010) 020, arXiv:0908.2991 [hep-ph].

[51] S. Chang, A. Pierce, and N. Weiner, "Momentum Dependent Dark Matter Scattering," *JCAP* **1001** (2010) 006, arXiv:0908.3192 [hep-ph].

[52] S. Chang, G. D. Kribs, D. Tucker-Smith, and N. Weiner, "Inelastic Dark Matter in Light of DAMA/LIBRA," *Phys.Rev.* **D79** (2009) 043513, arXiv:0807.2250 [hep-ph].

[53] D. Tucker-Smith and N. Weiner, "Inelastic dark matter," *Phys.Rev.* **D64** (2001) 043502, arXiv:hep-ph/0101138 [hep-ph].

[54] D. Tucker-Smith and N. Weiner, "The Status of inelastic dark matter," *Phys.Rev.* **D72** (2005) 063509, arXiv:hep-ph/0402065 [hep-ph].

[55] J. F. Gunion, D. Hooper, and B. McElrath, "Light neutralino dark matter in the NMSSM," *Phys.Rev.* **D73** (2006) 015011, arXiv:hep-ph/0509024 [hep-ph].

[56] D. Hooper and T. Plehn, "Supersymmetric dark matter: How light can the LSP be?," *Phys.Lett.* **B562** (2003) 18–27, arXiv:hep-ph/0212226 [hep-ph].

[57] A. Bottino, N. Fornengo, and S. Scopel, "Light relic neutralinos," *Phys.Rev.* **D67** (2003) 063519, arXiv:hep-ph/0212379 [hep-ph].

[58] A. Bottino, F. Donato, N. Fornengo, and S. Scopel, "Do current WIMP direct measurements constrain light relic neutralinos?," *Phys.Rev.* **D72** (2005) 083521, arXiv:hep-ph/0508270 [hep-ph].

[59] A. Bottino, F. Donato, N. Fornengo, and S. Scopel, "Interpreting the recent results on direct search for dark matter particles in terms of relic neutralino," *Phys.Rev.* **D78** (2008) 083520, arXiv:0806.4099 [hep-ph].

[60] A. Bottino, F. Donato, N. Fornengo, and S. Scopel, "Relic neutralinos and the two dark matter candidate events of the CDMS II experiment," *Phys.Rev.* **D81** (2010) 107302, arXiv:0912.4025 [hep-ph].

[61] J. L. Feng and J. Kumar, "The WIMPless Miracle: Dark-Matter Particles without Weak-Scale Masses or Weak Interactions," *Phys.Rev.Lett.* **101** (2008) 231301, arXiv:0803.4196 [hep-ph].

[62] D. E. Kaplan, M. A. Luty, and K. M. Zurek, "Asymmetric Dark Matter," *Phys.Rev.* **D79** (2009) 115016, arXiv:0901.4117 [hep-ph].

[63] A. L. Fitzpatrick, D. Hooper, and K. M. Zurek, "Implications of CoGeNT and DAMA for Light WIMP Dark Matter," *Phys.Rev.* **D81** (2010) 115005, arXiv:1003.0014 [hep-ph].

[64] S. Chang, J. Liu, A. Pierce, N. Weiner, and I. Yavin, "CoGeNT Interpretations," *JCAP* **1008** (2010) 018, arXiv:1004.0697 [hep-ph].

[65] S. Andreas, C. Arina, T. Hambye, F.-S. Ling, and M. H. Tytgat, "A light scalar WIMP through the Higgs portal and CoGeNT," *Phys.Rev.* **D82** (2010) 043522, arXiv:1003.2595 [hep-ph].

[66] R. Foot, "A CoGeNT confirmation of the DAMA signal," *Phys.Lett.* **B692** (2010) 65–69, arXiv:1004.1424 [hep-ph].

[67] R. Essig, J. Kaplan, P. Schuster, and N. Toro, "On the Origin of Light Dark Matter Species," *Submitted to Physical Review D* (2010) , arXiv:1004.0691 [hep-ph].

[68] N. Bozorgnia, G. B. Gelmini, and P. Gondolo, "Channeling in direct dark matter detection II: channeling fraction in Si and Ge crystals," *JCAP* **1011** (2010) 028, arXiv:1008.3676 [astro-ph.CO].

[69] C. Savage, G. Gelmini, P. Gondolo, and K. Freese, "XENON10/100 dark matter constraints in comparison with CoGeNT and DAMA: examining the Leff dependence," *Phys.Rev.* **D83** (2011) 055002, arXiv:1006.0972 [astro-ph.CO].

[70] E. Drobyshevski, "Channeling Effect and Improvement of the Efficiency of Charged Particle Registration with Crystal Scintillators," *Mod.Phys.Lett.* **A23** (2008) 3077–3085, arXiv:0706.3095 [physics.ins-det].

[71] R. Bernabei, P. Belli, F. Montecchia, F. Nozzoli, F. Cappella, *et al.*, "Possible implications of the channeling effect in NaI(Tl) crystals," *Eur.Phys.J.* **C53** (2008) 205–213, arXiv:0710.0288 [astro-ph].

[72] C. McCabe, "The Astrophysical Uncertainties Of Dark Matter Direct Detection Experiments," *Phys.Rev.* **D82** (2010) 023530, arXiv:1005.0579 [hep-ph].

[73] S. Chaudhury, P. Bhattacharjee, and R. Cowsik, "Direct detection of WIMPs : Implications of a self-consistent truncated isothermal model of the Milky Way's dark matter halo," *JCAP* **1009** (2010) 020, arXiv:1006.5588 [astro-ph.CO].

[74] **TEXONO Collaboration** Collaboration, S. Lin *et al.*, "New limits on spin-independent and spin-dependent couplings of low-mass WIMP dark matter with a germanium detector at a threshold of 220 eV," *Phys.Rev.* **D79** (2009) 061101, arXiv:0712.1645 [hep-ex].

[75] Y. Messous, "Calibration of a Ge crystal with nuclear recoils for the development of a dark matter detector," *Astropart.Phys.* **3** (1995) 361–366.

[76] P. Barbeau, J. Collar, and O. Tench, "Large-Mass Ultra-Low Noise Germanium Detectors: Performance and Applications in Neutrino and Astroparticle Physics," *JCAP* **0709** (2007) 009, arXiv:nucl-ex/0701012 [nucl-ex].

[77] P. Barbeau, J. Collar, and P. Whaley, "Design and Characterization of a Neutron Calibration Facility for the Study of sub-keV Nuclear Recoils," *Nucl.Instrum.Meth.* **A574** (2007) 385–391, arXiv:nucl-ex/0701011 [nucl-ex].

[78] P. Barbeau, *Neutrino and Astroparticle Physics with P-Type Point Contact High Purity Germanium Detectors*. PhD thesis, University of Chicago, 2009.

[79] R. Bernabei, P. Belli, F. Cappella, R. Cerulli, F. Montecchia, *et al.*, "Dark matter search," *Riv.Nuovo Cim.* **26N1** (2003) 1–73, arXiv:astro-ph/0307403 [astro-ph].

[80] K. Fushimi, H. Ejiri, H. Kinoshita, N. Kudomi, K. Kume, *et al.*, "Application of a large volume NaI scintillator to search for dark matter," *Phys.Rev.* **C47** (1993) 425–428.

[81] F. Cappella. Personal communication.

[82] V. Tretyak. Personal communication.

[83] V. Tretyak, "Semi-empirical calculation of quenching factors for ions in scintillators," *Astropart.Phys.* **33** (2010) 40–53, arXiv:0911.3041 [nucl-ex].

[84] J. Collar and D. McKinsey, "Comments on 'First Dark Matter Results from the XENON100 Experiment'," arXiv:1005.0838 [astro-ph.CO].

[85] J. Collar and D. McKinsey, "Response to arXiv:1005.2615," arXiv:1005.3723 [astro-ph.CO].

[86] J. Collar, "Comments on arXiv:1006.0972 'XENON10/100 dark matter constraints in comparison with CoGeNT and DAMA: examining the Leff dependence'," arXiv:1006.2031 [astro-ph.CO].

[87] D. Tovey, V. Kudryavtsev, M. Lehner, J. McMillan, C. Peak, *et al.*, "Measurement of scintillation efficiencies and pulse-shapes for nuclear recoils in NaI(Tl) and CaF-2(Eu) at low-energies for dark matter experiments," *Phys.Lett.* **B433** (1998) 150–155.

[88] H. Chagani, P. Majewski, E. Daw, V. Kudryavtsev, and N. Spooner, "Measurement of the quenching factor of Na recoils in NaI(Tl)," *JINST* **3** (2008) P06003, arXiv:0806.1916 [physics.ins-det].

[89] "Response of nai(tl) to x-rays and electrons," *Nuclear Instruments and Methods in Physics Research Section A: Accelerators, Spectrometers, Detectors and Associated Equipment* **411** no. 2ñ3, (1998) 351 – 364.

[90] J. Collar, "Certainty and uncertainty in dark matter searches," in *Exploring Low-Mass Dark Matter Candidates*, Pitt-PACC. November 14-16, 2011.

[91] J. N. Bahcall, "Exchange and Overlap Effects in Electron Capture and in Related Phenomena," *Phys.Rev.* **132** (1963) 362–367.

[92] T. Seidel, "CRESST," in *WONDER 2010 Workshop*. 2010.

[93] T. Schwetz, "Dark Matter direct detection and speculations on low-mass WIMPs," in *MPIK Seminar*. 2010.

[94] **XENON Collaboration** Collaboration, J. Angle *et al.*, "First Results from the XENON10 Dark Matter Experiment at the Gran Sasso National Laboratory," *Phys.Rev.Lett.* **100** (2008) 021303, arXiv:0706.0039 [astro-ph].

[95] **XENON10 Collaboration** Collaboration, J. Angle *et al.*, "Constraints on inelastic dark matter from XENON10," *Phys.Rev.* **D80** (2009) 115005, arXiv:0910.3698 [astro-ph.CO].

[96] A. Manzur, A. Curioni, L. Kastens, D. McKinsey, K. Ni, *et al.*, "Scintillation efficiency and ionization yield of liquid xenon for mono-energetic nuclear recoils down to 4 keV," *Phys.Rev.* **C81** (2010) 025808, arXiv:0909.1063 [physics.ins-det].

[97] J. Filippini, *A Search for WIMP Dark Matter Using the First Five-Tower Run of the Cryogenic Dark Matter Search*. PhD thesis, University of California at Berkeley, 2008.

[98] **CDMS Collaboration** Collaboration, J. Filippini, "WIMP hunting with the Cryogenic Dark Matter Search," *Nuovo Cim.* **C32N5-6** (2009) 45–52.

[99] G. Gerbier, E. Lesquoy, J. Rich, M. Spiro, C. Tao, *et al.*, "MEASUREMENT OF THE IONIZATION OF SLOW SILICON NUCLEI IN SILICON FOR THE CALIBRATION OF A SILICON DARK MATTER DETECTOR," *Phys.Rev.* **D42** (1990) 3211–3214.

[100] R. Ogburn, *A search for particle dark matter using cryogenic germanium and silicon detectors in the one- and two-tower runs of CDMS-II at Soudan*. PhD thesis, Standford University, 2008.

[101] **CDMS Collaboration** Collaboration, D. Akerib *et al.*, "A low-threshold analysis of CDMS shallow-site data," *Phys.Rev.* **D82** (2010) 122004, arXiv:1010.4290 [astro-ph.CO].

[102] D. Hooper, J. Collar, J. Hall, D. McKinsey, and C. Kelso, "A Consistent Dark Matter Interpretation For CoGeNT and DAMA/LIBRA," *Phys.Rev.* **D82** (2010) 123509, arXiv:1007.1005 [hep-ph].

[103] D. Hooper and L. Goodenough, "Dark Matter Annihilation in The Galactic Center As Seen by the Fermi Gamma Ray Space Telescope," *Phys.Lett.* **B697** (2011) 412–428, arXiv:1010.2752 [hep-ph].

[104] R. Schoenrich, J. Binney, and W. Dehnen, "Local Kinematics and the Local Standard of Rest," arXiv:0912.3693 [astro-ph.GA].

[105] A. M. Green, "Dependence of direct detection signals on the WIMP velocity distribution," *JCAP* **1010** (2010) 034, arXiv:1009.0916 [astro-ph.CO].

[106] J. Schmaler, "," in *DPG Spring Meeting*. 2011.

[107] F. Probst, "," in *Princeton Center for Theoretical Science Workshop*. 2010.

[108] T. Seidel, "CRESST-II," in *IDM 2010*. 2010.

[109] **CDMS-II Collaboration** Collaboration, Z. Ahmed *et al.*, "Results from a Low-Energy Analysis of the CDMS II Germanium Data," *Phys.Rev.Lett.* **106** (2011) 131302, arXiv:1011.2482 [astro-ph.CO].

[110] J. Collar. Personal communication.

[111] A. Drukier, K. Freese, and D. Spergel, "Detecting Cold Dark Matter Candidates," *Phys.Rev.* **D33** (1986) 3495–3508.

[112] C. Kelso and D. Hooper, "Prospects For Identifying Dark Matter With CoGeNT," *JCAP* **1102** (2011) 002, arXiv:1011.3076 [hep-ph].

[113] D. Hooper and T. Linden, "Gamma Rays From The Galactic Center and the WMAP Haze," *Phys.Rev.* **D83** (2011) 083517, arXiv:1011.4520 [astro-ph.HE].

[114] N. Bozorgnia, G. B. Gelmini, and P. Gondolo, "Channeling in direct dark matter detection I: channeling fraction in NaI (Tl) crystals," *JCAP* **1011** (2010) 019, arXiv:1006.3110 [astro-ph.CO].

[115] J. Collar, "A comparison between the low-energy spectra from CoGeNT and CDMS," arXiv:1103.3481 [astro-ph.CO].

[116] G. Plante, E. Aprile, R. Budnik, B. Choi, K. Giboni, *et al.*, "New Measurement of the Scintillation Efficiency of Low-Energy Nuclear Recoils in Liquid Xenon," *Phys.Rev.* **C84** (2011) 045805, arXiv:1104.2587 [nucl-ex].

[117] **XENON10 Collaboration** Collaboration, J. Angle *et al.*, "A search for light dark matter in XENON10 data," *Phys.Rev.Lett.* **107** (2011) 051301, arXiv:1104.3088 [astro-ph.CO].

[118] J. L. Feng, J. Kumar, D. Marfatia, and D. Sanford, "Isospin-Violating Dark Matter," *Phys.Lett.* **B703** (2011) 124–127, arXiv:1102.4331 [hep-ph].

[119] F. Dahl, "Indirect and Direct Detection of Dark Matter ," in *Aspen Center For Physics 2011 Winter Conference*. 2011.

[120] V. Barger, M. McCaskey, and G. Shaughnessy, "Complex Scalar Dark Matter vis-à-vis CoGeNT, DAMA/LIBRA and XENON100," *Phys.Rev.* **D82** (2010) 035019, arXiv:1005.3328 [hep-ph].

[121] K. J. Bae, H. D. Kim, and S. Shin, "Light neutralino dark matter with a very light Higgs for CoGeNT and DAMA/LIBRA data," *Phys.Rev.* **D82** (2010) 115014, arXiv:1005.5131 [hep-ph].

[122] Y. Mambrini, "The Kinetic dark-mixing in the light of CoGENT and XENON100," *JCAP* **1009** (2010) 022, arXiv:1006.3318 [hep-ph].

[123] A. V. Belikov, J. F. Gunion, D. Hooper, and T. M. Tait, "CoGeNT, DAMA, and Light Neutralino Dark Matter," *Phys.Lett.* **B705** (2011) 82–86, arXiv:1009.0549 [hep-ph].

[124] J. F. Gunion, A. V. Belikov, and D. Hooper, "CoGeNT, DAMA, and Neutralino Dark Matter in the Next-To-Minimal Supersymmetric Standard Model," arXiv:1009.2555 [hep-ph].

[125] M. R. Buckley, D. Hooper, and T. M. Tait, "Particle Physics Implications for CoGeNT, DAMA, and Fermi," *Phys.Lett.* **B702** (2011) 216–219, arXiv:1011.1499 [hep-ph].

[126] N. Fornengo, S. Scopel, and A. Bottino, "Discussing direct search of dark matter particles in the Minimal Supersymmetric extension of the Standard Model with light neutralinos," *Phys.Rev.* **D83** (2011) 015001, arXiv:1011.4743 [hep-ph].

[127] S. Shin, "Light neutralino dark matter in light Higgs scenario related with the CoGeNT and DAMA/LIBRA results," *PoS* **IDM2010** (2011) 094, arXiv:1011.6377 [hep-ph].

[128] M. H. Tytgat, "A light scalar WIMP through the Higgs portal?," *PoS* **IDM2010** (2011) 126, arXiv:1012.0576 [hep-ph].

[129] M. Buckley, P. Fileviez Perez, D. Hooper, and E. Neil, "Dark Forces At The Tevatron," *Phys.Lett.* **B702** (2011) 256–259, arXiv:1104.3145 [hep-ph].

[130] Y. Mambrini, "The ZZ' kinetic mixing in the light of the recent direct and indirect dark matter searches," *JCAP* **1107** (2011) 009, arXiv:1104.4799 [hep-ph].

[131] M. T. Frandsen, F. Kahlhoefer, J. March-Russell, C. McCabe, M. McCullough, *et al.*, "On the DAMA and CoGeNT Modulations," *Phys.Rev.* **D84** (2011) 041301, arXiv:1105.3734 [hep-ph].

[132] A. L. Fitzpatrick and K. M. Zurek, "Dark Moments and the DAMA-CoGeNT Puzzle," *Phys.Rev.* **D82** (2010) 075004, arXiv:1007.5325 [hep-ph].

[133] D. Hooper and C. Kelso, "Implications of CoGeNT's New Results For Dark Matter," *Phys.Rev.* **D84** (2011) 083001, arXiv:1106.1066 [hep-ph].

[134] J. Collar, "CoGENT and COUPP," in *TAUP 2011 Workshop*. 2011.

[135] J. Kopp, T. Schwetz, and J. Zupan, "Light Dark Matter in the light of CRESST-II," *JCAP* **1203** (2012) 001, arXiv:1110.2721 [hep-ph].

[136] A. Brown, S. Henry, H. Kraus, and C. McCabe, "Extending the CRESST-II commissioning run limits to lower masses," *Phys.Rev.* **D85** (2012) 021301, arXiv:1109.2589 [astro-ph.CO].

[137] R. Bernabei, P. Belli, F. Cappella, R. Cerulli, C. Dai, *et al.*, "Particle Dark Matter and DAMA/LIBRA," *AIP Conf.Proc.* **1223** (2010) 50–59, arXiv:0912.0660 [astro-ph.GA].

[138] A. Bottino, F. Donato, N. Fornengo, and S. Scopel, "Light neutralinos and WIMP direct searches," *Phys.Rev.* **D69** (2004) 037302, arXiv:hep-ph/0307303 [hep-ph].

[139] P. Gondolo and G. Gelmini, "Compatibility of DAMA dark matter detection with other searches," *Phys.Rev.* **D71** (2005) 123520, arXiv:hep-ph/0504010 [hep-ph].

[140] M. Farina, D. Pappadopulo, A. Strumia, and T. Volansky, "Can CoGeNT and DAMA Modulations Be Due to Dark Matter?," *JCAP* **1111** (2011) 010, arXiv:1107.0715 [hep-ph].

[141] D. Hooper and T. Linden, "On The Origin Of The Gamma Rays From The Galactic Center," *Phys.Rev.* **D84** (2011) 123005, arXiv:1110.0006 [astro-ph.HE].

[142] D. Hooper, D. P. Finkbeiner, and G. Dobler, "Possible evidence for dark matter annihilations from the excess microwave emission around the center of the Galaxy seen by the Wilkinson Microwave Anisotropy Probe," *Phys.Rev.* **D76** (2007) 083012, arXiv:0705.3655 [astro-ph].

[143] D. P. Finkbeiner, "WMAP microwave emission interpreted as dark matter annihilation in the inner galaxy," arXiv:astro-ph/0409027 [astro-ph].

[144] D. Fixsen, A. Kogut, S. Levin, M. Limon, P. Lubin, *et al.*, "ARCADE 2 Measurement of the Extra-Galactic Sky Temperature at 3-90 GHz," arXiv:0901.0555 [astro-ph.CO].

[145] M. Seiffert, D. Fixsen, A. Kogut, S. Levin, M. Limon, *et al.*, "Interpretation of the Extragalactic Radio Background," arXiv:0901.0559 [astro-ph.CO].

[146] N. Fornengo, R. Lineros, M. Regis, and M. Taoso, "Possibility of a Dark Matter Interpretation for the Excess in Isotropic Radio Emission Reported by ARCADE," *Phys.Rev.Lett.* **107** (2011) 271302, arXiv:1108.0569 [hep-ph].

[147] M. Regis. Personal communication.

[148] T. Linden, D. Hooper, and F. Yusef-Zadeh, "Dark Matter and Synchrotron Emission from Galactic Center Radio Filaments," *Astrophys.J.* **741** (2011) 95, arXiv:1106.5493 [astro-ph.HE].